NACA

RESEARCH MEMORANDUM

EFFECT OF BLADE-SECTION CAMBER ON AERODYNAMIC CHARACTERISTICS OF FULL-SCALE SUPERSONIC-TYPE PROPELLERS AT MACH NUMBERS TO 1.04

By Julian D. Maynard, John M. Swihart,
and Harry T. Norton, Jr.

Langley Aeronautical Laboratory
Langley Field, Va.

NATIONAL ADVISORY COMMITTEE
FOR AERONAUTICS

WASHINGTON

October 19, 1956

NATIONAL ADVISORY COMMITTEE FOR AERONAUTICS

RESEARCH MEMORANDUM

EFFECT OF BLADE-SECTION CAMBER ON AERODYNAMIC CHARACTERISTICS OF FULL-SCALE SUPERSONIC-TYPE PROPELLERS AT MACH NUMBERS TO 1.04

By Julian D. Maynard, John M. Swihart, and Harry T. Norton, Jr.

SUMMARY

An investigation of the aerodynamic characteristics of two full-scale supersonic-type propellers has been made in the Langley 16-foot transonic tunnel with the 6,000-horsepower propeller dynamometer. The tests covered a range of blade angles at forward Mach numbers up to 1.04. One of the propellers had symmetrical NACA 16-series airfoil sections, and the other propeller was similar except for the incorporation of blade-section camber and a slight difference in pitch distribution. Both propellers were designed for an advance ratio of 2.2 and a Mach number of 0.95 at an altitude of 35,000 feet. Limitation of the maximum dynamometer rotational speed did not permit testing at the design condition of operation.

The results showed that the cambered propeller was more efficient at off-design conditions of operation and could operate efficiently over a wider range of advance ratio. However, calculations indicated that the symmetrical propeller had a slightly higher efficiency at the design condition of operation. At an advance ratio of 3.6, the cambered propeller was more efficient than the symmetrical propeller over a Mach number range from 0.6 to 1.04. The loss in maximum efficiency due to compressibility effects began at a Mach number of about 0.75 and amounted to 22 percent for either propeller at a Mach number of 1.04. The cambered propeller was found to absorb considerably more power, and stall flutter occurred at higher thrust coefficients for the cambered propeller than for the symmetrical propeller. The feathering blade angle of the cambered propeller was found to be 85.4°, measured at the 0.75 radius, and the negative thrust characteristics of this propeller make it very effective when used as a brake.

INTRODUCTION

Pressure distributions obtained in recent years (refs. 1 to 7) on the blade sections of operating propellers at high speeds have indicated that these airfoils have aerodynamic characteristics that are different from those of two-dimensional airfoils or wings, particularly for blade sections near the tip. Factors, or a combination of them, which might explain this phenomenon include the effects of blade interference or a cascade effect, the tip-relieving or aspect-ratio effects, the effects of radial boundary-layer flow, and the effects of a Mach number gradient along the blades. At present, there is no theory or calculation procedure for propellers which adequately takes into account all these factors, and it is necessary, therefore, that the aerodynamic characteristics of propellers designed to operate at transonic speeds be determined experimentally to justify the assumptions necessary with respect to airfoil data and propeller theory.

A previous investigation of the effects of blade-section camber on the aerodynamic characteristics of propellers operating at Mach numbers up to 0.65 (ref. 8) indicated important advantages for camber in the take-off and climb performance of propellers. However, in the early designs of propellers to operate in the transonic-speed range, it was considered necessary to reduce the blade-section camber to very low values and even to zero to obtain higher critical Mach numbers for the blade sections which would be operating at low supersonic speeds. The first wind-tunnel investigation of a full-scale supersonic-type propeller at Mach numbers to 0.96 was reported in reference 9. This propeller had thin symmetrical 16-series airfoil sections from the spinner to the tip, and the aerodynamic characteristics reported in reference 9 were considered satisfactory. However, in an investigation of the effect of blade-section camber on the static characteristics of three NACA propellers, it was found that the flutter-speed coefficient increased with an increase in the blade-section camber (ref. 10). This indicated that the stall-flutter characteristics of supersonic propellers, about which the structural designers were concerned, might be improved by incorporating some camber in the blade sections. Furthermore, there was some indication in reference 8 that although the critical tip Mach number of propellers is lowered by an increase in blade-section camber, the supercritical tip Mach number at which recovery of thrust occurs is lower for a propeller having the higher cambered sections than for one having the lower cambered sections. For these reasons, it seemed desirable to investigate the effects of blade-section camber on the aerodynamic characteristics of a supersonic-type propeller and to determine the stall-flutter characteristics where possible.

A propeller was obtained, therefore, which had the same plan-form and thickness ratios as the supersonic propeller of reference 9, but the

blade sections were cambered and there was a slight difference in pitch distribution. The purpose of this investigation is to determine the characteristics of this cambered propeller to provide a comparison with the data presented in reference 9 for the symmetrical propeller. The investigation will indicate the effects of blade-section camber on the aerodynamic characteristics of supersonic-type propellers. A second purpose is to extend the Mach number range of the tests to low supersonic values for both propeller designs, and perhaps to obtain some indication of the effects of blade-section camber on the flutter characteristics of supersonic-type propellers.

This paper presents the results of the aerodynamic tests as plots of propeller efficiency and the thrust and power coefficients plotted against propeller advance ratio for a range of forward Mach numbers up to about 1.04. Limitations of the testing equipment prevent a complete and thorough analysis of the effect of blade-section camber, and the brief analysis presented herein includes only the primary effects of camber on propeller performance. In addition, a few tests were made with the cambered propeller to determine its feathering blade angle and to determine its aerodynamic characteristics at low and negative blade angles.

SYMBOLS

b	blade width (chord), ft
C_P	power coefficient, $\frac{P}{\rho n^3 D^5}$
C_T	thrust coefficient, $\frac{T}{\rho n^2 D^4}$
c_{l_d}	section design lift coefficient
D	propeller diameter, ft
h	blade-section maximum thickness, ft
J	advance ratio, $\frac{V}{nD}$
L/D	lift-drag ratio

M	Mach number of advance
M_t	helical tip Mach number, $M\sqrt{1 + \left(\frac{\pi}{J}\right)^2}$
M_x	helical Mach number at station x, $M\sqrt{1 + \left(\frac{\pi x}{J}\right)^2}$
n	propeller rotational speed, rps
P	power, ft-lb/sec
p	static pressure, lb/sq ft
Q	torque, ft-lb
q	dynamic pressure, $\frac{1}{2}\rho V^2$, lb/sq ft
R	propeller tip radius, ft
r	radius to a blade element, ft
T	thrust, lb
V	velocity of advance, fps
x	fraction of propeller tip radius, r/R
$\beta_{0.75R}$	blade angle at 0.75R, deg
η	efficiency
ρ	air density, slugs/cu ft

Subscript:

o	free stream

APPARATUS

Langley 16-Foot Transonic Tunnel

The investigation was conducted in the Langley 16-foot transonic tunnel which is an atmospheric type with longitudinal slots in the test section. These slots permit wall-interference-free testing to the maximum tunnel speed as limited by the maximum power of the drive system. Details of the wind tunnel are given in reference 11.

Propeller Dynamometer

Details of the 6,000-horsepower dynamometer are given in reference 12, and the instrumentation used in the present tests is the same as that described in reference 9. The arrangement of the dynamometer in the test section is also the same as that described in reference 9 with the following exceptions: the plane of rotation of the propeller was moved forward three feet to increase the distance between the propeller and the leading edge of the dynamometer support strut, and a fairing was placed between the support struts of the two dynamometer units (see sketch in fig. 1). These changes were made to place the propeller in a region where the Mach number would be higher and to alleviate to some extent the axial Mach number gradient at the plane of the propeller. These changes may be seen by comparing figure 1 of reference 9 with figure 1 of this paper. The length of the cylindrical fairing ahead of the propeller spinner was reduced from approximately 2.4 to 2.1 propeller diameters by the relocation of the propeller plane of rotation. As in reference 9, the boundary-layer thickness in the propeller plane due to the cylindrical fairing was computed to be of small enough magnitude to produce no noticeable effect on the operating propeller. Figure 2 shows photographs of the dynamometer installed in the Langley 16-foot transonic tunnel.

Propellers

The three-bladed solid steel propellers used in this investigation were designed by the Curtiss-Wright Corporation (design nos. 109622 and 109626) and were 9.75 feet in diameter. The two designs were similar except for the incorporation of blade-section camber in the 109626 design and a slight difference in pitch distribution. Both designs had a blade width of 14 inches from the spinner surface to the tip and the thickness ratio of both designs varied from 0.058 at the spinner to 0.02 at the tip. The blade-form characteristics are shown in figure 3.

The determination of the design-lift-coefficient curve in figure 3 was based on a desire to obtain the maximum camber in the blade sections without resorting to a concave thrust surface and without changing the thickness distribution from that of the 109622 design. Beginning at the 16.75-inch radial station, a camber was determined on the basis of an NACA 16-series airfoil (ref. 13) with the thrust surface coincident with the chord line at the 50-percent-chord station. When the section ordinates were calculated by using this camber, concavity of the thrust surface near the trailing edge resulted. Therefore, the camber was successively reduced until this concavity was eliminated. This procedure was repeated for several radial stations along the blade until there was no concavity of the thrust surface at any point along the blade radius. Since the slope of the mean line of the 16-series airfoil is zero at the 50-percent-chord station, the procedure used results in blade sections having the maximum camber without concavity in the thrust surface. It is apparent, however, that the resulting camber is not necessarily that which yields maximum lift-drag ratio of the blade section.

Having established the distribution of blade-section camber, or design lift coefficient, for the 109626 blades, the designers made a strip analysis of the propeller operating at 2,600 rpm and a forward Mach number of 0.95 at an altitude of 35,000 feet (the design condition). As a result of this analysis, the designers decided to use a pitch distribution slightly different from that of the 109622 design to obtain a slightly higher efficiency. The maximum difference in pitch distribution between the two blade designs amounts to about 2.5°. About half of this maximum difference in pitch distribution may be accounted for by the difference in angle for zero lift for cambered and symmetrical 16-series airfoils.

Strain gages were mounted on one of the blades of each propeller to monitor the vibratory bending and torsional stresses. The build-up of adhesive material surrounding the gages was kept to a minimum so as to change the blade contour as little as possible.

The natural torsional frequency of both the 109622 and 109626 blades was about 85 cycles per second, as determined from static bench tests of the two designs.

Wake Survey Rakes

Wake survey rakes were mounted as shown in figures 1 and 2(b) with the orifices of the probes 53 inches downstream of the propeller plane and 2 feet ahead of the rake strut leading edge. The rake strut was made up of 8-percent-thick circular-arc airfoils with a constant 2-foot chord. Further details of the survey rakes are not discussed here because the wake survey data are not presented in this paper.

TESTS

Most of the tests were made at constant values of forward Mach number, and a range of advance ratio was covered by varying the propeller rotational speed. One group of tests was made to cover a range of blade angles at low forward speeds by operating the propeller at a constant rotational speed of 1,600 rpm while varying the tunnel airspeed to obtain a range of advance ratio.

All the tests were made at fixed-blade angle settings. A few tests were made on the cambered propeller (design no. 109626) at low and negative blade angles while operating the tunnel at a constant Mach number of 0.13. Also, the thrust and power characteristics of the cambered propeller were obtained at several Mach numbers in the blade-angle range for propeller feathering conditions. In these tests, the propeller was rotated first in the right-hand, or normal, rotational direction and then in the left-hand, or reverse, rotational direction. This method was used to determine the feathering blade angle because the dynamometer bearings would be damaged by vibration if the tunnel were operated without rotating the propeller shaft.

The range of the tests was limited by either the maximum dynamometer rotational speed (2,200 rpm without overloading), the maximum available dynamometer power (6,000 horsepower without overloading) or propeller blade flutter. The rotational-speed limitation did not permit testing of either of the propellers at the design condition of operation (2,600 rpm, $J = 2.2$). During some of the tests at 1,600 rpm, the tunnel airspeed was lowered until flutter was indicated by the blade stresses but, because of the danger involved, little data were recorded. The range of blade angles covered at the various Mach numbers and at a constant rotational speed of 1,600 rpm is shown in table I for both the symmetrical propeller (design number 109622) and the cambered propeller (design number 109626). Figure numbers are also shown in table I to facilitate location of the data presented in this paper and also in reference 9.

CALIBRATIONS

Tunnel Airspeed

A calibration of the tunnel airstream was made with the dynamometer positioned in the test section with no propeller installed. The Mach number at which the tests were made was indicated by a Mach meter that was referenced to the static pressure in the tank (surrounding the test section) at a point about 13 feet upstream of the propeller location. The relationship between the Mach number at the propeller plane (without

propeller) and the Mach number determined from the tank static pressure was established in the same manner as in reference 11.

The longitudinal Mach number distribution as measured by static-pressure orifices near the center line of one of the tunnel-wall flats and along the dynamometer body is shown in figure 1. The data points are not shown in figure 1, but a comparison of the results obtained from the tunnel-wall orifices with those obtained from the dynamometer body orifices indicated a negligible radial Mach number difference across the propeller plane. As in reference 9, this difference amounted to about 0.005 at the propeller plane of rotation for the highest Mach number of the tests. An attempt was made to determine this radial Mach number gradient in more detail by installing a survey rake so that the probes would lie along the propeller plane. However, the presence of this rake, which extended from the propeller spinner to the tunnel wall, affected the velocity in the tunnel at the higher Mach numbers so that the results were not reliable. The curves in figure 1 represent faired values of the Mach number as determined from the static-pressure measurements along the tunnel wall and along the dynamometer body without the rake mounted in the propeller plane of rotation. Evidence that propeller operation has little significant effect on tunnel-wall pressures is presented in a later section of this paper. Figure 1 shows that the longitudinal Mach number distribution is relatively smooth up to a Mach number of about 0.8. Above this Mach number there is some interference arising at the triadic support plates and near the leading edge of the dynamometer support strut; however, the axial Mach number gradient is still small in the regions immediately ahead of and behind the propeller location. From the foregoing considerations, it has been concluded that the propeller data presented in the present paper do not include any detrimental effects that may arise from propeller operation in a nonuniform airstream and that the values of stream Mach number obtained from the tunnel-wall orifices are the values experienced by the operating propeller.

Dynamometer Calibration

Calibrations of the thrust and torque meters were made in a manner similar to that for the 2,000-horsepower propeller dynamometer described in reference 14. The thrust system was loaded to cover a 10,000-pound range, and the torque system was loaded to cover a 12,000-foot-pound range. The calibrations were straight lines when the indicated loads were plotted against the applied loads, and the slopes of the lines were determined by the method of least squares. The probable error in the thrust scale readings was ± 4.5 pounds and the probable error in the total torque readings was ± 1.7 foot-pounds.

REDUCTION OF DATA

Thrust

Propeller thrust as used in this paper is defined as the shaft tension produced by the aerodynamic forces acting on the propeller blades from the spinner to the blade tips.

The aerodynamic forces on the rotating spinner were determined by operating the tunnel and dynamometer over a range of airspeed and rotational speed with no propeller installed and recording the readings of the thrust scales. The difference in pressure between the upstream face and downstream face of the rotating spinner was recorded simultaneously with the thrust readings. A plot was made of the thrust scale readings against the spinner-juncture pressure differences and, within the accuracy of the measurements, the variation was linear for all combinations of spinner rotational speed and tunnel airspeed. With this relation determined, the spinner-juncture pressure difference was measured for test points with the propeller operating and the corresponding value of thrust was subtracted from the indicated scale readings as a tare force. Propeller thrust is, therefore, the indicated thrust of the propeller minus the spinner tare force created by the difference in spinner-juncture pressure between the upstream and downstream faces of the spinner, the spinner skin-friction drag being less than the accuracy of the thrust readings.

The variation of this spinner tare force with airstream Mach number is very interesting. (See fig. 4.) In the tests reported in reference 9 the Mach number did not exceed 0.96, and the spinner tare force was always positive (to be subtracted from the indicated thrust) and did not exceed 100 pounds. However, in the present tests, where the Mach number exceeded 1.0, the spinner tare force became negative (to be added to the indicated thrust) and reached values as high as 500 pounds when the Mach number was approximately 1.0. These large spinner tare forces represent an appreciable part of the measured thrust, and an effort was made to learn more about the aerodynamics causing the large spinner-juncture pressure differences. Attempts to obtain good shadowgraph pictures were unsuccessful, but during one of the propeller tests spinner-surface pressures were measured through the propeller plane of rotation and between the blades of the three-bladed propeller. The results of these measurements are shown in figure 5 and serve to verify the large pressure differences obtained on the upstream and downstream faces of the spinner at a Mach number of 1.0.

Torque

Torque tare readings were obtained simultaneously with the thrust tare readings during the tare runs. As in reference 9, the torque tare

forces varied very little with dynamometer rotational speed but varied linearly with tunnel airspeed. The maximum torque tare correction was 46 foot-pounds at a Mach number of 1.04. This variation of torque with tunnel airspeed was caused by a deflection of the dynamometer support strut under aerodynamic load and, to a lesser extent, inherent vibration of the dynamometer.

The torque tare forces for all rotational speeds were plotted against a function of tunnel airspeed and a faired line was drawn through the points, so that the small variation of torque with rotational speed was neglected. The net propeller torque was the indicated torque reading minus the torque tare as determined from the linear variation with tunnel airspeed.

Wind-Tunnel Wall Correction

The data shown in reference 9 indicate that no wall correction should be necessary for tests of three-bladed 10-foot-diameter propellers in the Langley 16-foot transonic tunnel over the range of Mach numbers and thrust coefficients presented. In order to substantiate these data and to check the validity at higher test Mach numbers, some measurements of the tunnel-wall static pressures were made with the propeller operating. Figure 6 shows the results of these measurements as the variation of Mach number with tunnel station for conditions of low propeller thrust and high propeller thrust at nominal Mach numbers of about 0.8 and 1.04. The variation of Mach number with tunnel station for the condition of no propeller operating is also shown in figure 6 for comparison. At the subsonic speed, the Mach number with the propeller operating was within one percent of the values obtained without the propeller, and the tunnel longitudinal Mach number gradient with the propeller operating was essentially the same as that obtained without the propeller. At the supersonic speed, however, propeller operation caused a small Mach number gradient through the propeller plane of rotation. For the condition of high propeller thrust where the propeller efficiency is near its maximum value, the effect of propeller operation on the tunnel Mach number at the propeller plane is small, and the difference is believed to be within the accuracy of the measurements. Since propeller operation had no significant effect on the tunnel wall pressures at subsonic speeds and since the effect at supersonic speeds and high propeller thrust was small and perhaps within the accuracy of the measurements, no wind-tunnel wall correction has been applied to the data presented in this paper.

Accuracy

For conditions near maximum efficiency, it is estimated that the propeller data presented in this paper are accurate to one percent based

on the static calibrations. The estimated error in Mach number is ±0.01 and the maximum propeller rotational speed error is ±1/4 rpm.

RESULTS AND DISCUSSION

Presentation of Basic Results

The aerodynamic data obtained in tests of the Curtiss-Wright cambered propeller (design no. 109626) are presented in figures 7 to 17 as faired curves of thrust coefficient, power coefficient, propeller efficiency, airstream Mach number, and helical tip Mach number plotted against propeller advance ratio. The data test points are included on the plots of thrust and power coefficients. Figure 18 presents the data obtained in tests of the Curtiss-Wright symmetrical propeller (design no. 109622) at Mach numbers of 1.01, 1.02, and 1.04. These data were obtained to extend the Mach number range of the tests presented in reference 9, which included data for Mach numbers to only 0.96.

Effect of Blade-Section Camber at Subcritical Speeds

It was not possible to test either the cambered or the symmetrical propeller at the design operating conditions since the maximum rotational speed of the dynamometer did not permit operation at an advance ratio of 2.2 at a forward Mach number of 0.95. In order to obtain the propeller characteristics in the lower range of advance ratio a series of tests were made at a constant rotational speed of 1,600 rpm, and in these tests the forward Mach number did not exceed about 0.6. The results from these tests of the two propellers (109622 propeller tests from ref. 9) are compared in figure 19 to show the effect of blade-section camber on envelope efficiency and on the thrust and power coefficients for maximum efficiency. The cambered propeller was from 6 to 3.5 percent more efficient than the symmetrical propeller over the range of advance ratio of the tests (J = 1.0 to 2.4). This shows that the cambered propeller operates more efficiently at off-design conditions than the symmetrical propeller. Both the thrust and power coefficients for maximum efficiency increased more rapidly with advance ratio for the cambered propeller than for the symmetrical propeller. At an advance ratio of 2.2 the thrust coefficient was 25 percent greater for the cambered propeller than for the symmetrical propeller, whereas the power coefficient was only 20 percent greater. Only at advance ratios less than 1.3 did the cambered propeller produce less thrust (at maximum efficiency) than the symmetrical propeller, and at these low advance ratios the cambered propeller absorbed considerably less power.

Since airplane propellers operate over a range of advance ratio at constant rotational speed and torque and since blade-section camber affects the power-absorption qualities of a propeller, the data for the two propellers have been compared at two values of constant power coefficient for a rotational speed of 1,600 rpm. This comparison is shown in figure 20 for power coefficients of 0.12 and 0.18. Figure 20 shows that for advance ratios up to 2.4, the propeller with cambered blade sections produces more thrust than the propeller with symmetrical blade sections when the two propellers are absorbing the same power. This is particularly true at the lower values of advance ratio corresponding to take-off and climb conditions of operation. For example, at an advance ratio of 1.0, the cambered propeller was 7 percent more efficient than the symmetrical propeller when the power coefficient was constant at either 0.12 or 0.18.

An explanation for the higher efficiency at subcritical speeds of the propeller with cambered blade sections may be seen in figure 21 which shows the effect of design lift coefficient, or camber, on the lift-drag ratio of 4-percent-thick 16-series airfoil sections at a Mach number of 0.7. The curves in figure 21 were taken from reference 15, and they show that the lift-drag ratio increases rapidly with increasing design lift coefficient to some maximum value which depends upon the operating lift coefficient. For an operating lift coefficient of 0.4 the lift-drag ratio increases from about 35 to 84 when the airfoil is changed from a symmetrical one ($c_{l_d} = 0$) to one having a design lift coefficient of 0.3. The curves in figure 21 also show that the increase in lift-drag ratio with design lift coefficient is greater when the airfoil is operating at a lift coefficient of 0.4 than when operating at a lift coefficient of 0.2. This serves to explain the higher efficiency of the cambered propeller at the lower values of advance ratio corresponding to the high thrust required for take-off and climb conditions of operation, and, in general, accounts for the higher efficiency of the cambered propeller at off-design conditions of operation. This characteristic of the cambered propeller is expected because reference 15 shows that the operating lift coefficient for maximum lift-drag ratio is higher at a given blade-section Mach number for the cambered 16-series airfoils than for the symmetrical airfoils.

Effect of Blade-Section Camber on Propeller Characteristics at Transonic Speeds

The variation of envelope efficiency with advance ratio for the Curtiss-Wright cambered propeller (design no. 109626) is shown in figure 22 for constant values of Mach number from 0.60 to 1.04. As pointed out in reference 9 for the symmetrical propeller, a notable feature of

the envelope efficiency curves for these supersonic propellers is the small loss in efficiency at the higher values of advance ratio. This characteristic is more pronounced for the cambered propeller than for the symmetrical propeller, as shown in figure 23, wherein the envelope efficiency of the two propellers is compared at Mach numbers of 0.80, 0.89, and 0.96. Since both propellers were designed for an advance ratio of 2.2, the envelope efficiency would be expected to reach a maximum value at this advance ratio. However, the envelope efficiency of the cambered propeller decreases very slowly with an increase in advance ratio, so that the efficiency is quite high at an advance ratio of twice the design value. The curves in figure 23 show that the cambered propeller (109626) will operate efficiently over a wide range of advance ratio.

Although the design value of advance ratio (2.2) could not be reached at the higher Mach numbers, a comparison of the two propellers has been made at an advance ratio of 3.6 to show the effect of blade-section camber on propeller characteristics up to a Mach number of 1.04. An advance ratio of 3.6 was chosen because in the supersonic tests of the symmetrical propeller at a blade angle of 60° the efficiency was about a maximum at this advance ratio (fig. 18). Figure 24 shows this comparison of the envelope efficiency and the thrust and power coefficients for maximum efficiency of the two propellers over a Mach number range from 0.6 to 1.04. Over this speed range the cambered propeller was from 2 to 4.5 percent more efficient than the symmetrical propeller. Both propellers began showing the characteristic loss in efficiency caused by compressibility effects at a Mach number of about 0.75, the loss amounting to 22 percent for either of the propellers at the highest Mach number of the tests. At a Mach number of 1.0, the difference in efficiency between the two propellers was small. At the highest Mach number of the tests (1.04), the efficiency of the cambered propeller was about 67 percent compared to about 62.5 percent for the symmetrical propeller.

The thrust and power coefficients for maximum efficiency were quite different for the two propellers over the Mach number range of the tests. Figure 24 shows that the thrust and power for the symmetrical propeller began a fairly steady increase at a Mach number of 0.75 and continued to increase to the highest Mach number of the tests. The thrust and power for the cambered propeller also began to increase at a Mach number of 0.75, but the increase was more rapid, and at a Mach number of about 0.95 the thrust and power reached a maximum and began to decrease with an increase in Mach number. At a Mach number of 0.95 the power coefficient for maximum efficiency was 53 percent greater for the cambered propeller, and the thrust coefficient for maximum efficiency was about 60 percent greater for the cambered propeller than for the symmetrical propeller.

Design Considerations

The relatively high efficiency of the cambered propeller (design no. 109626) shown in figures 22, 23, and 24 at an advance ratio of 3.6 suggests that the blade sections were operating at or near their maximum lift-drag ratio at this condition of operation. A brief analysis was made, therefore, to determine the propeller operating conditions for which the cambered blade sections of the 109626 propeller would be operating at their maximum lift-drag ratio. Reference 15 presents the blade-section design lift coefficient (NACA 16-series airfoils) for maximum lift-drag ratio plotted against thickness ratio for constant values of Mach number. Although these curves do not extend to thickness ratios of less than 4 percent, an extrapolation indicates that for Mach numbers greater than 0.95 the design lift coefficient for maximum lift-drag ratio is affected very little by thickness ratios of less than 5 percent. Since the blade sections of the cambered propeller are less than 5 percent thick from about the 0.3 radius to the propeller tip, a plot was made to show the variation with blade-section Mach number of the design lift coefficient for maximum lift-drag ratio for 16-series sections less than 5 percent thick. This variation is shown in figure 25 by the curve of long dashes and indicates that for a blade-section Mach number of 0.95 the design lift coefficient should be 0.38. For a blade-section Mach number of 1.5, the design lift coefficient should be reduced to zero. Obviously, the blade sections of the symmetrical propeller (design no. 109622) should have had some camber unless all the blade sections were to operate at Mach numbers greater than 1.5.

For comparison with the optimum variation of camber shown in figure 25, the design lift coefficients of the blade sections of the cambered propeller (design no. 109626) were plotted against the blade-section Mach numbers for three operating conditions. At the design condition of operation, an advance ratio of 2.2 and a Mach number of 0.95, the blade sections of the cambered propeller operate at Mach numbers far in excess of those necessary for maximum lift-drag ratio. At a higher advance ratio, 3.6, and a Mach number of 1.0, the blade sections of the cambered propeller operate at section speeds nearer to those for maximum lift-drag ratio. At a Mach number of 0.95 and an advance ratio of 3.6 the section speeds over the most effective part of the blade radius are very near to those required for maximum lift-drag ratio. The curves in figure 25 show, therefore, that the blade sections of the cambered propeller (design no. 109626) are overcambered for the design condition of operation, and that the propeller as built should operate at the design Mach number (0.95) more efficiently at an advance ratio higher than the design value. At this higher advance ratio (3.6), the curves in figure 25 also show that the blade sections of the cambered propeller should operate more efficiently than the blade sections of the symmetrical propeller.

It should be pointed out that the curve in figure 25 showing the design lift coefficient for maximum lift-drag ratio was determined from considerations of two-dimensional airfoil characteristics only; and, as mentioned in the introduction to this paper, there is evidence that propeller blade sections have aerodynamic characteristics that are different from those of two-dimensional airfoils. Specifically, pressure distributions obtained in recent years on the blade sections of operating propellers show that at zero angle of attack of the chord line the value of lift coefficient is appreciably less than the design value for which the section is cambered. There is evidently an induced camber, or an effective reduction in camber, of a section when it operates as part of a three-dimensional airfoil producing lift and an induced angle of attack. This three-dimensional characteristic is discussed in reference 16, which shows that the effective camber in the middle and outer radii of a propeller blade is smaller than the geometrical camber. For this reason the curve in figure 25 showing the design lift coefficient for maximum lift-drag ratio should be shifted perhaps to slightly higher values of design lift coefficient, particularly for the blade sections along the middle and outer radii. However, the curve (long dashes) in figure 25 is considered adequate for the purpose of the brief analysis presented in this paper.

Comparison of Experimental and Calculated Values of Propeller Efficiency

Strip theory calculations have been made for the efficiency of the cambered propeller by using the method described in reference 14, and the results of these calculations are shown on figures 7(c) and 22. The calculated values of efficiency are within 1.5 percent of the measured values. This agreement may be considered excellent, but because it was necessary to use extensive extrapolations of existing airfoil data, the agreement may have been fortuitous. For operating conditions where the blade-section speeds were in the transonic region, both lift and drag were rapidly changing, making both interpolation and extrapolation of airfoil characteristics questionable. For such operating conditions, the agreement of calculated with experimental values of thrust and power coefficients ranged from fair to poor. However, it is believed that propeller efficiency may be calculated with reasonable accuracy by using subsonic strip theory when the two-dimensional airfoil characteristics are known.

Since it was not possible to test the cambered propeller at the design operating condition, a calculation of propeller efficiency was made for an advance ratio of 2.2 and a Mach number of 0.95. This calculated efficiency for the cambered propeller was about 70 percent, which compares with a calculated value of about 73 percent for the symmetrical

propeller reported in reference 9. The fact that the calculated value of efficiency is less for the cambered propeller than for the symmetrical propeller at the design operating condition is not surprising when the analysis presented in figure 25 is considered. At the design operating condition the blade-section speeds are such that very little camber, or none, is required for maximum lift-drag ratio of the most effective sections along the blade radius. For the cambered propeller (design no. 109626) the blade-section design lift coefficient is too high for maximum lift-drag ratio at the section speeds attained at the design operating condition.

Effect of Strain Gages on Propeller Efficiency

In all tests of the cambered propeller (design no. 109626) strain gages were cemented to the surface of one of the propeller blades. However, in the tests of the symmetrical propeller reported in reference 9, the strain gages were removed and some tests repeated to obtain the effect of the gages on propeller efficiency. These tests indicated that the strain gages had no effect on propeller efficiency at Mach numbers up to 0.88. At a higher Mach number (0.96), the effect of the strain gages was to reduce propeller efficiency by about 2 percent. In the present tests the bonding material for the gages was built up in a manner similar to that used on the symmetrical propeller for the tests reported in reference 9, so that the strain-gage installations for the two propellers were very nearly the same. It seems reasonable to assume, therefore, that the effect of the strain gages on propeller efficiency was very nearly the same in the present tests as for the tests reported in reference 9.

Stall-Flutter Data

Although stall flutter was encountered on several occasions during the tests of the cambered propeller (design no. 109626), very little data were obtained on these occasions because of the hazardous nature of operation with sustained flutter of the propeller blades. However, during the constant rotational speed tests at 1,600 rpm some data were recorded when flutter was detected both audibly and by the strain gages. The values of advance ratio at which flutter occurred have been indicated on the curves of thrust and power coefficient shown in figure 7. On other occasions when flutter was detected the propeller rotational speed was reduced before any data could be obtained. However, based on the experience of the dynamometer operators and the meager data obtained, a flutter boundary has been sketched on figure 7 which indicates that stall flutter characteristics may be improved by the use of cambered blade sections. The flutter boundaries presented in figure 7(a) show that thrust coefficients for the cambered propeller were about 20 percent higher than those for the symmetrical propeller when stall flutter was encountered.

Propeller Characteristics at Low and Negative Blade Angles

Tests at low and negative blade angles were made at a Mach number of 0.13 for the cambered propeller (design no. 109626) only, and the results are shown in figure 26. Propeller stall flutter or heavy vibration of the dynamometer was encountered in most of these tests and the data obtained were limited. A solid line is shown connecting the points where sustained stall flutter (torsional stress over ±9,000 psi) occurred at blade angles of -13.6° and -8.6°. At blade angles of -3.6° and 1.4°, the usual type of stall flutter with large responses in torsion was not observed, but heavy side and vertical accelerations of the dynamometer limited the tests. The exact cause of these vibrations is unknown but it may be possible that these vibrations were caused by wake flutter. Intermittent stall flutter with low torsional stresses (±1,000 to ±3,000 psi) was encountered at a blade angle of 6.4° near an advance ratio of 1.0; however, the flutter disappeared when the advance ratio was decreased further. It is believed that the propeller was operating in stall flutter at a blade angle of 6.4° near an advance ratio of 1.0, and that stall flutter did not occur at blade angles of 11.4° and 16.4° because the propeller was operated below an advance ratio of 1.0 for the entire test. It is not possible to establish the flutter boundary from the present data; therefore, great care must be taken to avoid sustained stall flutter at these low and negative blade angles.

With the foregoing flutter considerations in mind, the thrust coefficient curves in figure 26 have been extrapolated to advance ratios around unity, and a crossplot has been made in figure 27 to show the variation of negative thrust coefficient with blade angle at several constant values of advance ratio from 0.8 to 2.0. The curves in figure 27 show the increase in negative thrust coefficient as the blade angle at the 0.75 radius changes from low positive values to negative values. In order to obtain a better idea of the braking capabilities of the cambered propeller, the curves in figure 27 were used to calculate the variation of negative thrust in pounds with velocity in miles per hour for several blade angles at a constant rotational speed of 1,200 rpm. The results of these calculations are presented in figure 28. For a blade angle of -8° at the 0.75 radius, the negative thrust changes from 8,180 pounds at a velocity of 260 miles per hour to 2,400 pounds when the velocity is reduced to 110 miles per hour; this indicates the effectiveness of the propeller as a brake.

Feathering Conditions for the Cambered Propeller

Characteristics of the cambered propeller (design number 109626) are shown in figure 29 at blade angles near the feathering angle for Mach numbers of 0.3, 0.5, and 0.7. Note that instead of the usual coefficients, values of T/qD^2 and Q/qD^3 have been plotted against nD/V for convenience in determining the feathering blade angle. There is very

little difference in the data at the various subsonic Mach numbers, and a single curve has been drawn between the data obtained at positive and negative values of nD/V. The sign convention used in calculating values of nD/V is that rotational speeds are negative when in the left-hand direction of rotation and positive when in the right-hand direction of rotation. The faired values of the thrust and torque coefficients at zero rotational speed have been plotted against blade angle in figure 30 to determine the feathering blade angle and to obtain a value of negative thrust or drag of the propeller when in the feathered condition. Figure 30 shows that the cambered propeller (design number 109626) will be feathered when the blade angle at the 0.75 radius is 85.4°. The negative thrust, or drag, of the propeller in the feathered condition will be $0.007qD^2$, which amounts to about 153 pounds at 300 miles per hour (sea-level density).

CONCLUSIONS

Tests of two three-bladed supersonic propellers have been made on the 6,000-horsepower propeller dynamometer in the Langley 16-foot transonic tunnel over a range of blade angles at forward Mach numbers up to 1.04. One of the propellers, Curtiss-Wright design number 109622, had symmetrical NACA 16-series airfoil sections. The other propeller, Curtiss-Wright design number 109626, was similar except for the incorporation of blade-section camber and a slight difference in pitch distribution. Both propellers were designed for an advance ratio of 2.2 and a Mach number of 0.95 at an altitude of 35,000 feet. The results of the investigation indicate the following conclusions:

1. The cambered propeller was more efficient at off-design conditions of operation and could operate efficiently over a wider range of advance ratio. However, calculations indicated that the symmetrical propeller had a slightly higher efficiency at the design condition of operation.

2. A brief analysis indicates that the blade sections of the cambered propeller were overcambered for the design condition of operation and that the propeller as built should operate at the design Mach number (0.95) more efficiently at an advance ratio higher than the design value.

3. Comparison of the two propellers at an advance ratio of 3.6 showed:

(a) The maximum efficiency was greater for the cambered propeller than for the symmetrical propeller over a Mach number range from 0.6 to 1.04.

(b) The loss in maximum efficiency due to compressibility effects began at a Mach number of about 0.75 and amounted to 22 percent for either propeller at a Mach number of 1.04.

(c) At a Mach number of 0.95 the thrust and power coefficients for maximum efficiency were 60 and 53 percent greater, respectively, for the cambered propeller than for the symmetrical propeller.

4. Comparison of the two propellers at a constant rotational speed of 1,600 rpm and Mach numbers less than 0.6 showed:

(a) The maximum efficiency was from 6 to 3.5 percent greater for the cambered propeller than for the symmetrical propeller over a range of advance ratio from 1.0 to 2.4.

(b) At an advance ratio of 2.2 the thrust coefficient for maximum efficiency was 25 percent greater for the cambered propeller than for the symmetrical propeller, while the power coefficient was only 20 percent greater.

(c) At an advance ratio of 1.0, corresponding to a climb condition of operation, the cambered propeller was 7 percent more efficient than the symmetrical propeller when the power coefficient was constant at either 0.12 or 0.18.

(d) Stall flutter occurs at thrust coefficients which are greater for the cambered propeller than for the symmetrical propeller.

5. The negative thrust characteristics of the cambered propeller make it very effective when used as a brake, but care must be taken to avoid propeller flutter at low and negative blade angles.

6. The feathering blade angle of the cambered propeller is 85.4°, measured at the 0.75 radius, and the drag of this propeller in the feathered condition amounts to 153 pounds at 300 miles per hour (sea-level density).

Langley Aeronautical Laboratory,
National Advisory Committee for Aeronautics,
Langley Field, Va., May 2, 1956.

REFERENCES

1. Maynard, Julian D., and Murphy, Maurice P.: Pressure Distributions on the Blade Sections of the NACA 10-(3)(066)-033 Propeller Under Operating Conditions. NACA RM L9L12, 1950.

2. Gray, W. H., and Hunt, Robert M.: Pressure Distributions on the Blade Sections of the NACA 10-(3)(049)-033 Propeller Under Operating Conditions. NACA RM L9L23, 1950.

3. Johnson, Peter J.: Pressure Distributions on the Blade Sections of the NACA 10-(3)(090)-03 Propeller Under Operating Conditions. NACA RM L50A26, 1950.

4. Evans, Albert J., and Luchuk, Wallace: Pressure Distributions on the Blade Sections of the NACA 10-(5)(066)-03 Propeller Under Operating Conditions. NACA RM L50B21, 1950.

5. Steinberg, Seymour, and Milling, Robert W.: Pressure Distributions on the Blade Sections of the NACA 10-(0)(066)-03 Propeller Under Operating Conditions. NACA RM L50C03, 1950.

6. Evans, Albert J., and Liner, George: Preliminary Investigation To Determine Propeller Section Characteristics by Measuring the Pressure Distribution on an NACA 10-(3)(08)-03 Propeller Under Operating Conditions. NACA RM L8E11, 1948.

7. Igoe, William B. and Davidson, Robert E.: Propeller Induced Angles of Attack and Section Angles of Attack for the NACA 10-(3)(066)-03, 10-(3)(049)-03, 10-(3)(090)-03, 10-(5)(066)-03 and 10-(0)(066)-03 Propellers. NACA RM L51L06, 1952.

8. Maynard, Julian D., and Salters, Leland B., Jr.: Aerodynamic Characteristics at High Speeds of Related Full-Scale Propellers Having Different Blade-Section Cambers. NACA RM L8E06, 1948.

9. Evans, Albert J., and Liner, George: A Wind-Tunnel Investigation of the Aerodynamic Characteristics of a Full-Scale Supersonic-Type Three-Blade Propeller at Mach Numbers to 0.96. NACA RM L53F01, 1953.

10. Allis, Arthur E., and Swihart, John M.: The Effect of Blade-Section Camber on the Stall-Flutter Characteristics of Three NACA Propellers at Zero Advance. NACA RM L53B17, 1953.

11. Ward, Vernon G., Whitcomb, Charles F., and Pearson, Merwin D.: Air-Flow and Power Characteristics of the Langley 16-Foot Transonic Tunnel With Slotted Test Section. NACA RM L52E01, 1952.

12. Wood, John H., and Swihart, John M.: The Effect of Blade-Section Camber on the Static Characteristics of Three NACA Propellers. NACA RM L51L28, 1952.

13. Stack, John: Tests of Airfoils Designed to Delay the Compressibility Burble. NACA Rep. 763. 1943. (Supersedes NACA TN 976.)

14. Corson, Blake W., Jr., and Maynard, Julian D.: The Langley 2,000-Horsepower Propeller Dynamometer and Tests at High Speed of an NACA 10-(3)(08)-03 Two-Blade Propeller. NACA TN 2859, 1952. (Supersedes NACA RM L7L29.)

15. Anon.: Propeller Performance Analysis. Aerodynamic Characteristics. NACA 16 Series Airfoils. Rep. No. C-2000, Curtiss-Wright Corp., Propeller Div. (Caldwell, N. J.), Dec. 2, 1948.

16. Strassl, H.: Camber Corrections for Screw Profiles. Reps. and Translations No. 52, British M.A.P. Völkenrode, Apr. 1, 1946.

TABLE I.- RANGE OF BLADE ANGLES COVERED IN TESTS OF TWO CURTISS-WRIGHT SUPERSONIC PROPELLERS (DESIGN NOS. 109622 AND 109626)

Figure	Mach number	Rotational speed, rpm	Blade angle at 0.75 radius, 0.75R, deg
Cambered propeller (design no. 109626)			
26	0.13	Varied	-13.6, -8.6, -3.6, 1.4, 6.4, 11.4, and 16.4
29	0.30	Varied	71.4, 81.4, and 91.4
29	0.50	Varied	71.4, 81.4, and 91.4
29	0.70	Varied	71.4, 81.4, and 91.4
7	Varied	1,600	21.6, 26.6, 31.6, 36.6, 41.6, and 46.8
8	0.60	Varied	46.8, 52.2, 55.6, 61.8, and 64.4
9	0.70	Varied	46.8, 52.2, 56.1, 61.6, and 64.4
10	0.74	Varied	52.2, 55.6, and 61.6
11	0.80	Varied	55.6, 61.6, and 64.4
12	0.84	Varied	55.6, 61.6, and 64.4
13	0.89	Varied	55.6, 61.8, and 64.4
14	0.96	Varied	61.6 and 64.4
15	1.00	Varied	61.6 and 64.4
16	1.02	Varied	56.1 and 61.6
17	1.04	Varied	61.6 and 64.4
Symmetrical propeller (design no. 109622)			
[a]6	Varied	1,600	20.2, 25.2, 30.2, 35.2, 40.2, 45.4, and 50.8
[a]7	0.60	Varied	50.8, 54.7, and 60.2
[a]8	0.70	Varied	45.4, 50.8, 54.7, and 60.2
[a]9	0.74	Varied	50.8, 54.7, and 60.2
[a]10	0.80	Varied	50.8, 54.7, and 60.2
[a]11	0.84	Varied	50.8 and 54.7
[a]12	0.89	Varied	50.8, 54.7, and 60.2
[a]13	0.93	Varied	54.7 and 60.2
[a]14	0.96	Varied	54.7 and 60.2
18	1.01	Varied	60.0
18	1.02	Varied	60.0
18	1.04	Varied	60.0

[a]These figure numbers refer to figures in reference 9.

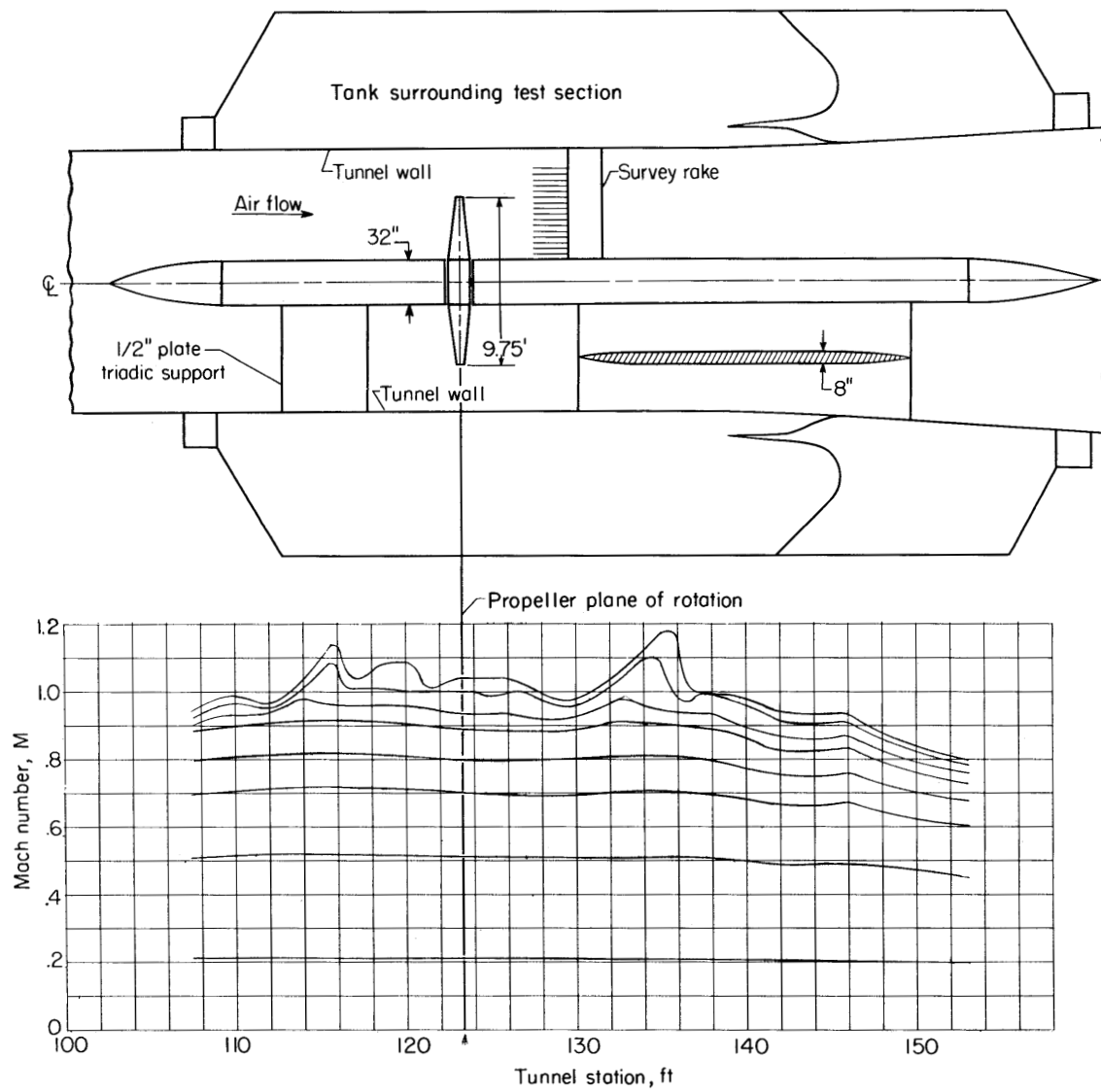

Figure 1.- Mach number distribution in the Langley 16-foot transonic tunnel test section with dynamometer installed (without propeller).

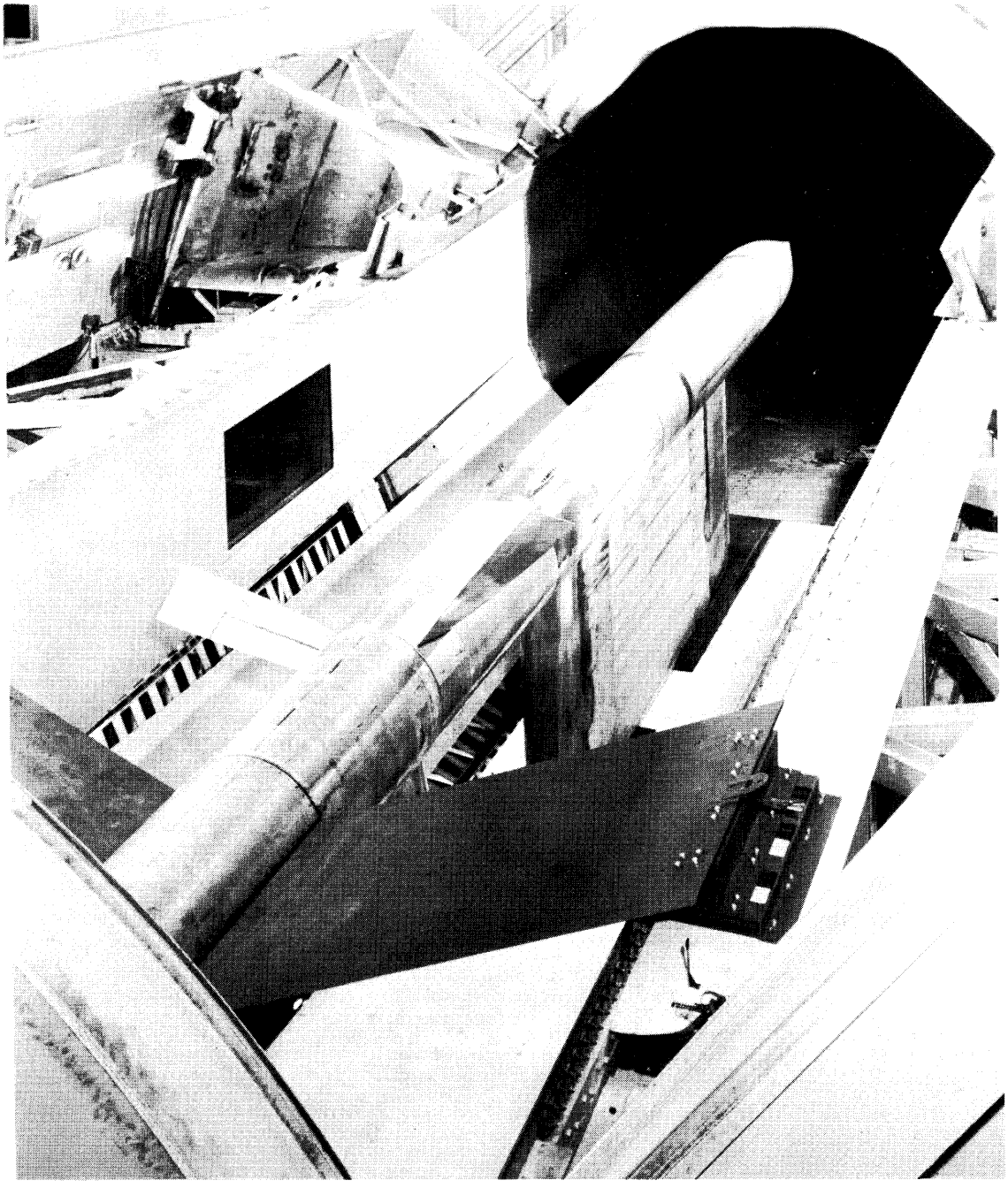

(a) Upper portion of test section raised. L-86110

Figure 2.- The 6,000-horsepower propeller dynamometer mounted in the Langley 16-foot transonic tunnel (view looking downstream).

L-86111

(b) Upper portion of test section in place. Wake survey rakes may be seen in this view.

Figure 2.- Concluded.

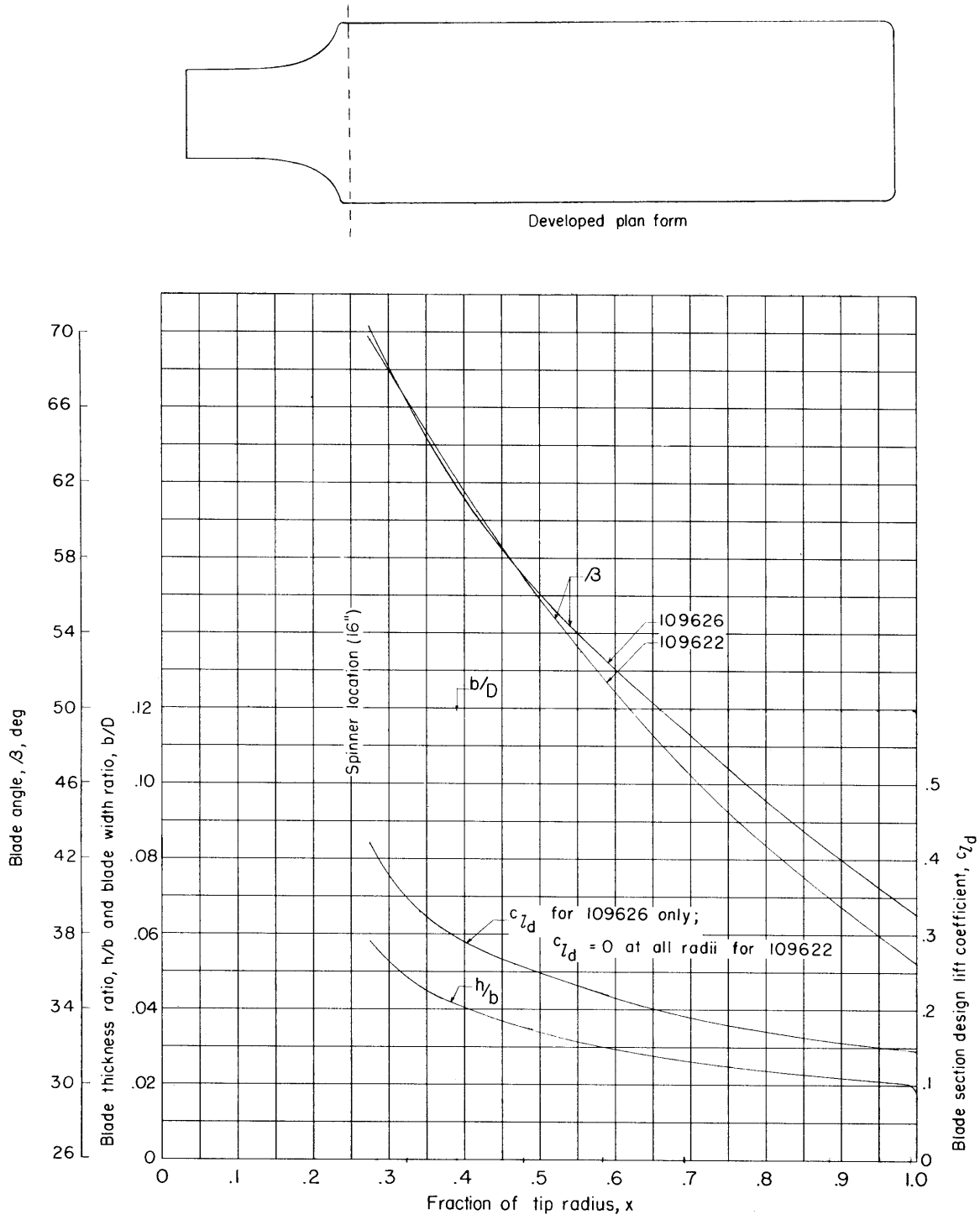

Figure 3.- Blade-form characteristics of two Curtiss-Wright supersonic propellers (design nos. 109622 and 109626).

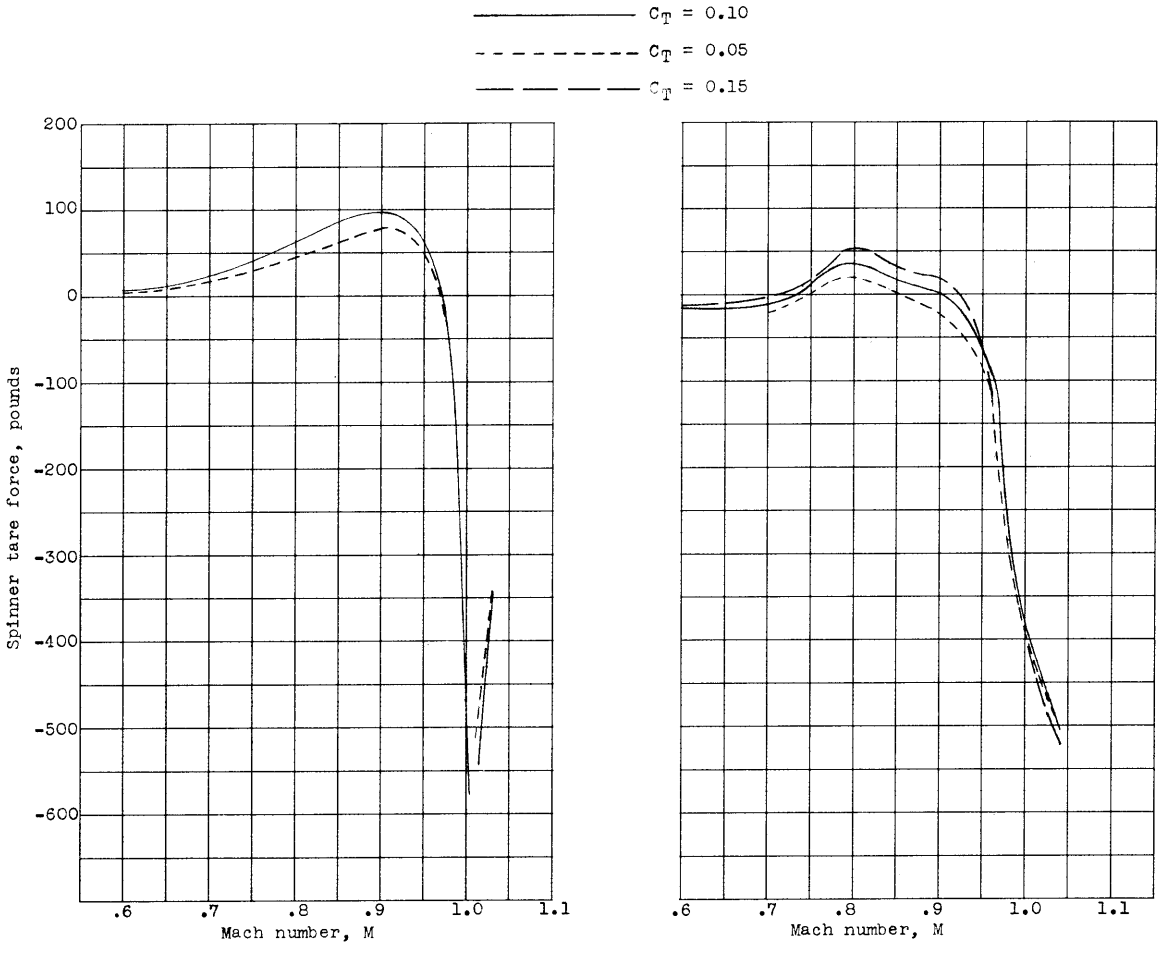

(a) Symmetrical propeller (design no. 109622); $\beta_{0.75R} = 60.0^{\circ}$.

(b) Cambered propeller (design no. 109626); $\beta_{0.75R} = 61.6^{\circ}$.

Figure 4.- Variation of the spinner tare force with Mach number for constant values of thrust coefficient.

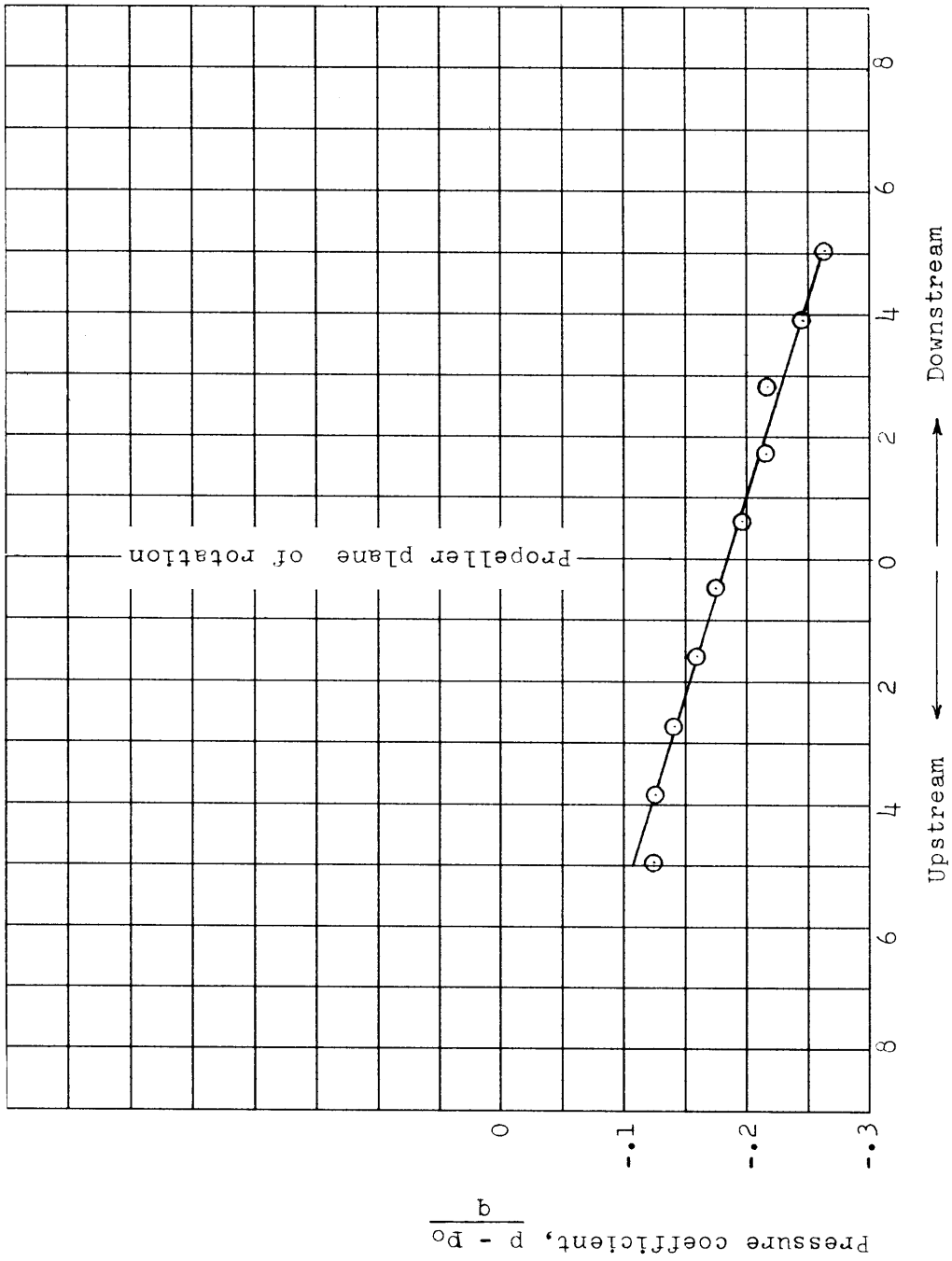

Figure 5.- Variation of spinner surface pressures through the propeller plane of rotation at a Mach number of 1.0. $J = 3.69$; $\beta_{0.75R} = 61.8^{\circ}$.

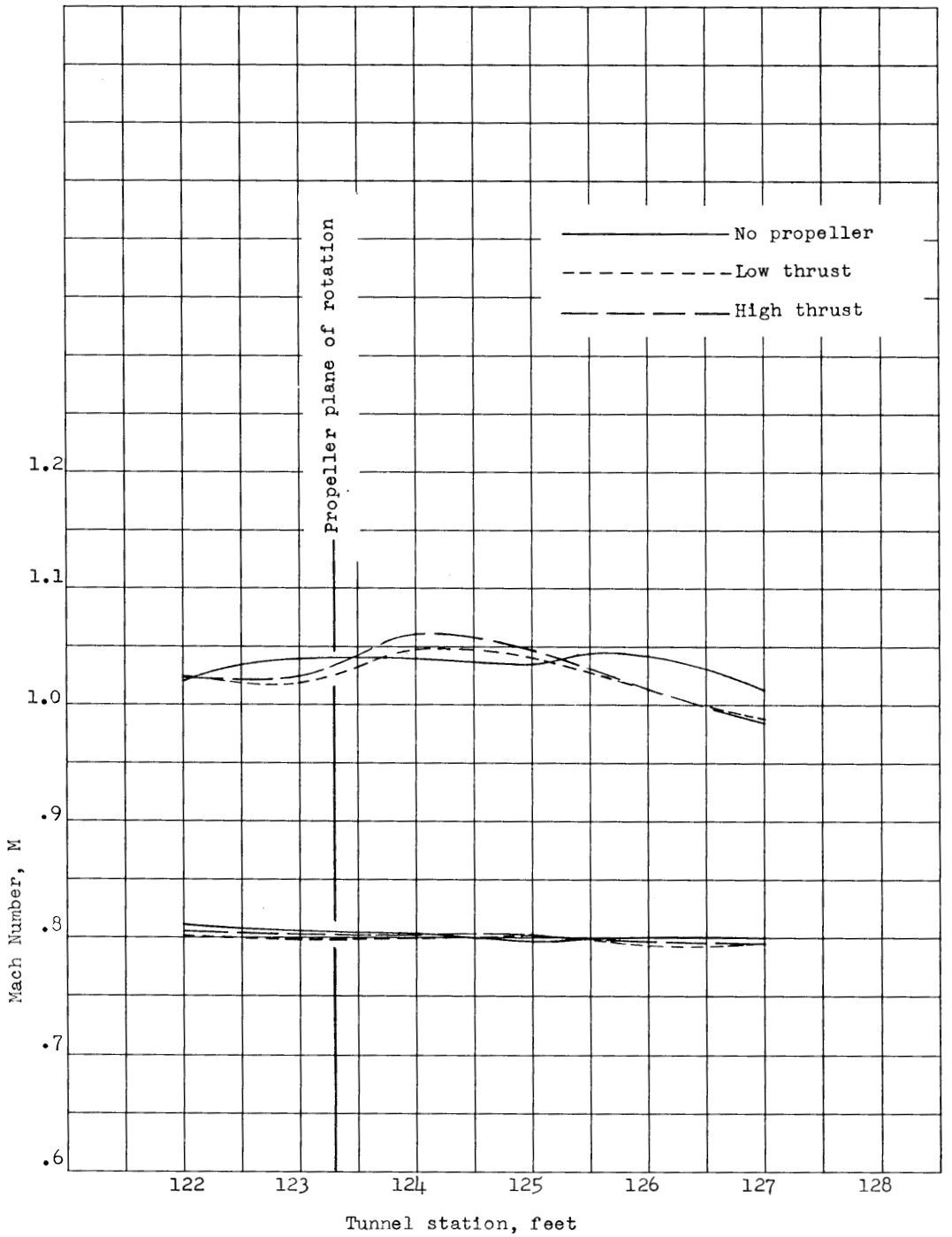

Figure 6.- Effect of propeller operation on the Mach number distribution in the vicinity of the propeller as determined by tunnel-wall measurements.

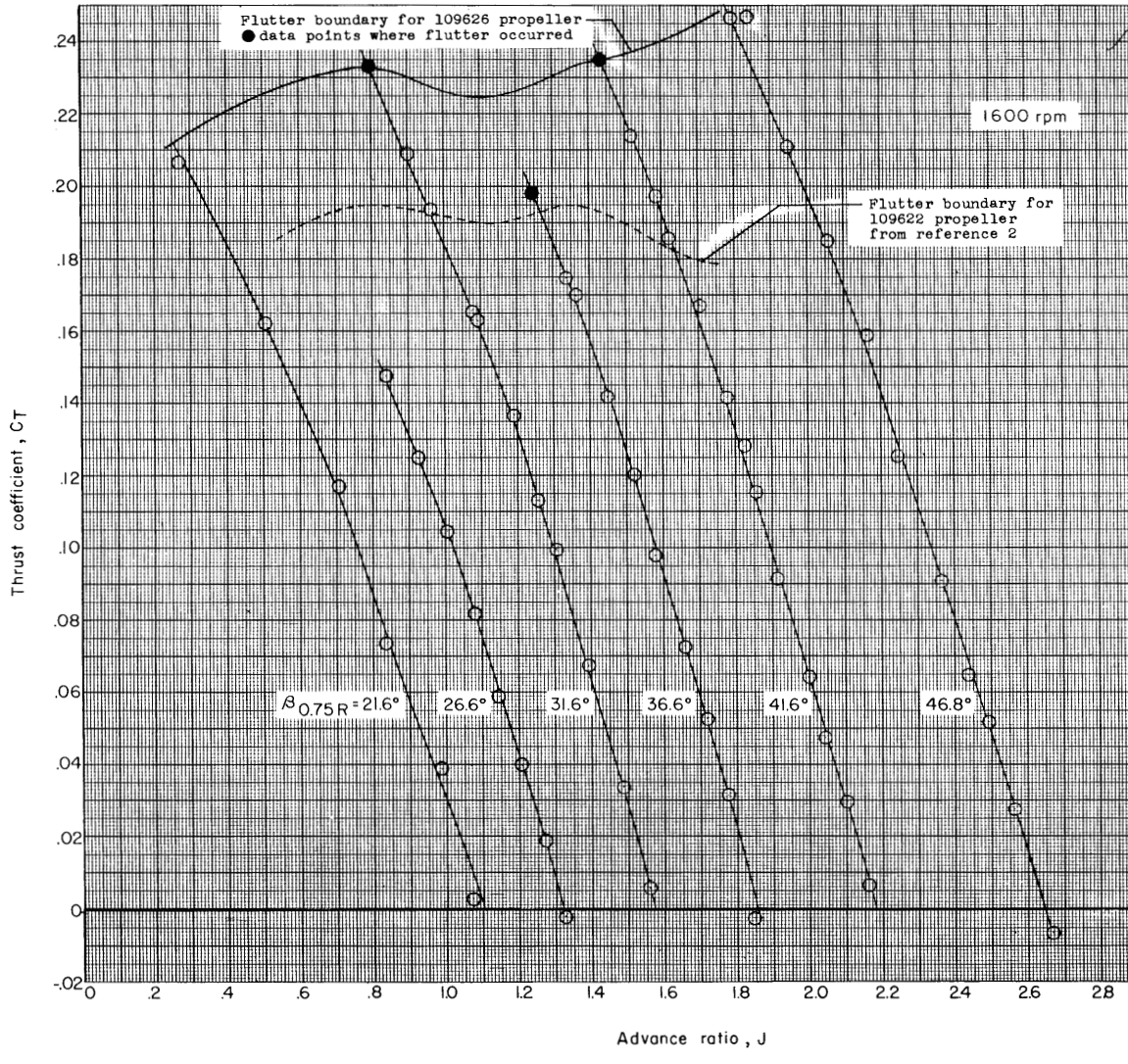

(a) Thrust coefficient.

Figure 7.- Characteristics of the Curtiss-Wright cambered propeller (design no. 109626). Rotational speed, 1,600 rpm; M < 0.64.

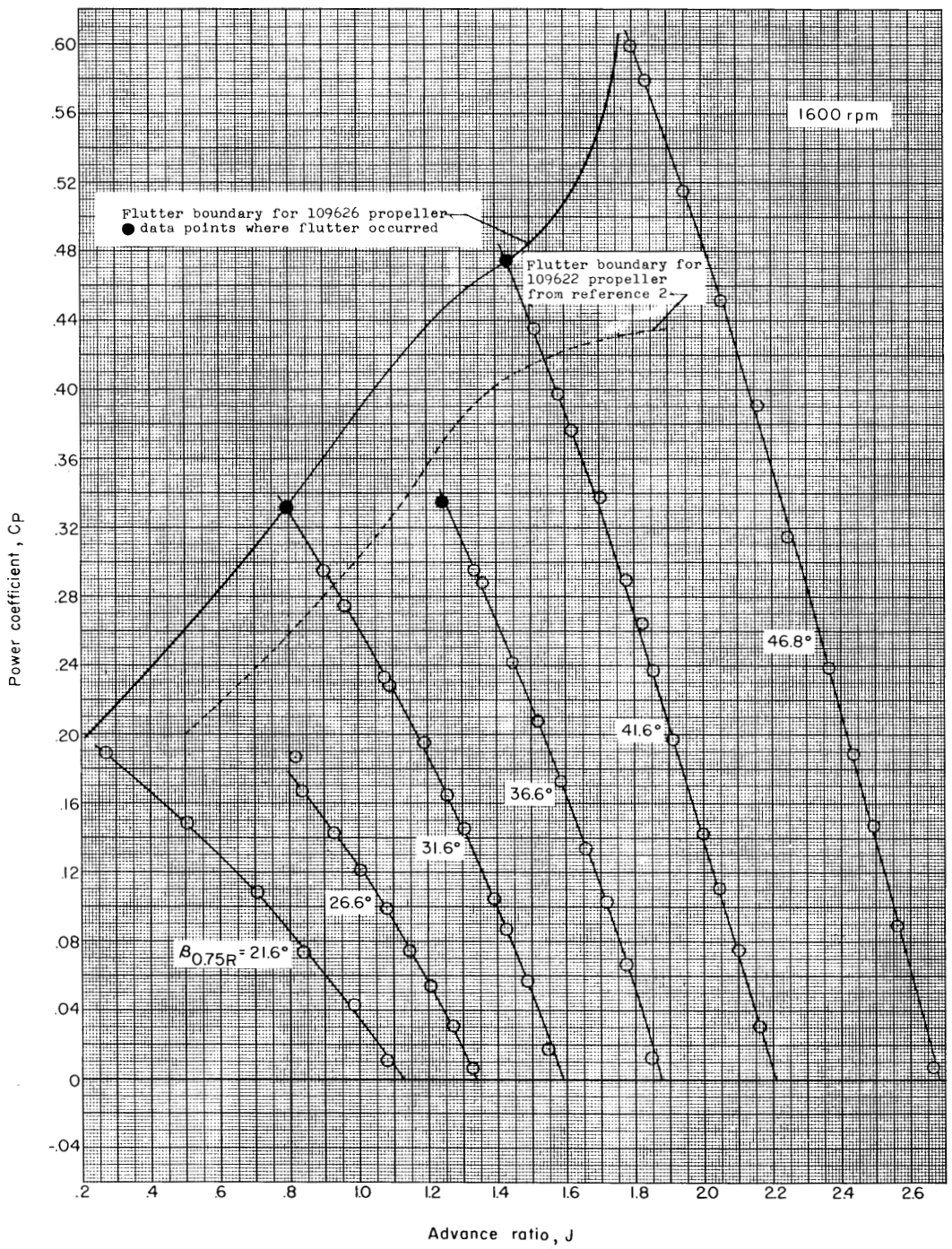

(b) Power coefficient.

Figure 7.- Continued.

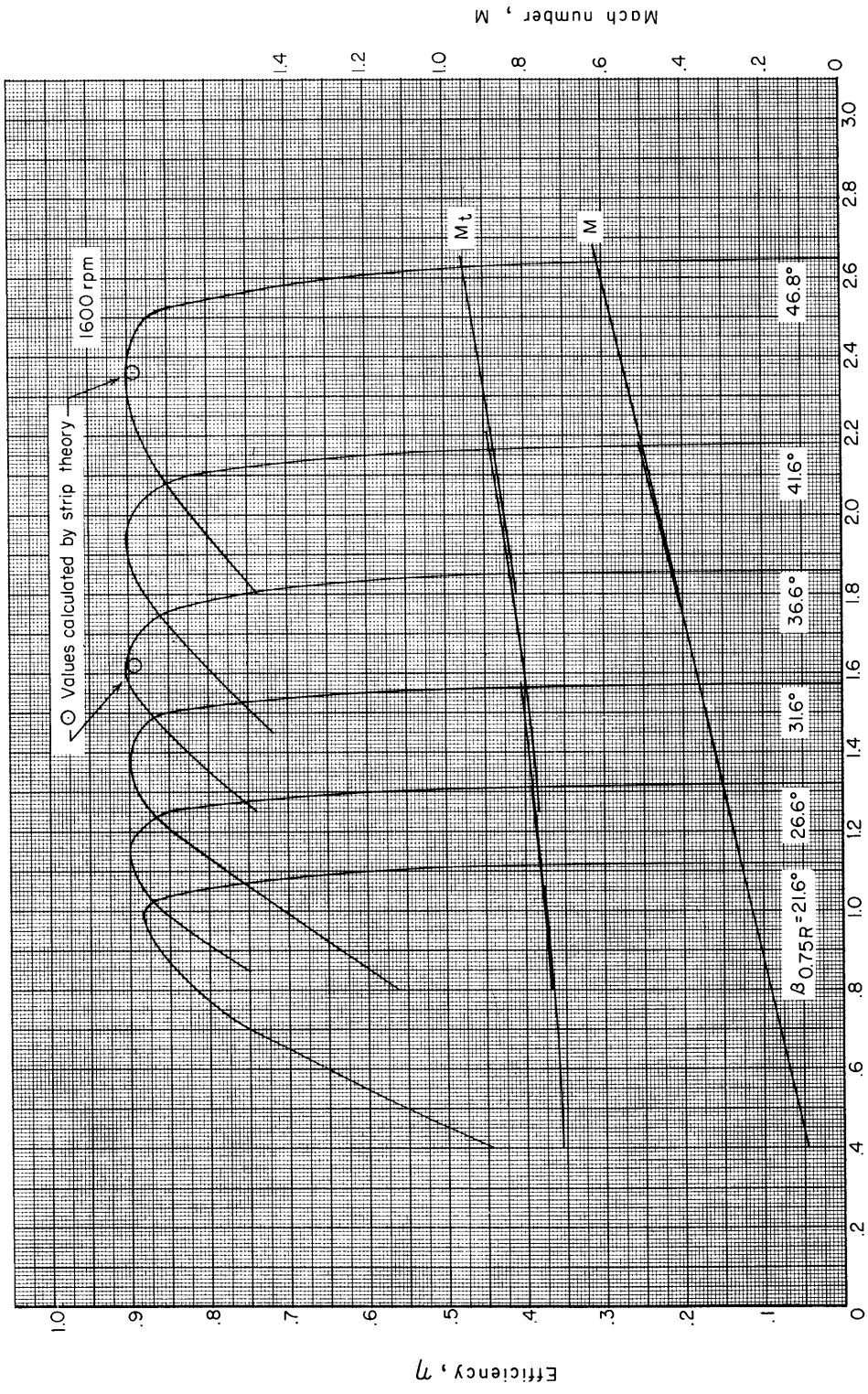

(c) Efficiency.

Figure 7.- Concluded.

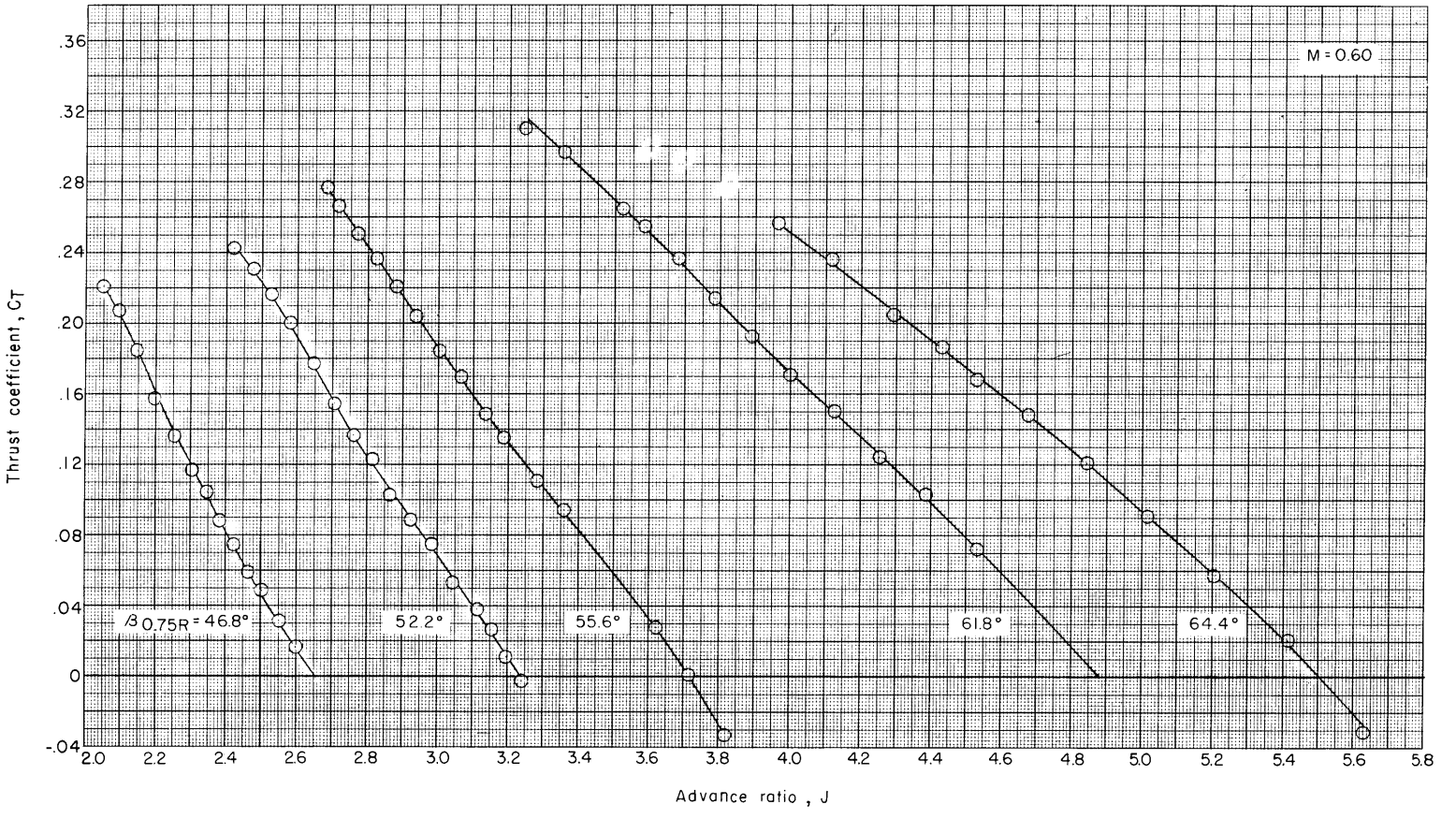

(a) Thrust coefficient.

Figure 8.- Characteristics of the Curtiss-Wright cambered propeller (design no. 109626). Forward Mach number, 0.60.

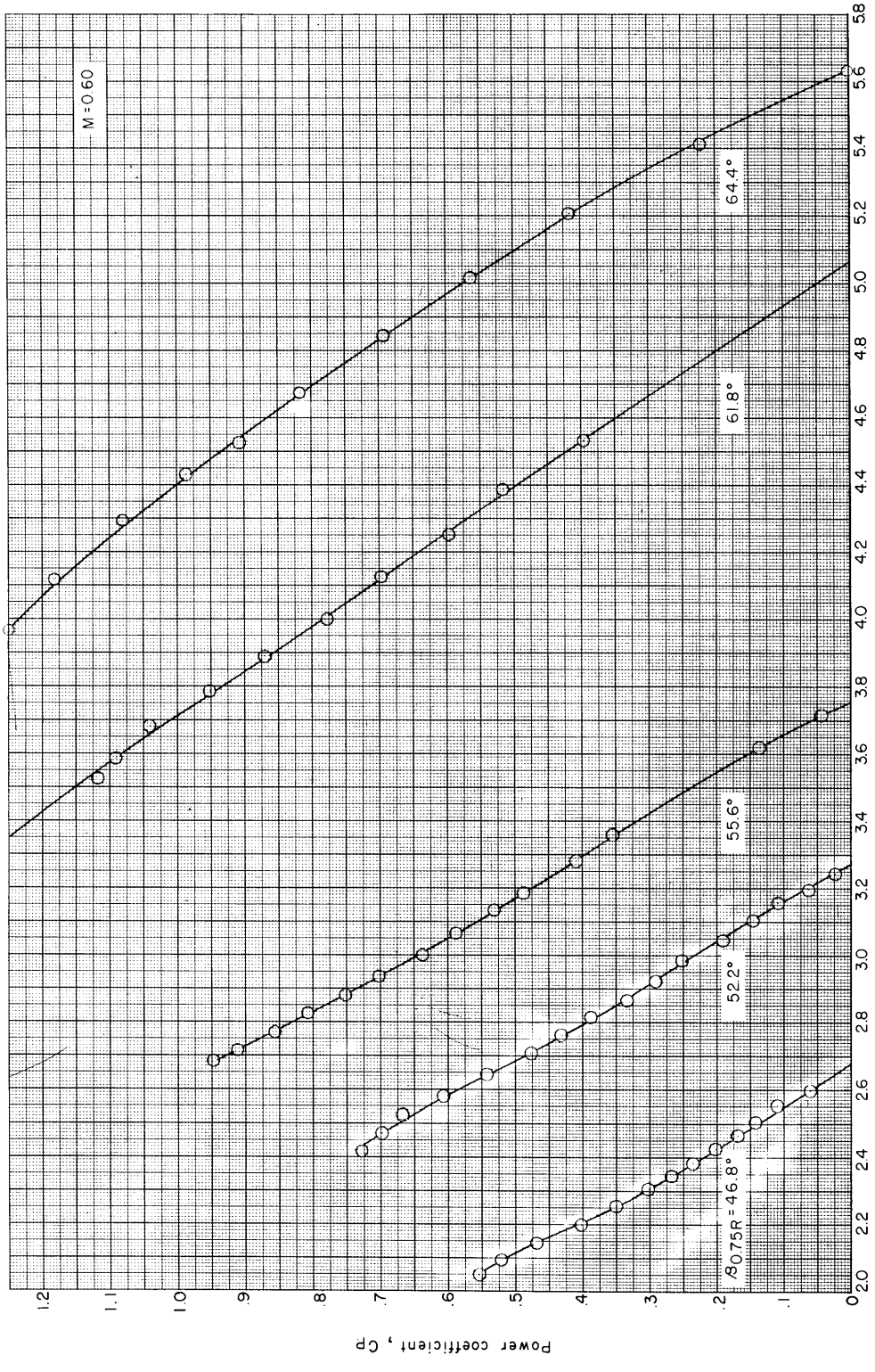

(b) Power coefficient.

Figure 8.- Continued.

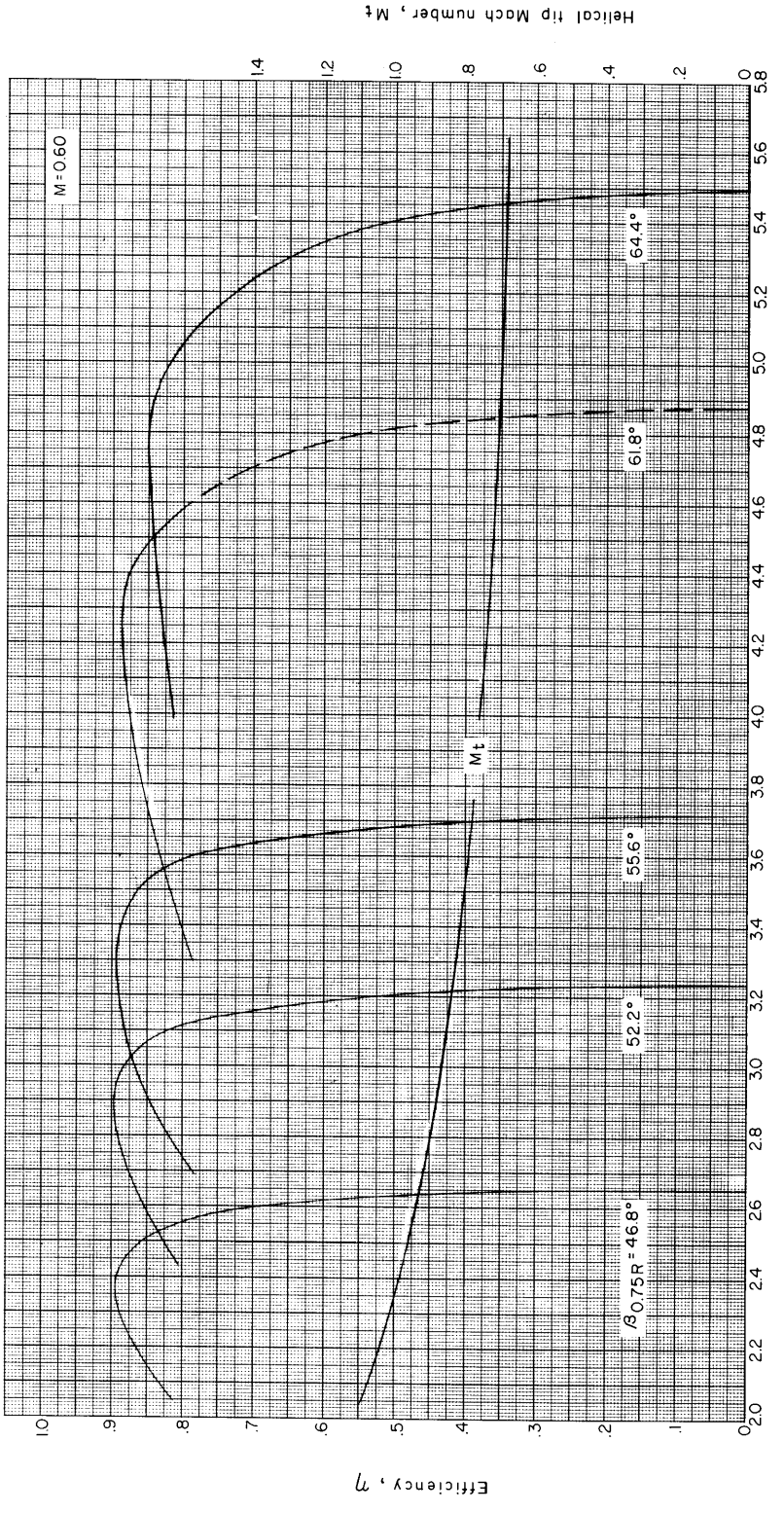

(c) Efficiency.

Figure 8.- Concluded.

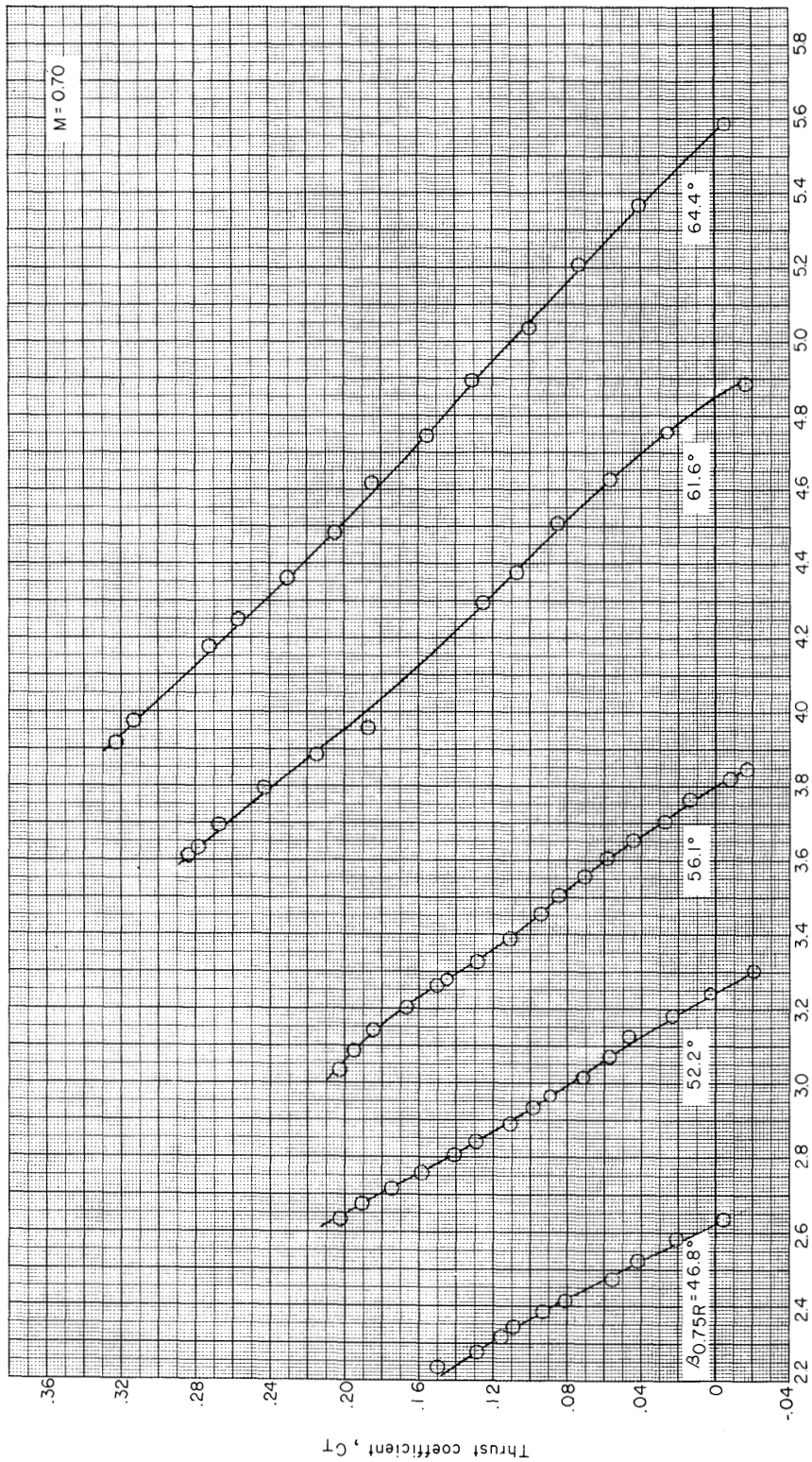

(a) Thrust coefficient.

Figure 9.- Characteristics of the Curtiss-Wright cambered propeller (design no. 109626). Forward Mach number, 0.70.

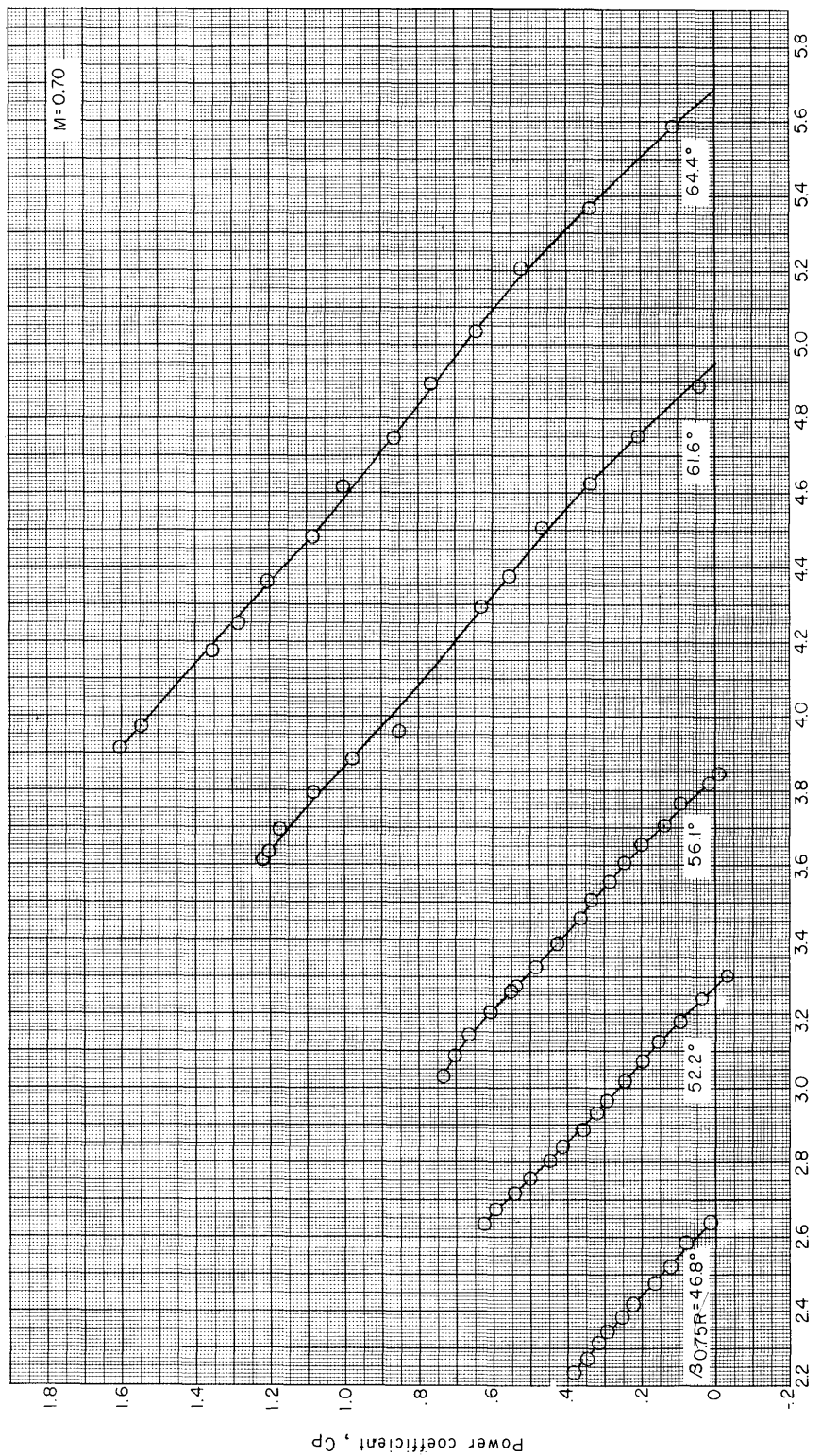

(b) Power coefficient.

Figure 9.- Continued.

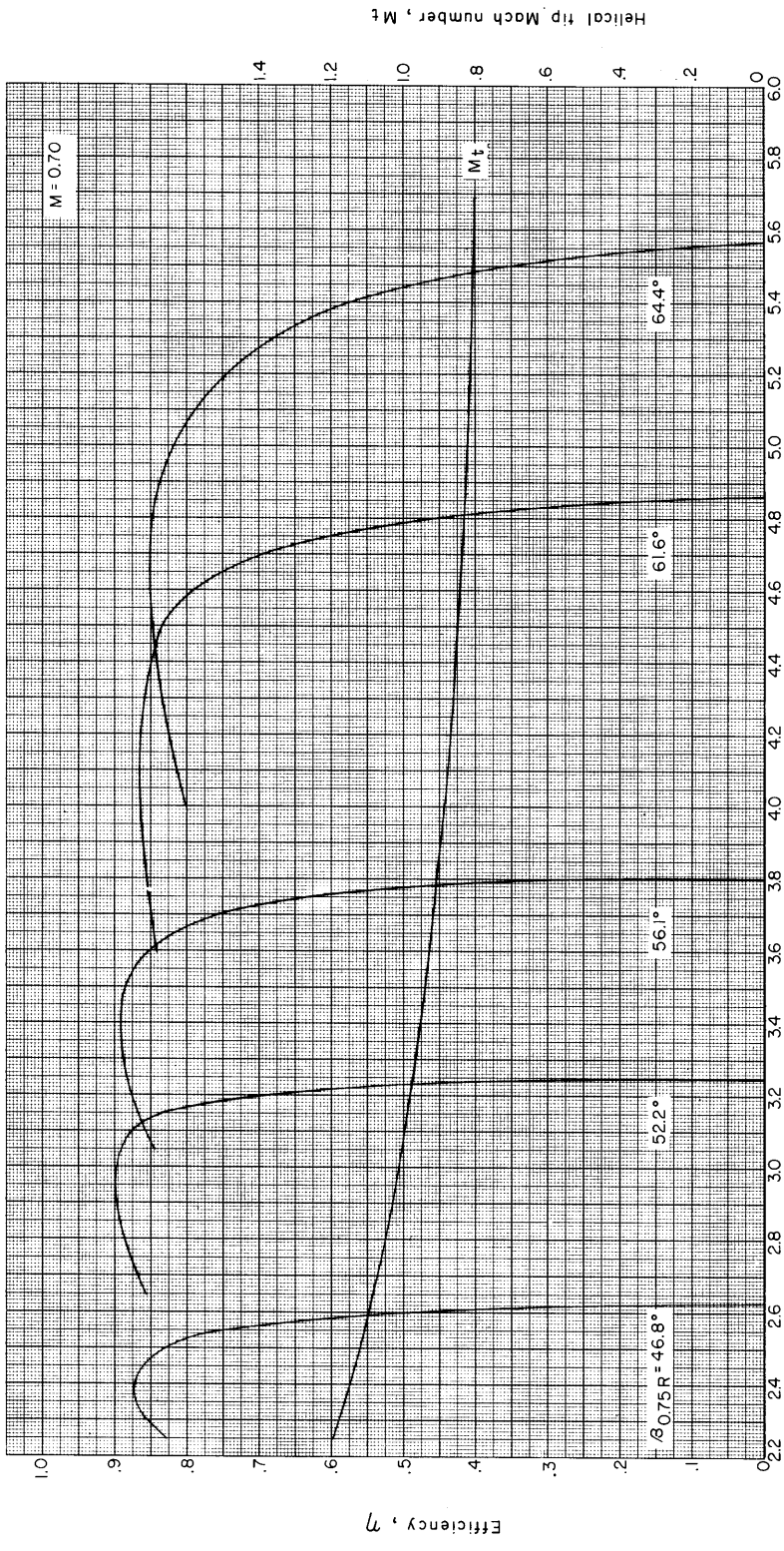

(c) Efficiency.

Figure 9.- Concluded.

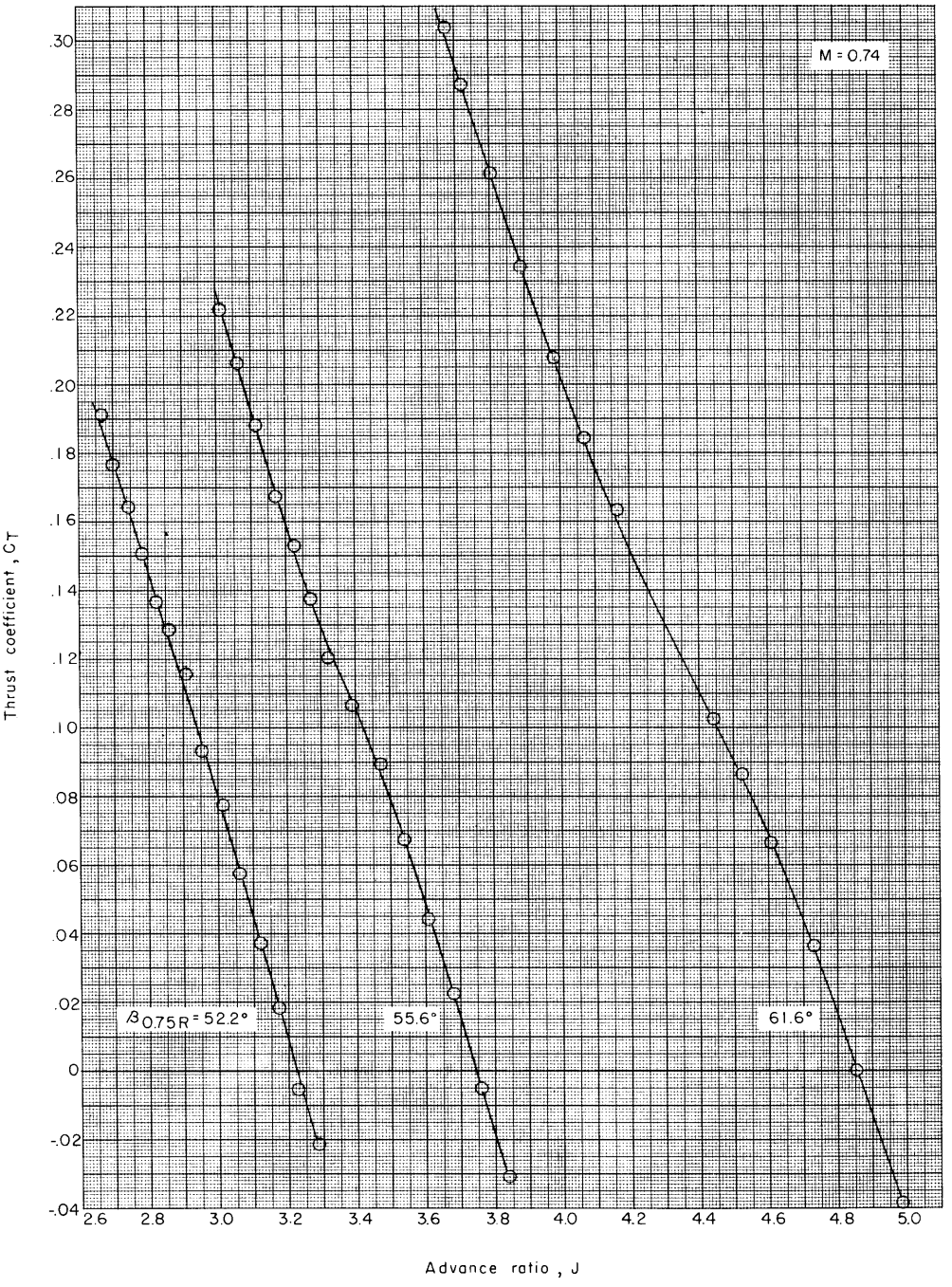

(a) Thrust coefficient.

Figure 10.- Characteristics of the Curtiss-Wright cambered propeller (design no. 109626). Forward Mach number, 0.74.

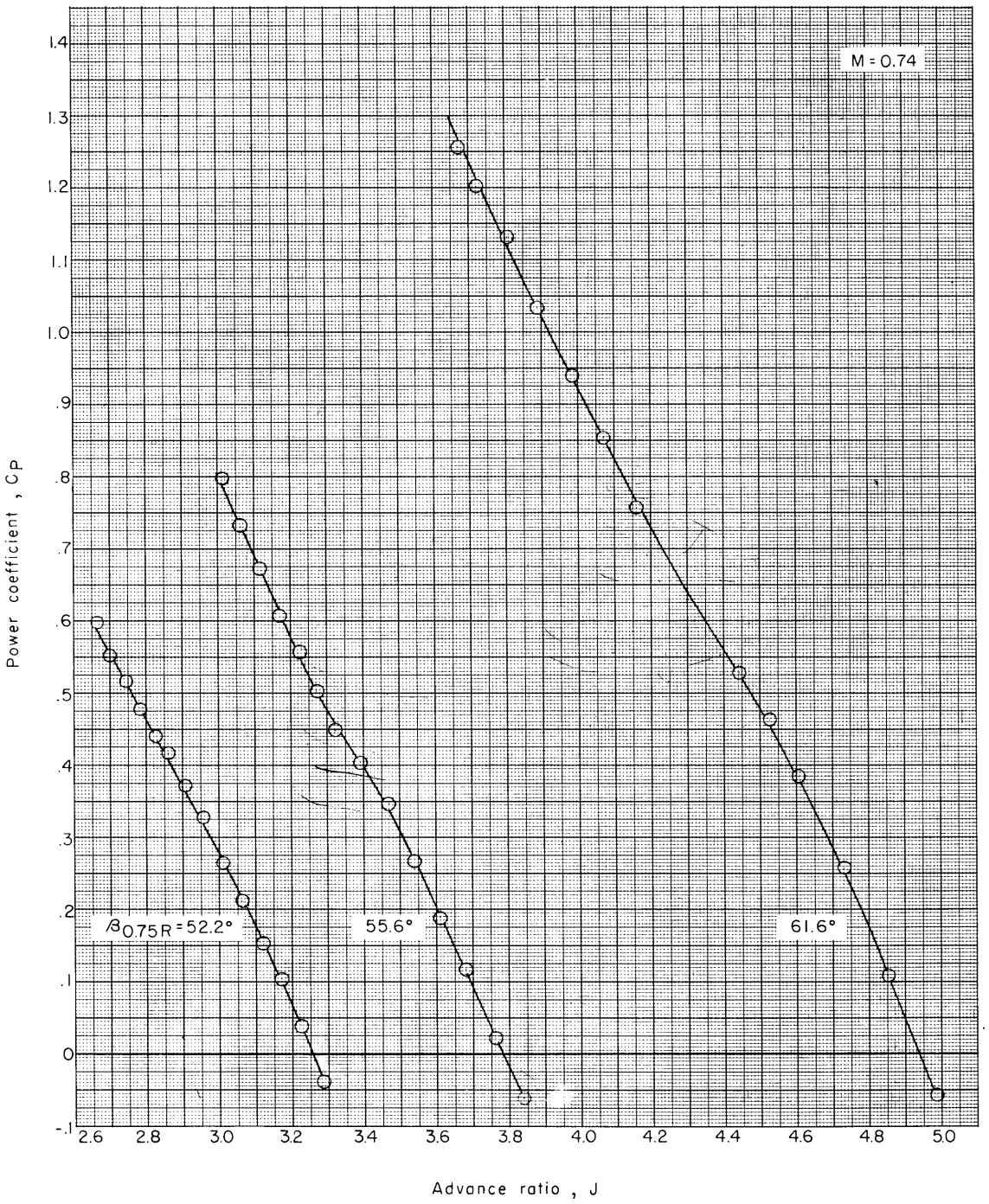

(b) Power coefficient.

Figure 10.- Continued.

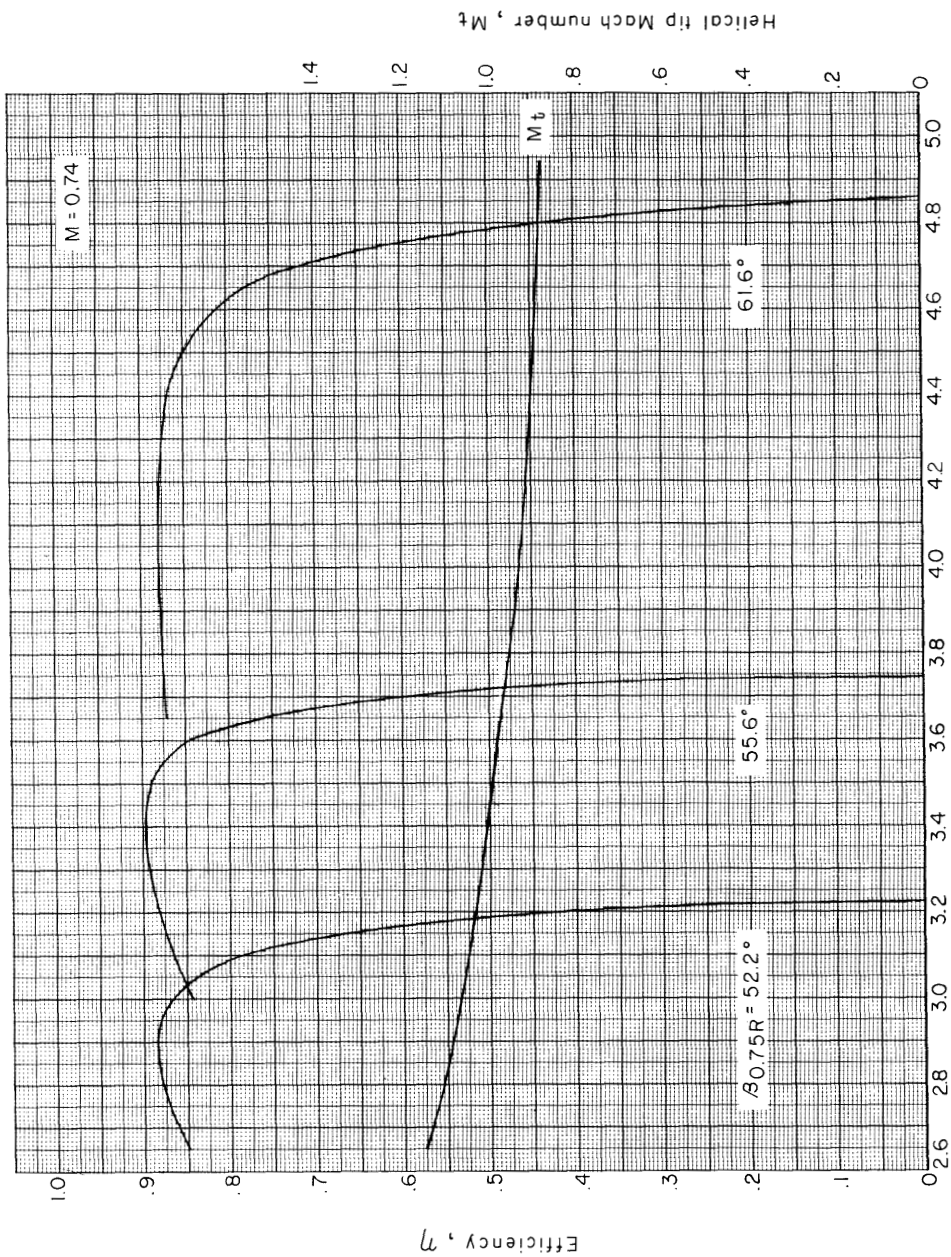

(c) Efficiency.

Figure 10.- Concluded.

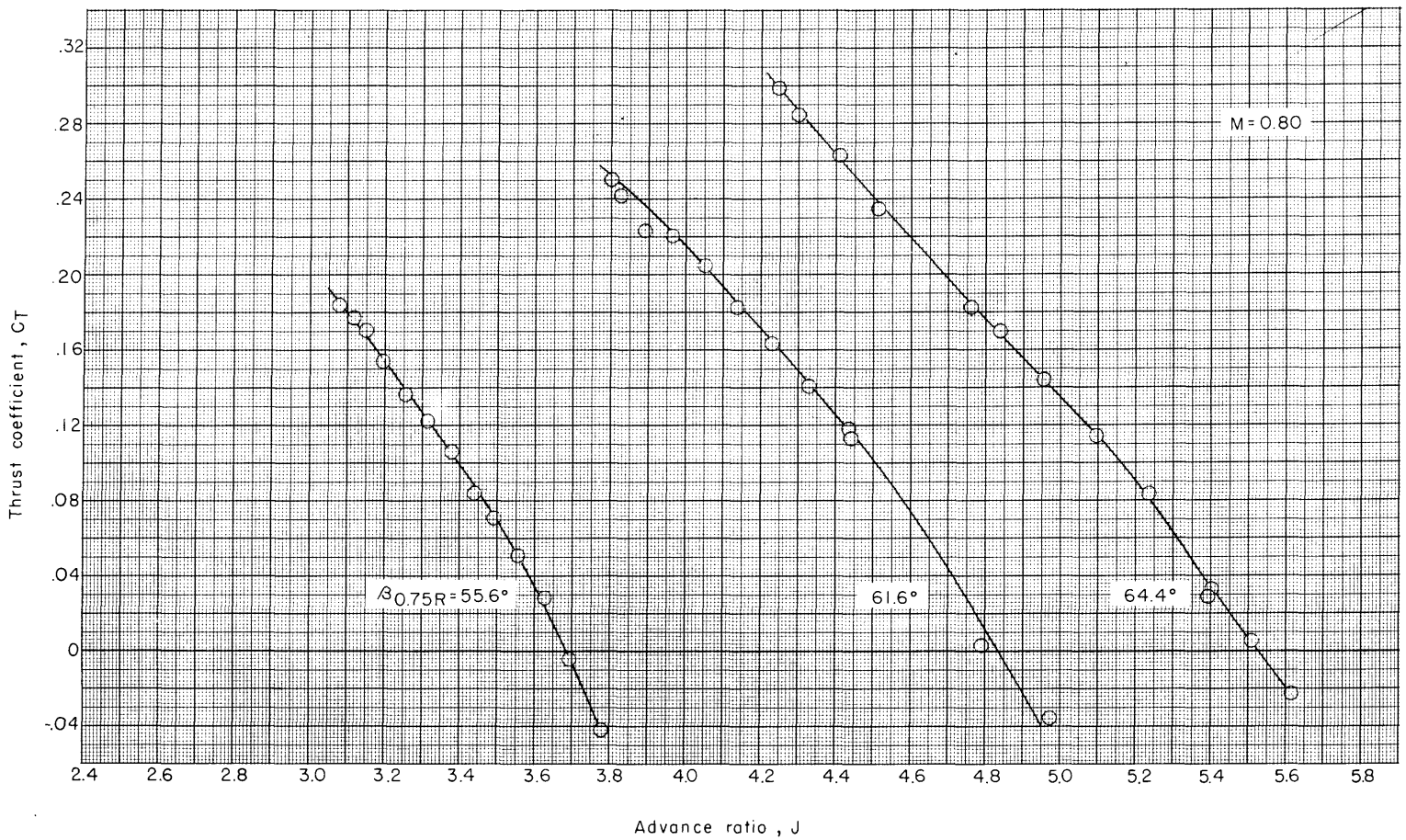

(a) Thrust coefficient.

Figure 11.- Characteristics of the Curtiss-Wright cambered propeller (design no. 109626). Forward Mach number, 0.80.

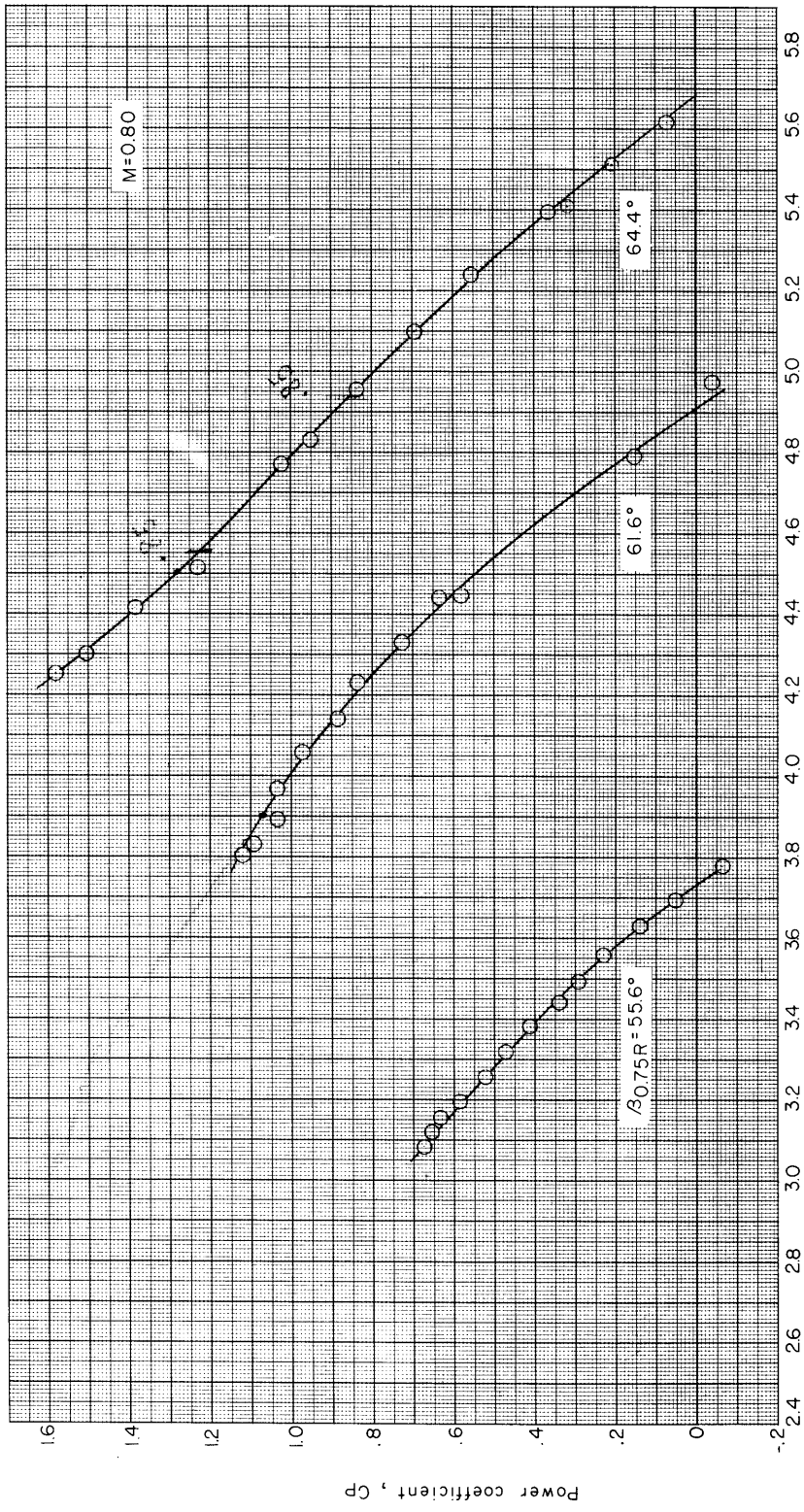

(b) Power coefficient.

Figure 11.- Continued.

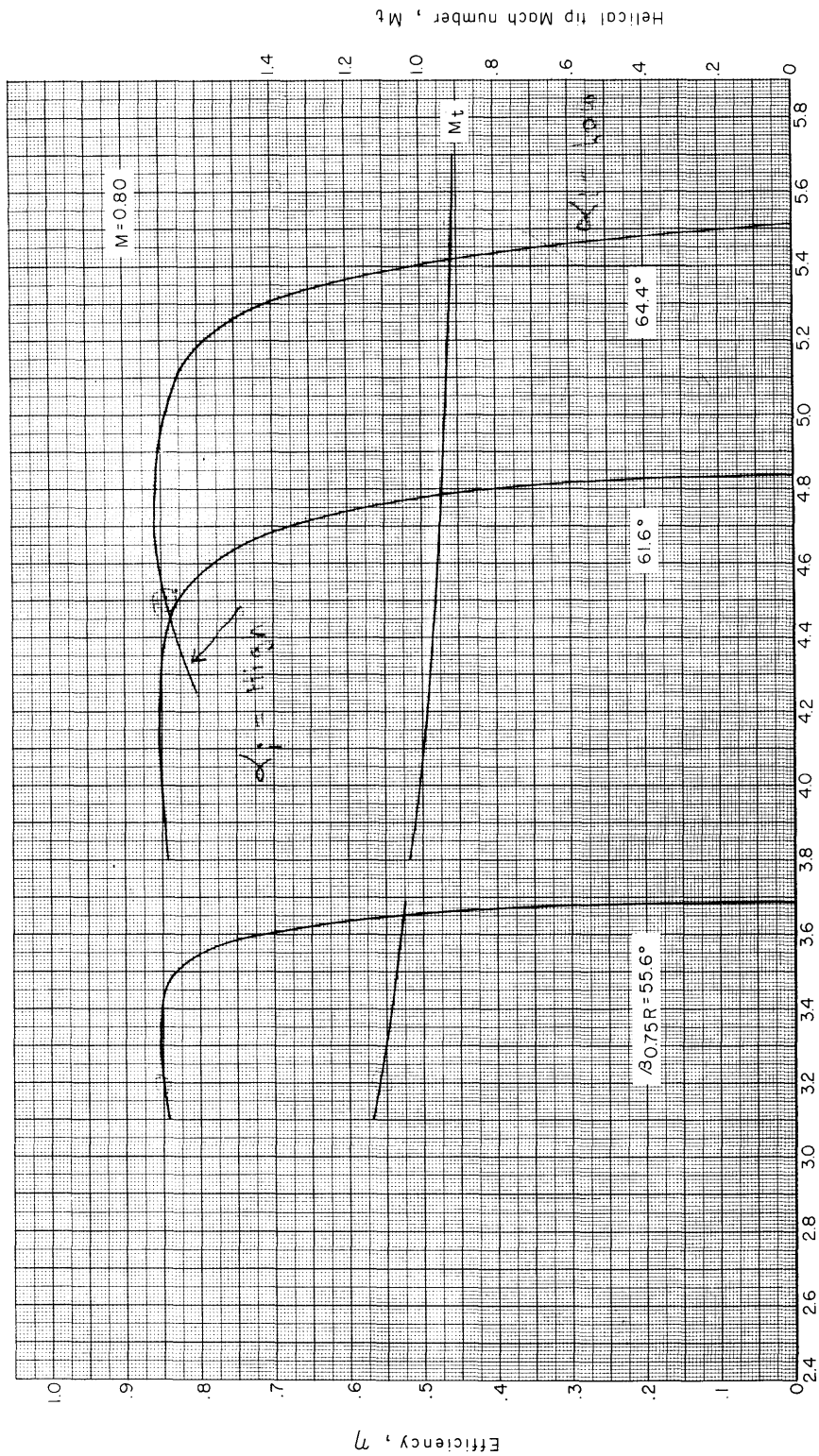

(c) Efficiency.

Figure 11.- Concluded.

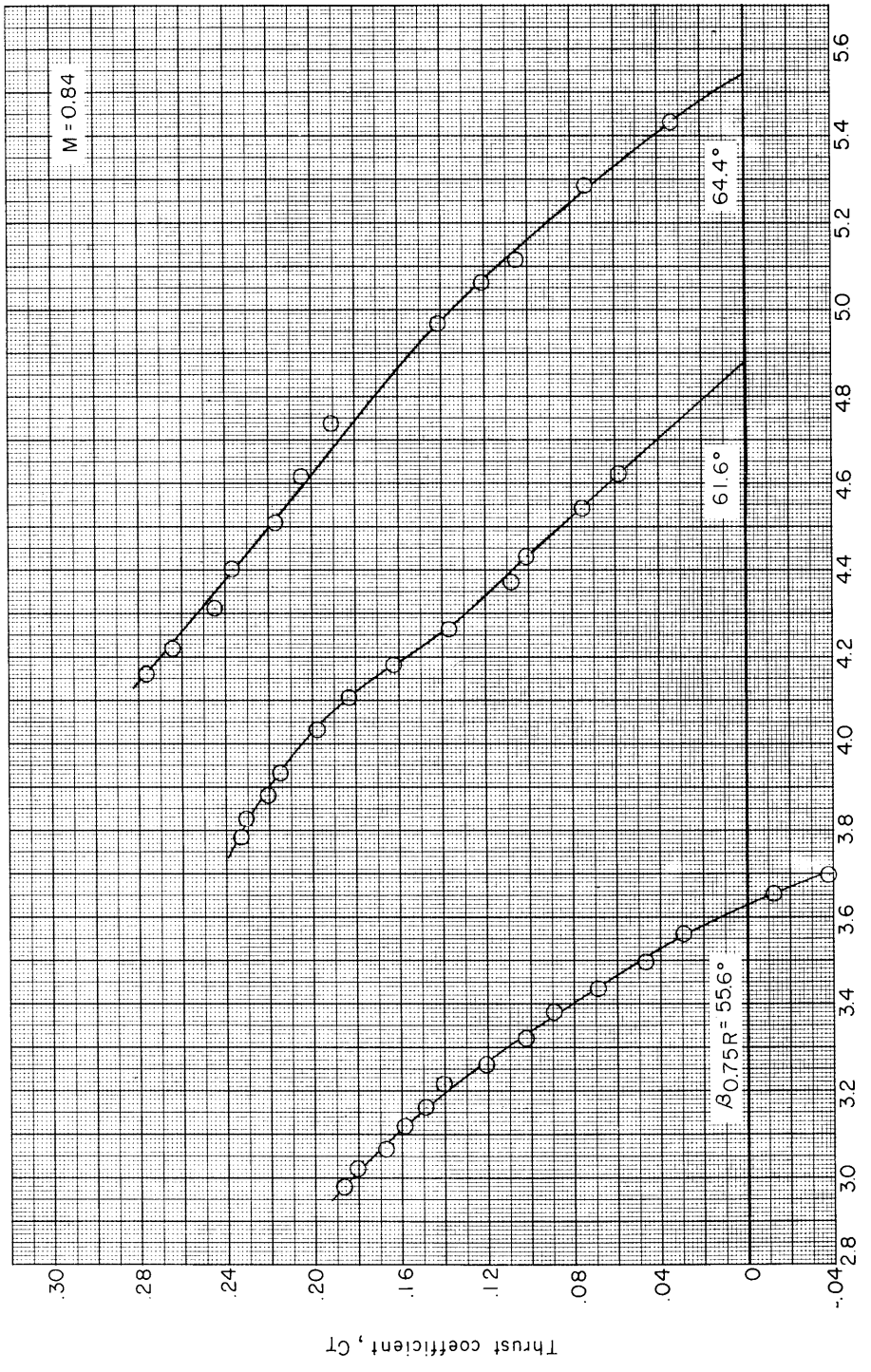

(a) Thrust coefficient.

Figure 12.- Characteristics of the Curtiss-Wright cambered propeller (design no. 109626). Forward Mach number, 0.84.

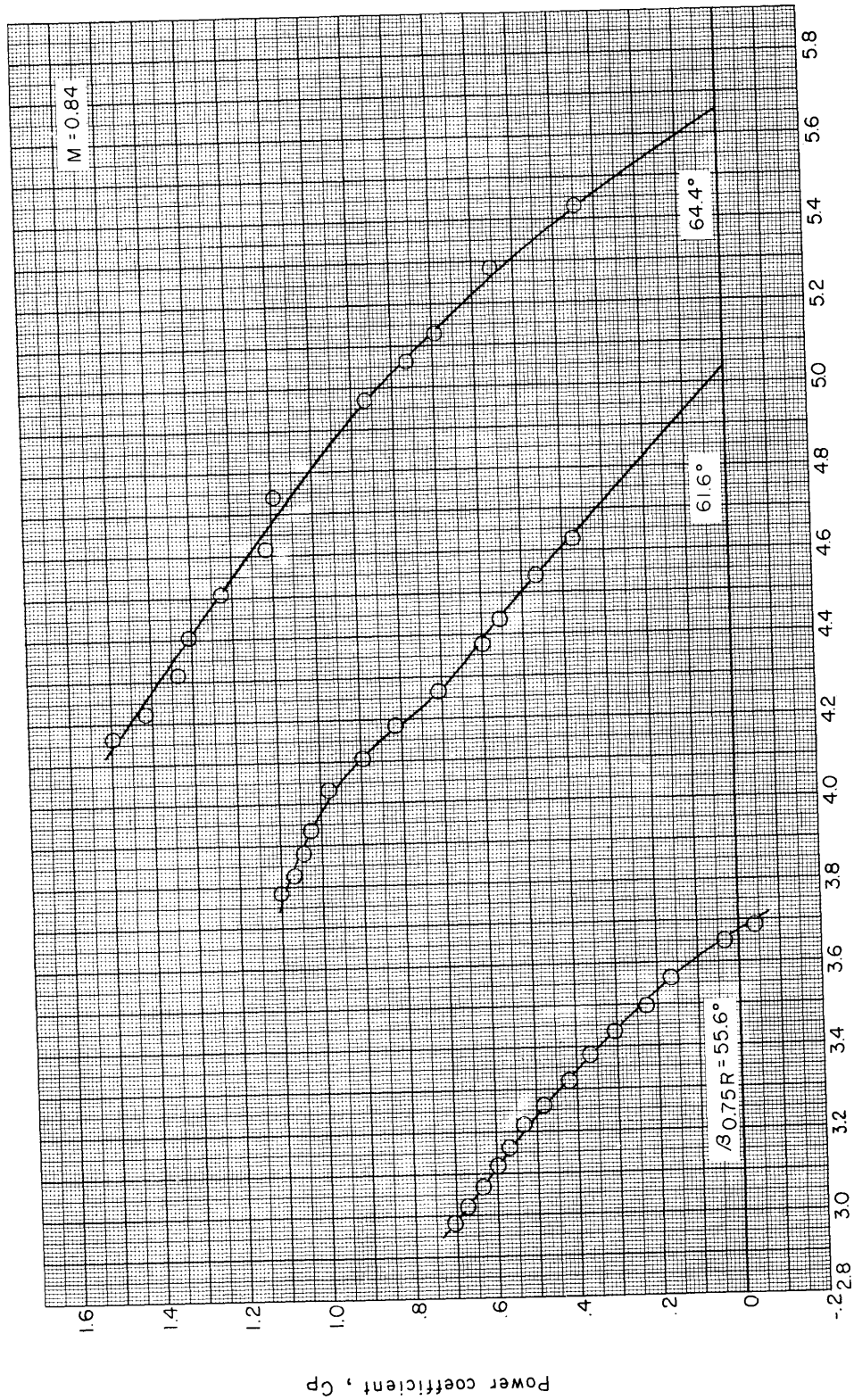

(b) Power coefficient.

Figure 12.- Continued.

(c) Efficiency.

Figure 12.- Concluded.

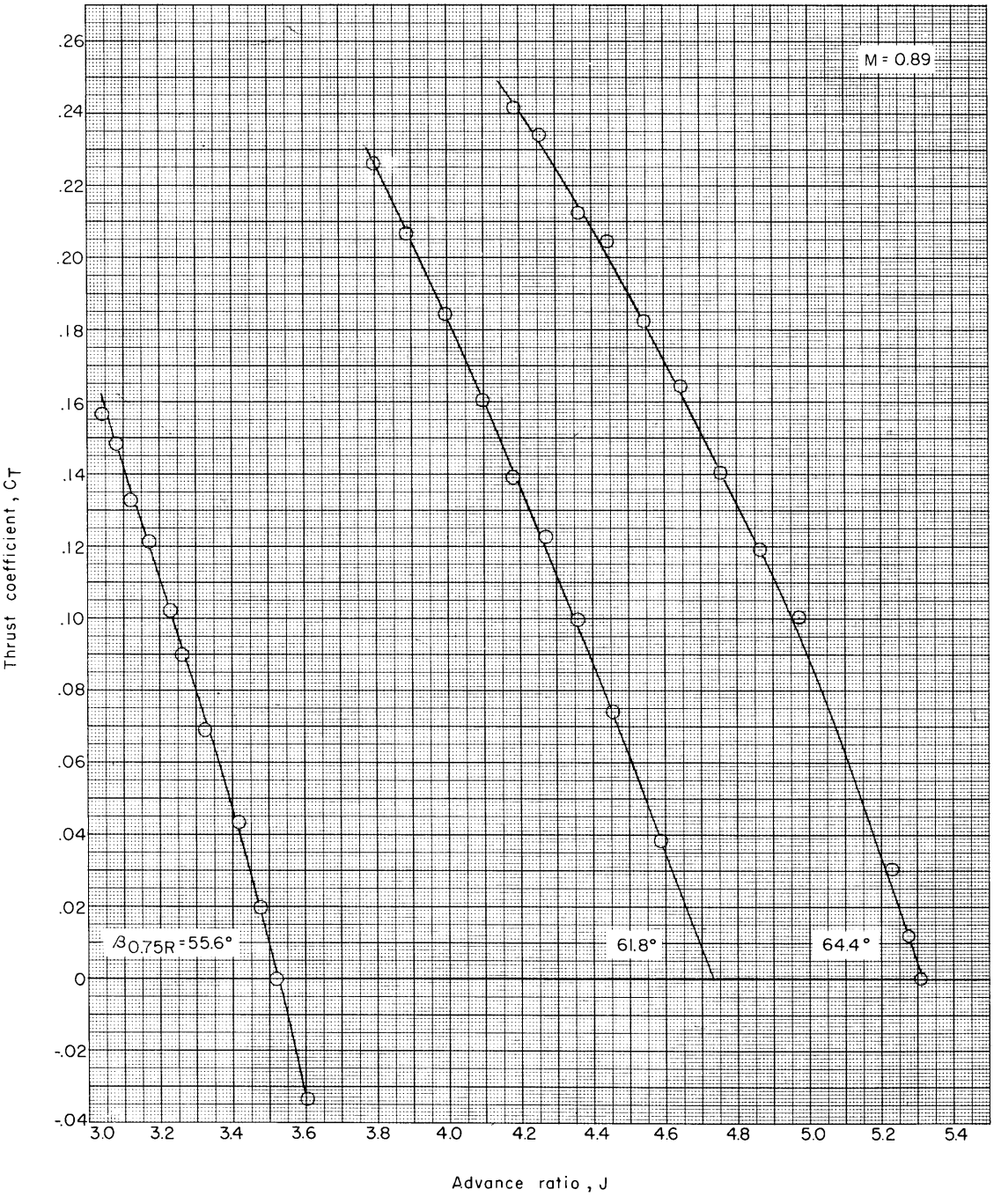

(a) Thrust coefficient.

Figure 13.- Characteristics of the Curtiss-Wright cambered propeller (design no. 109626). Forward Mach number, 0.89.

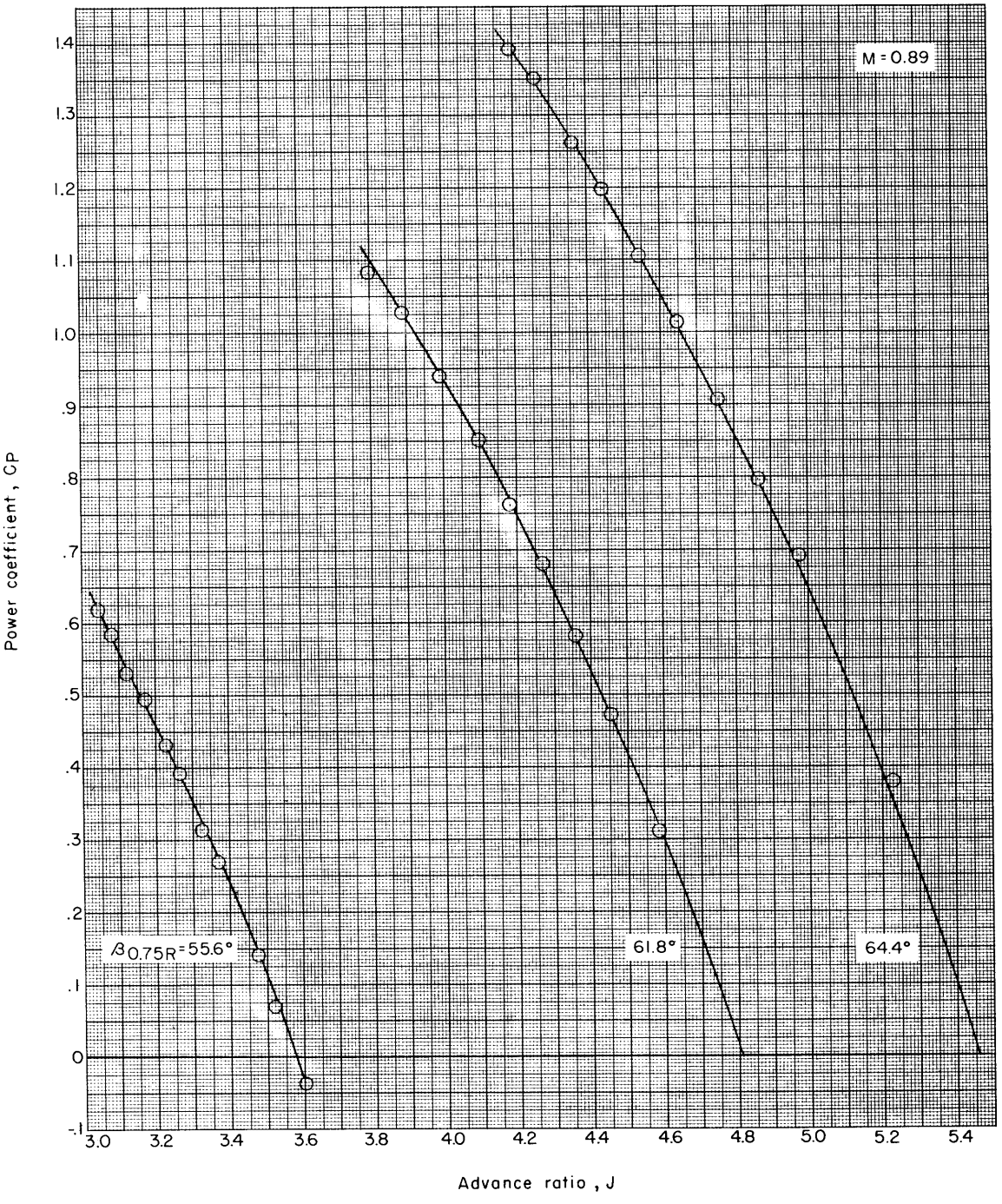

(b) Power coefficient.

Figure 13.- Continued.

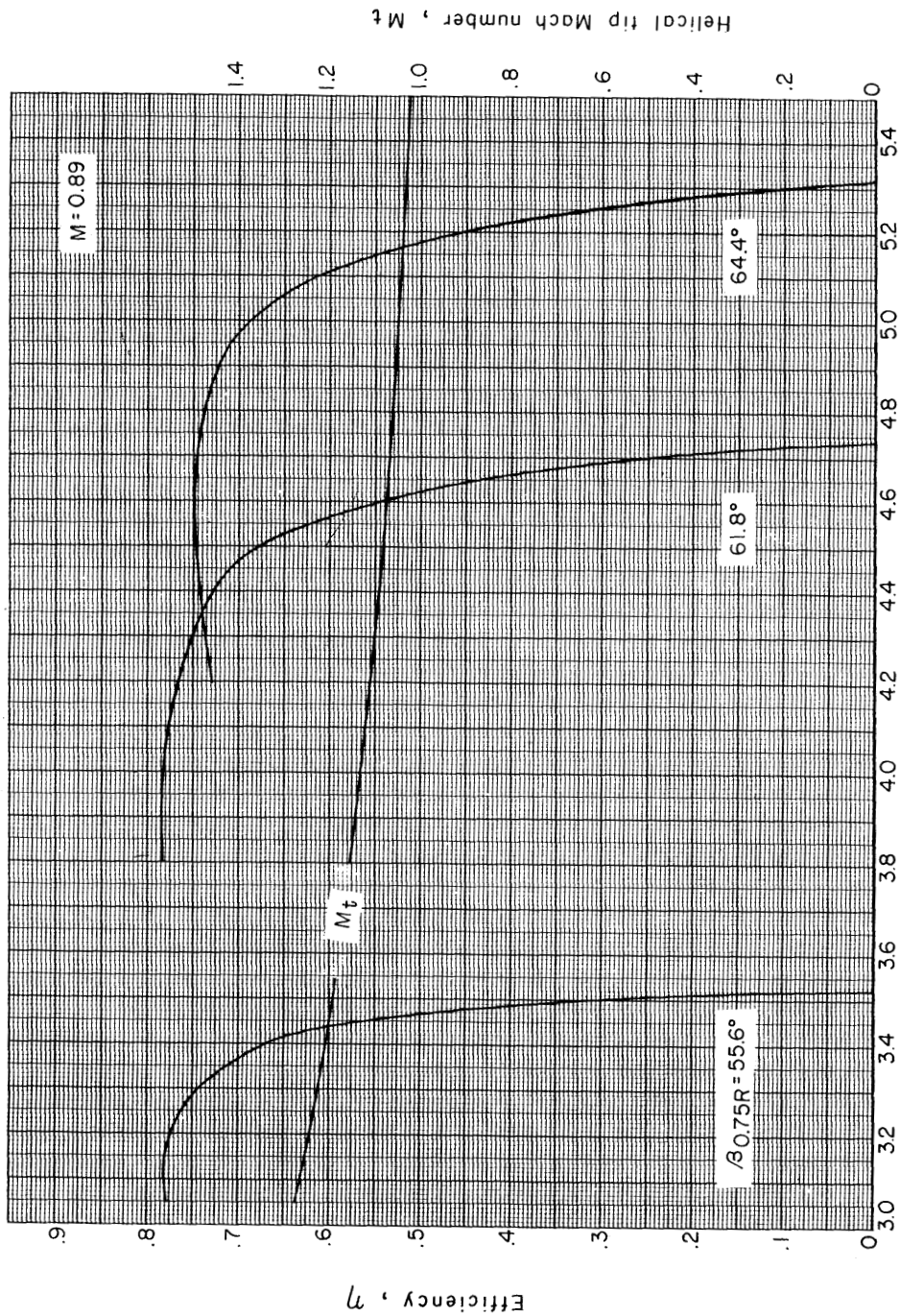

(c) Efficiency.

Figure 13.- Concluded.

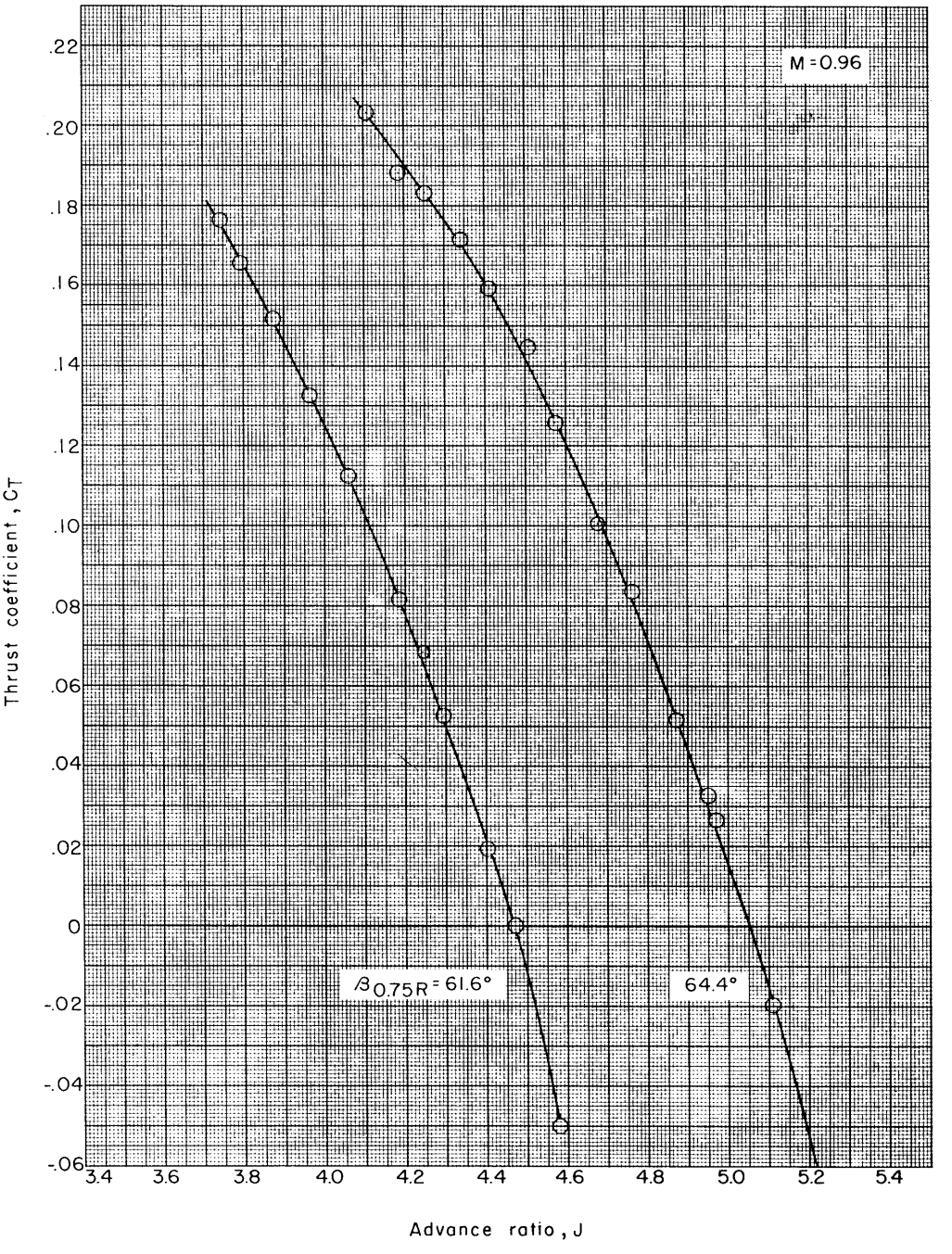

(a) Thrust coefficient.

Figure 14.- Characteristics of the Curtiss-Wright cambered propeller (design no. 109626). Forward Mach number, 0.96.

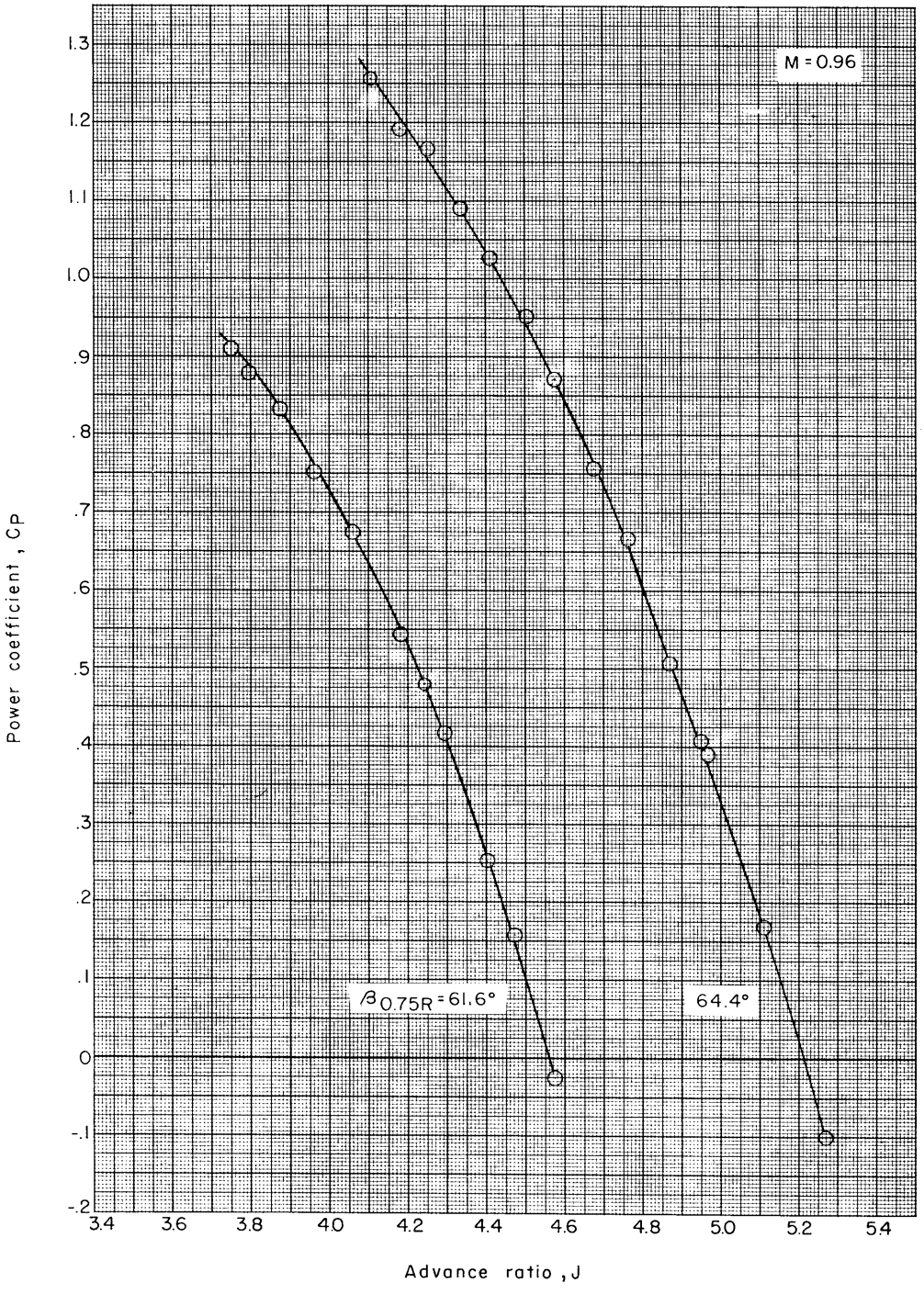

(b) Power coefficient.

Figure 14.- Continued.

(c) Efficiency.

Figure 14.- Concluded.

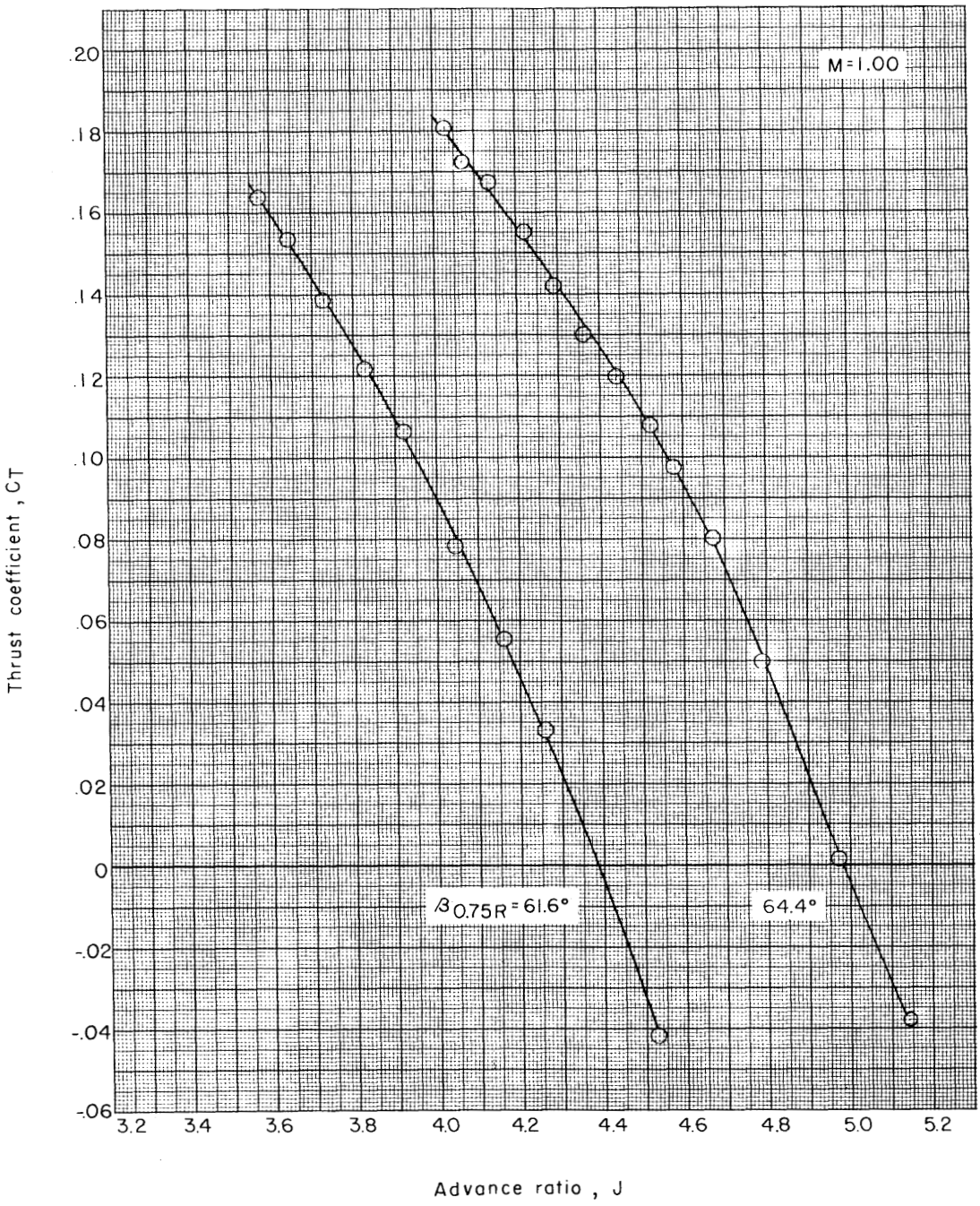

(a) Thrust coefficient.

Figure 15.- Characteristics of the Curtiss-Wright cambered propeller (design no. 109626). Forward Mach number, 1.00.

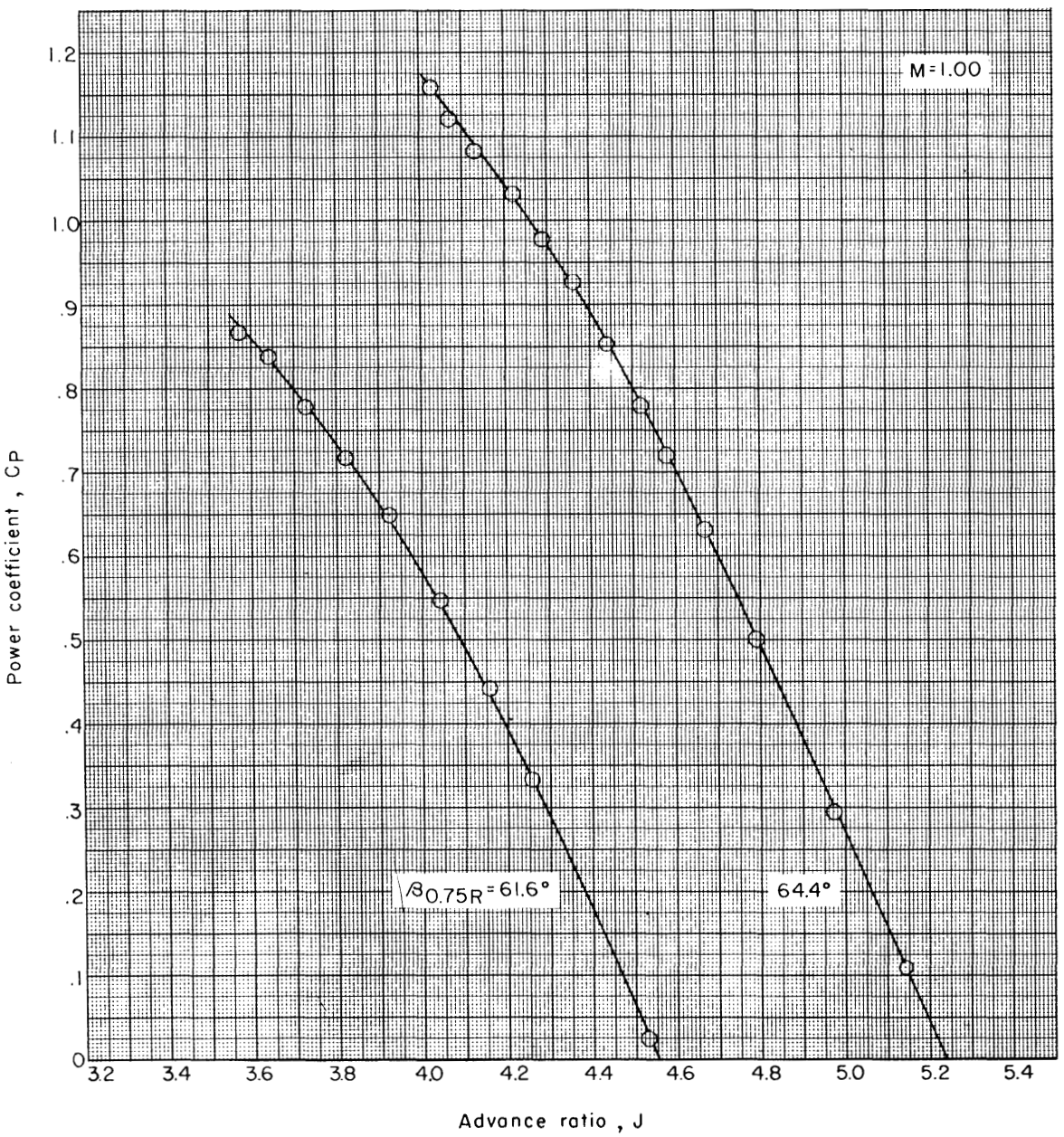

(b) Power coefficient.

Figure 15.- Continued.

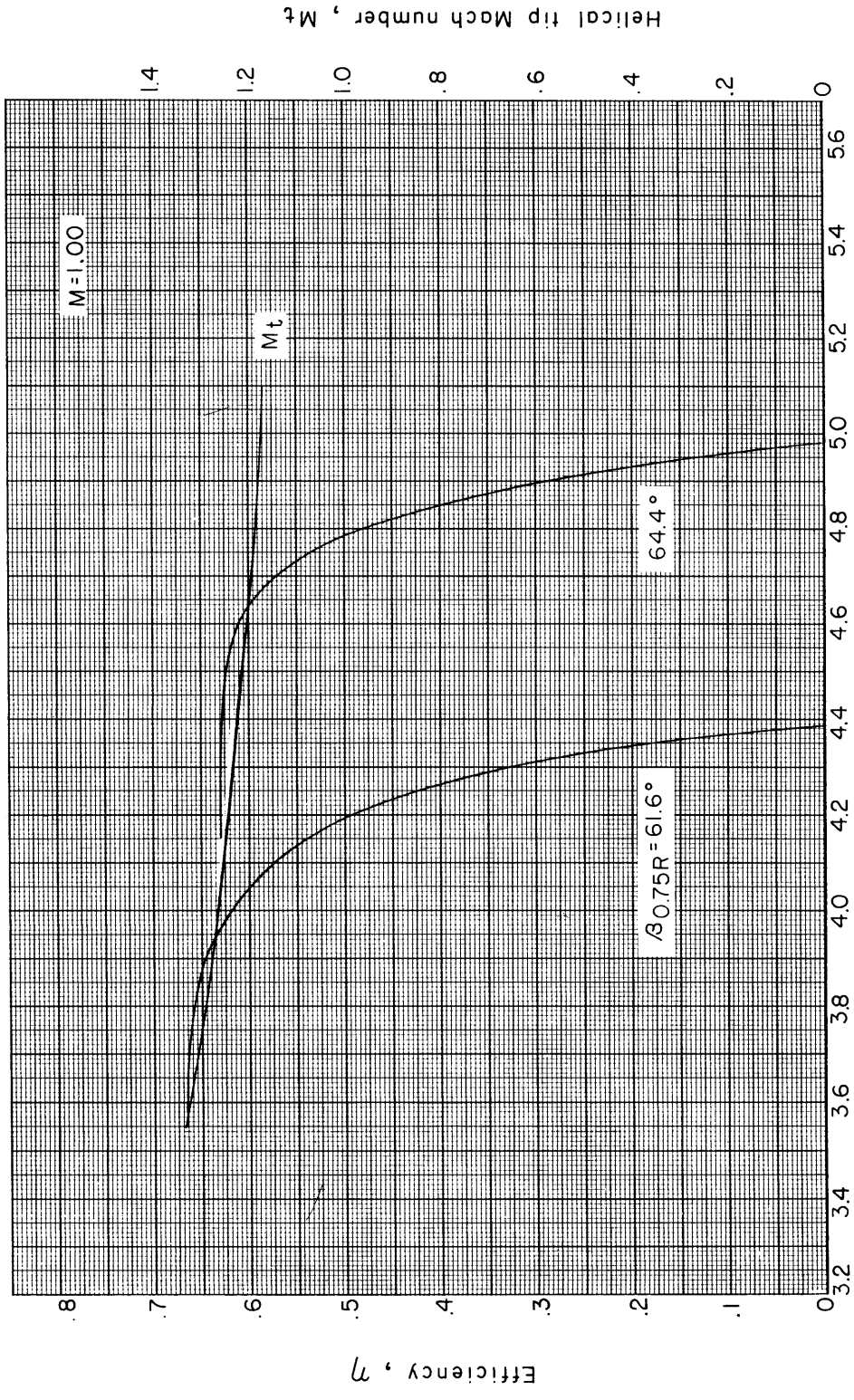

(c) Efficiency.

Figure 15.- Concluded.

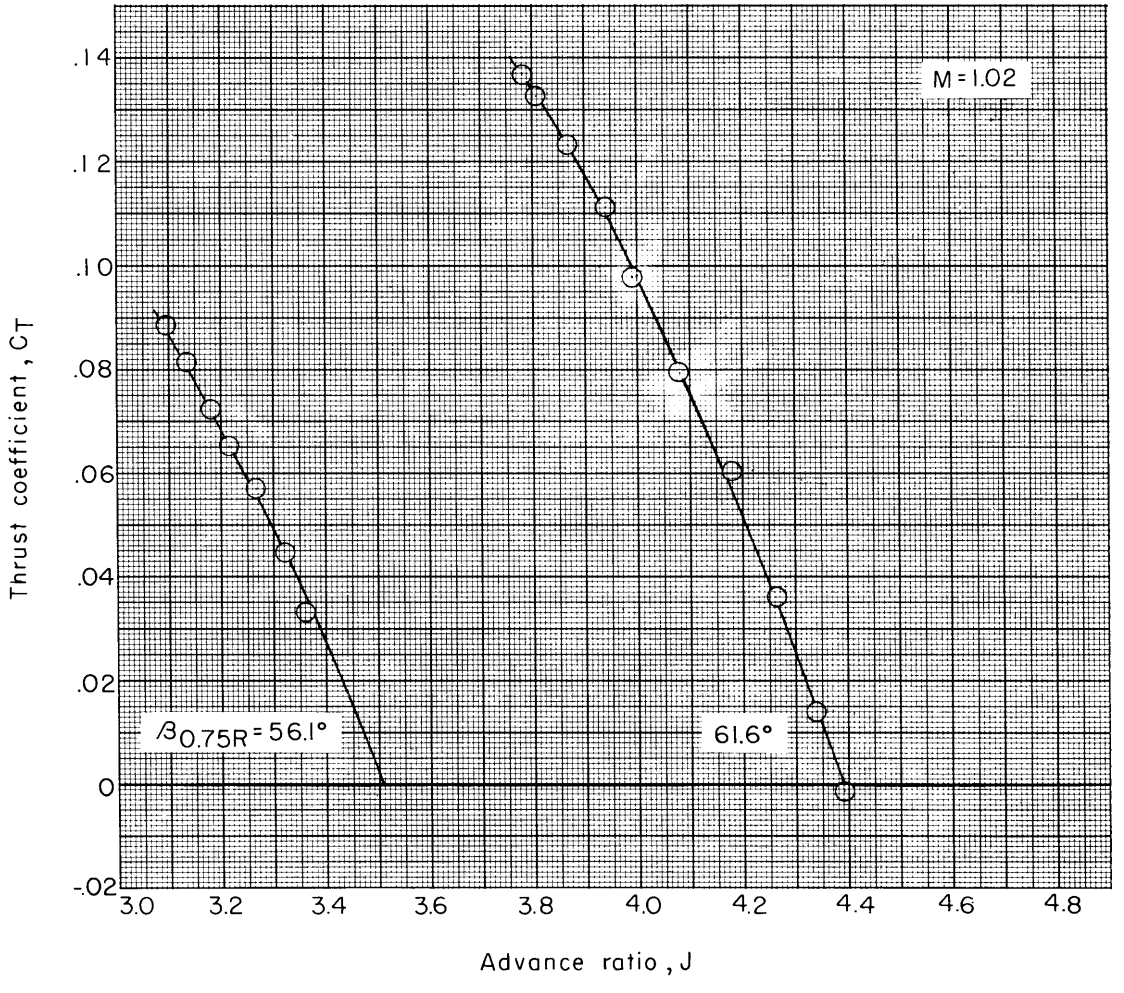

(a) Thrust coefficient.

Figure 16.- Characteristics of the Curtiss-Wright cambered propeller (design no. 109626). Forward Mach number, 1.02.

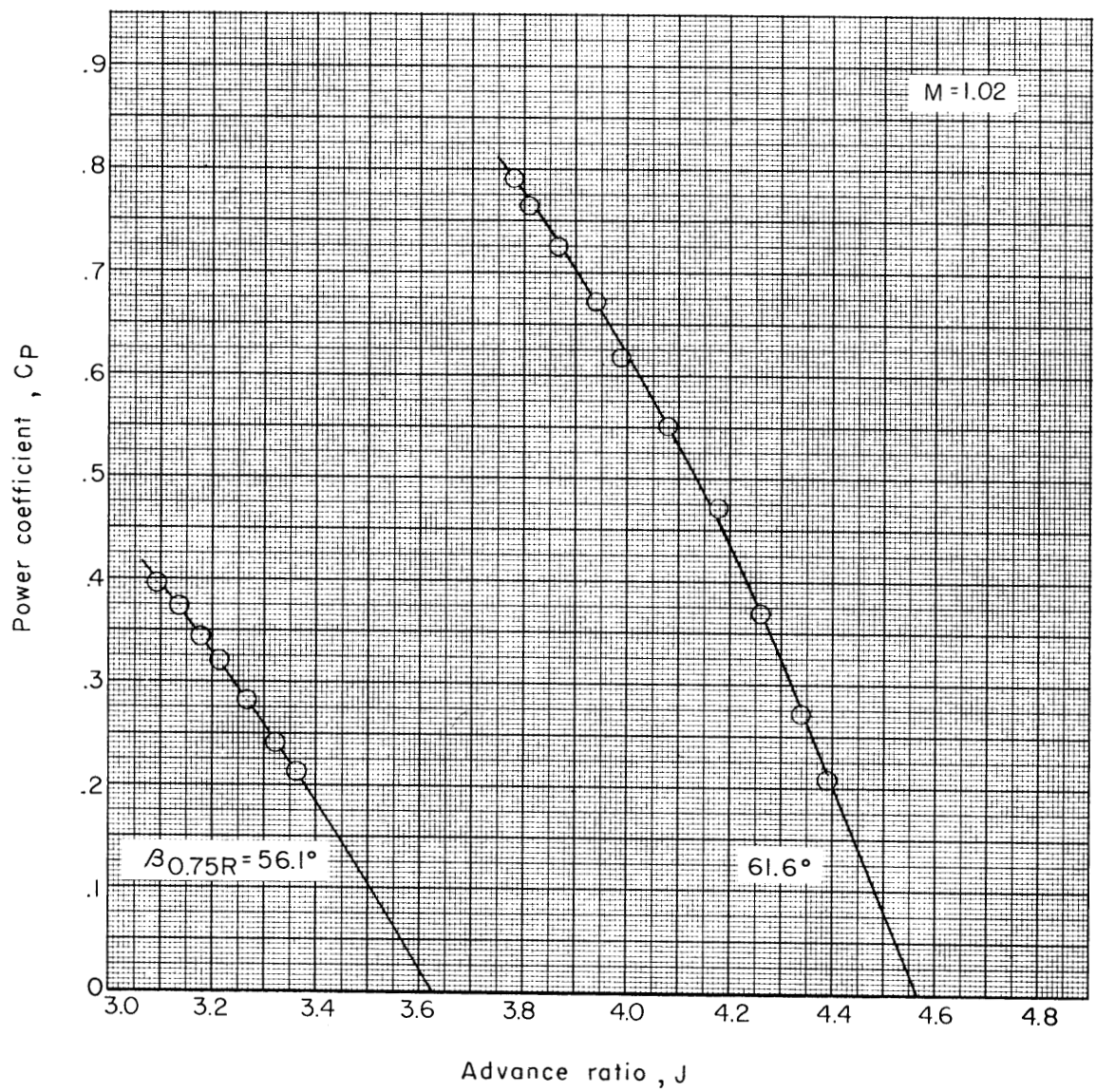

(b) Power coefficient.

Figure 16.- Continued.

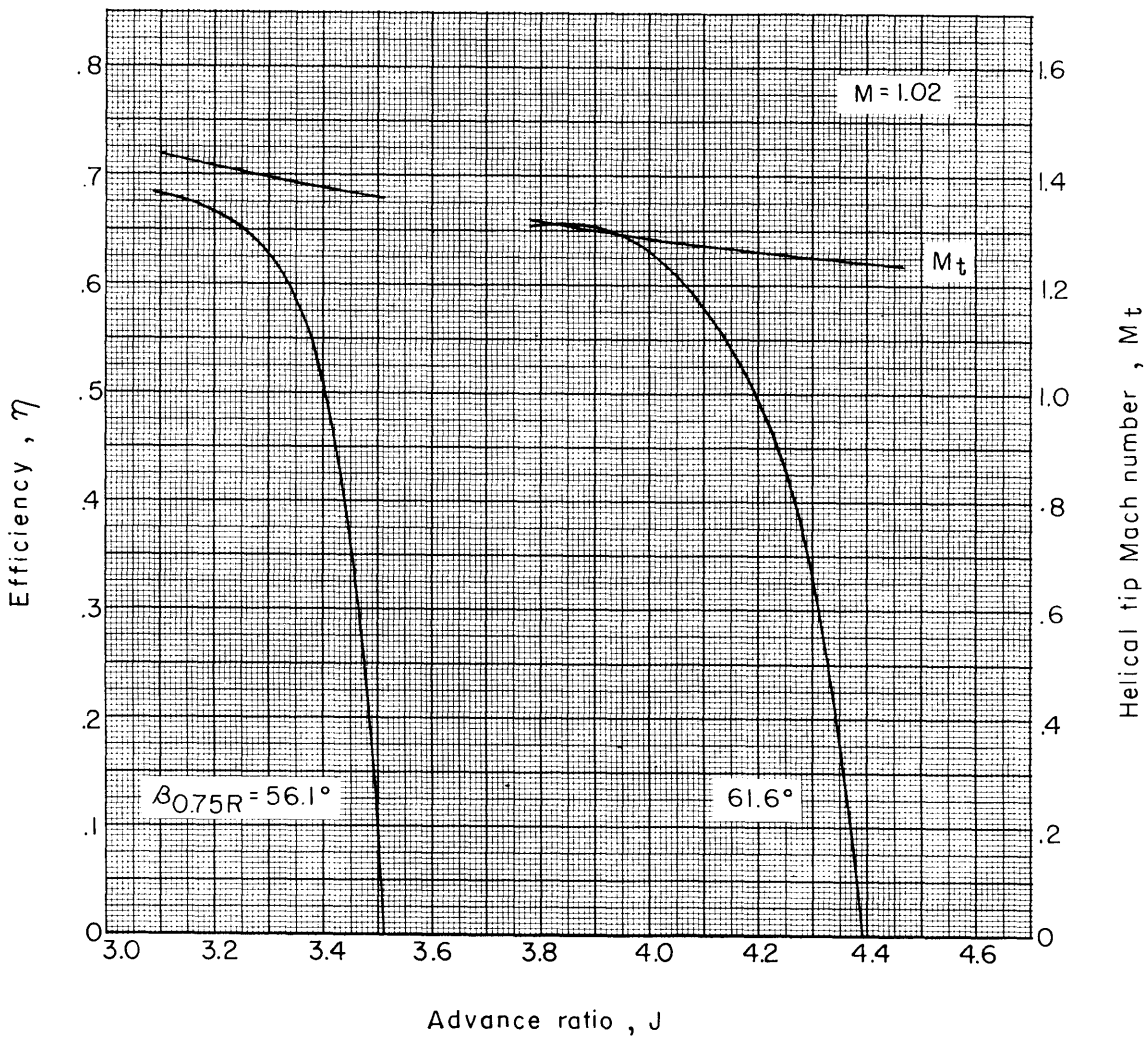

(c) Efficiency.

Figure 16.- Concluded.

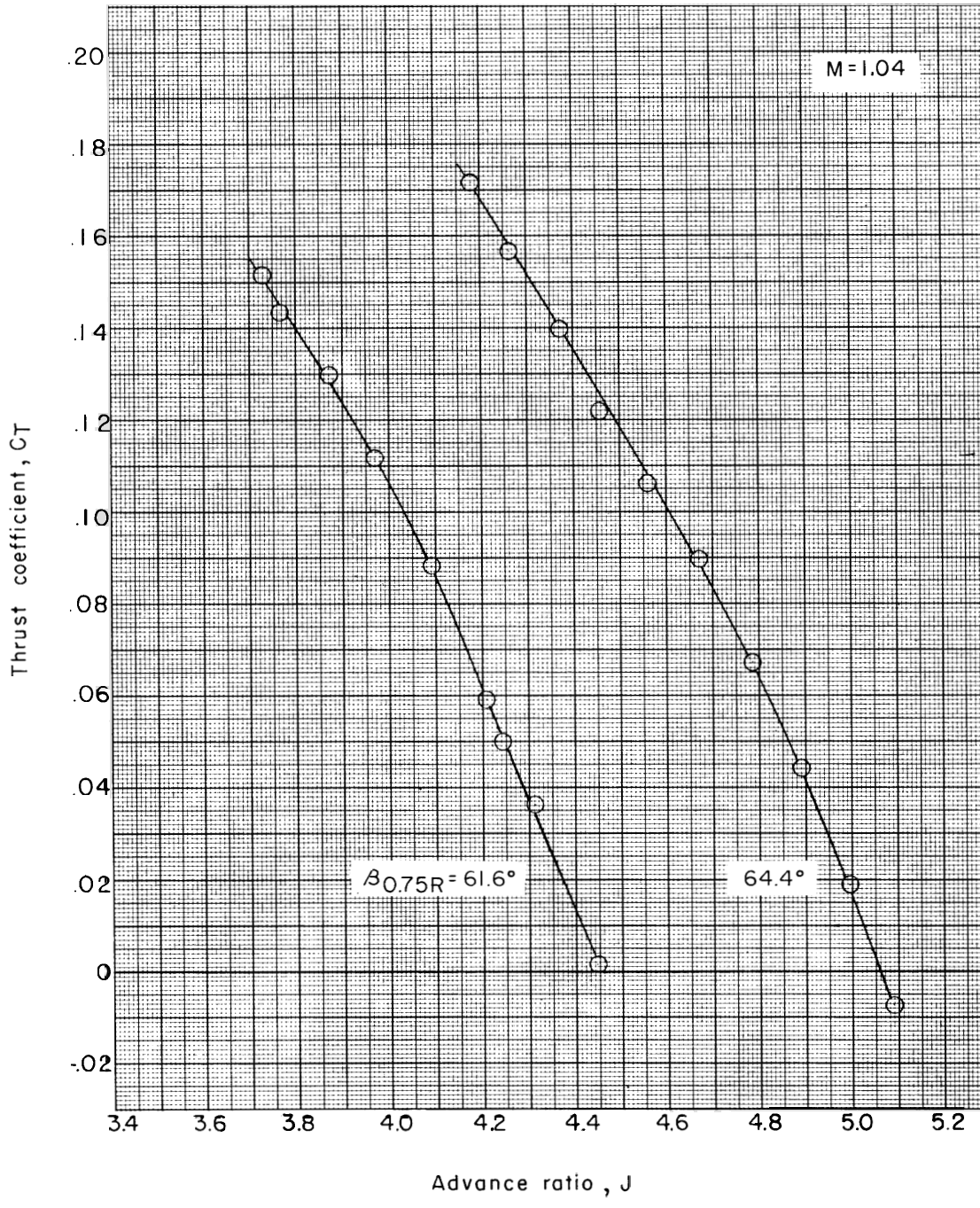

(a) Thrust coefficient.

Figure 17.- Characteristics of the Curtiss-Wright cambered propeller (design no. 109626). Forward Mach number, 1.04.

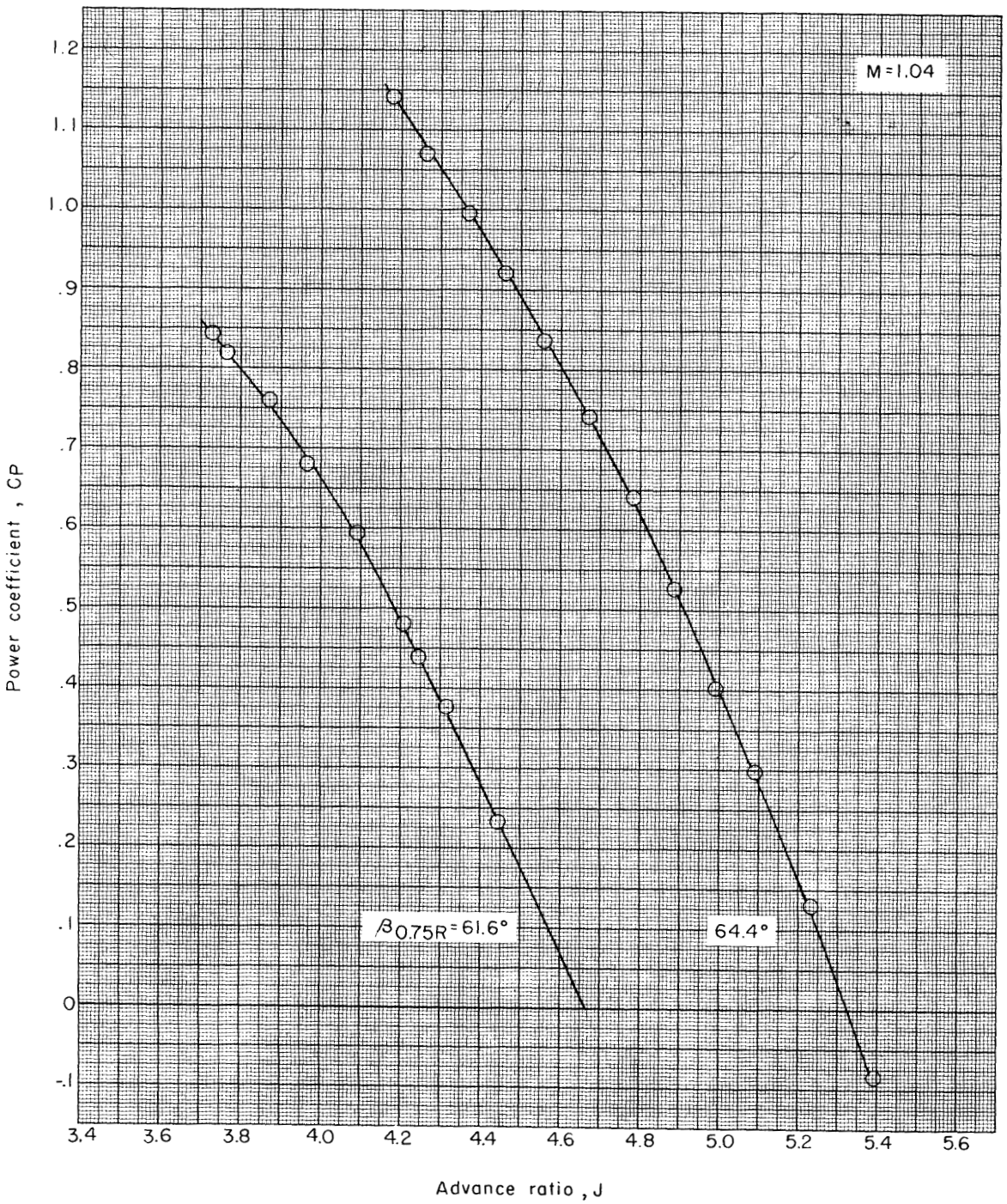

(b) Power coefficient.

Figure 17.- Continued.

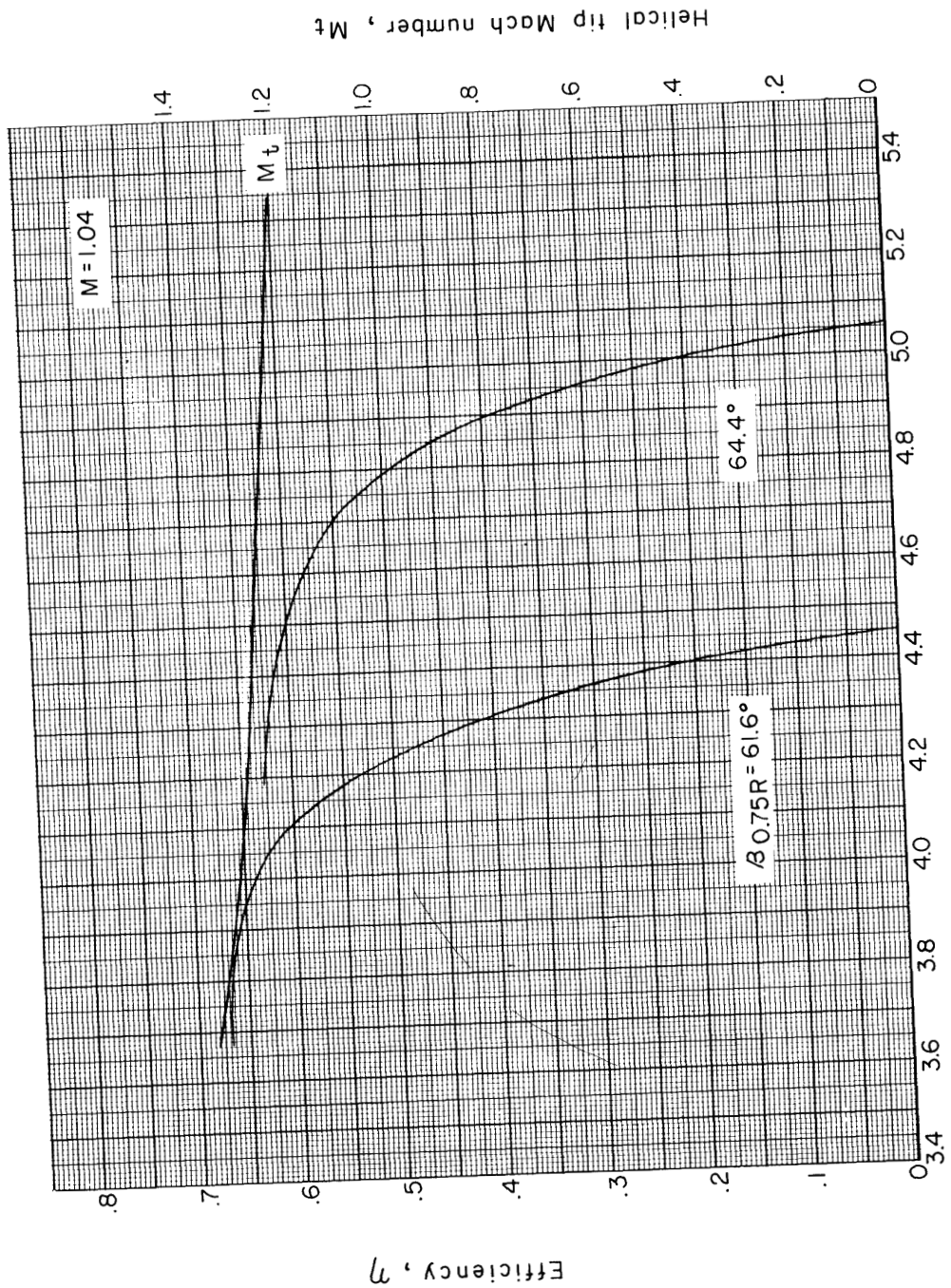

(c) Efficiency.

Figure 17.- Concluded.

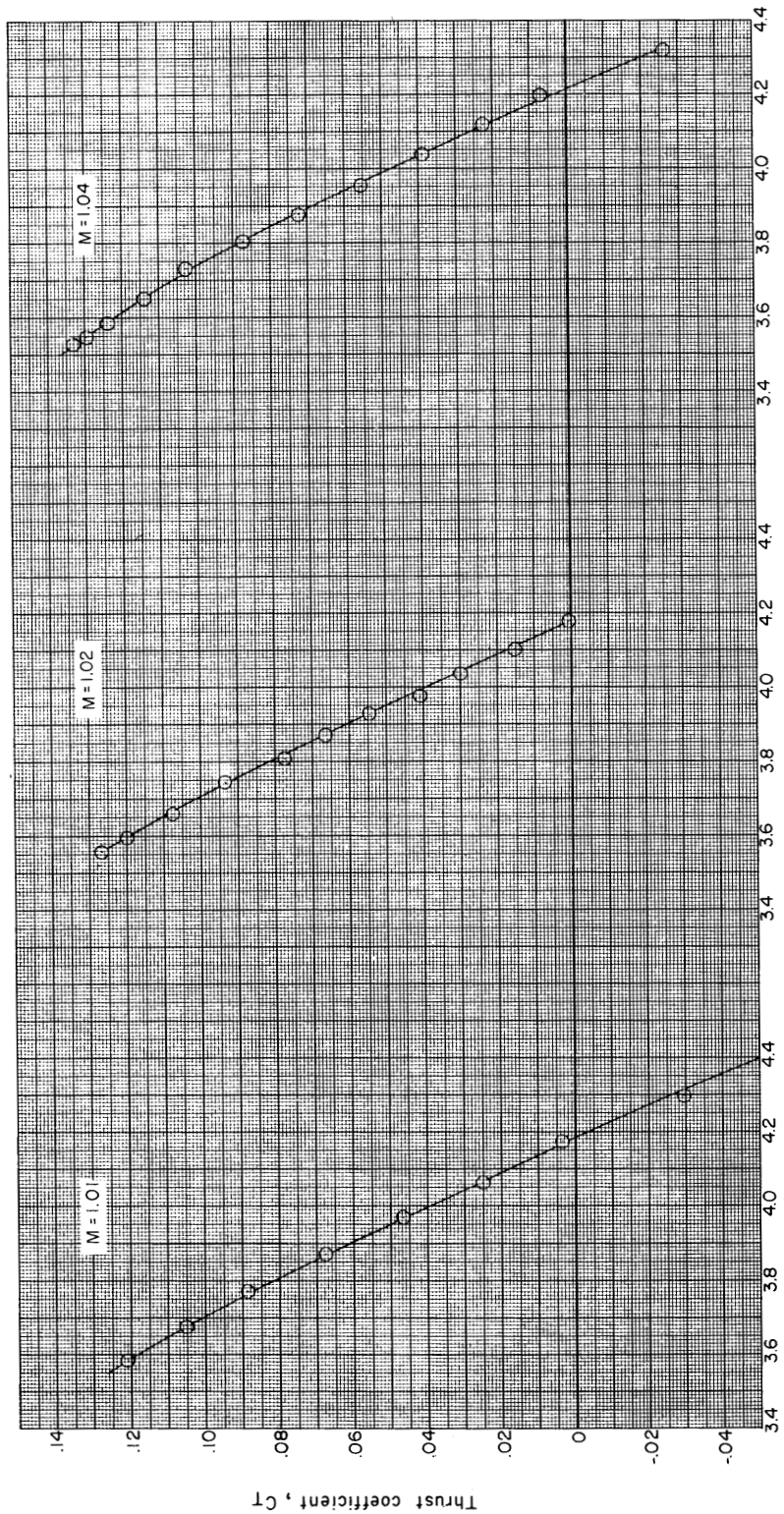

(a) Thrust coefficient.

Figure 18.- Characteristics of the Curtiss-Wright symmetrical propeller (design no. 109622). Blade angle, $\beta_{0.75R} = 60.0^{\circ}$.

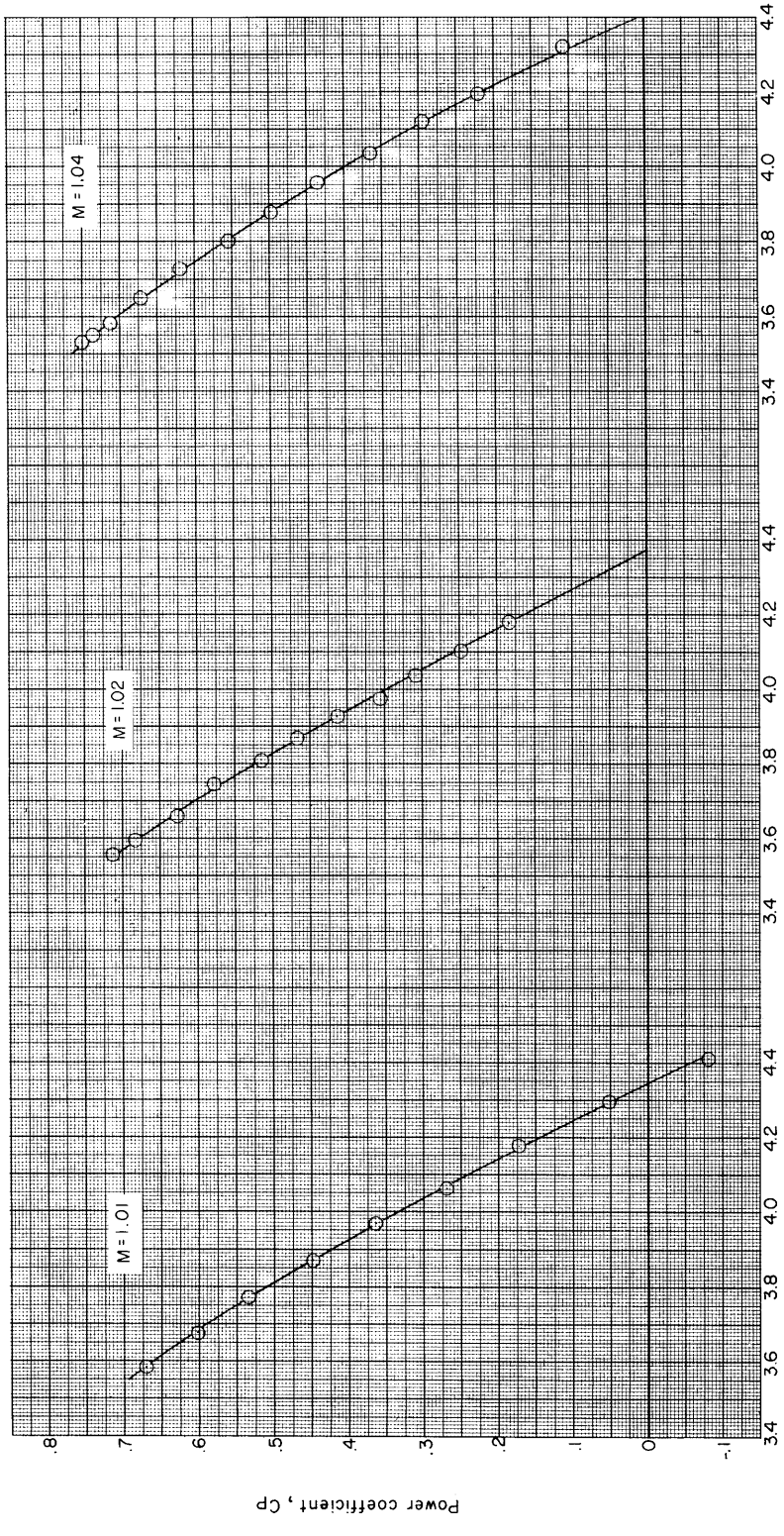

(b) Power coefficient.

Figure 18.- Continued.

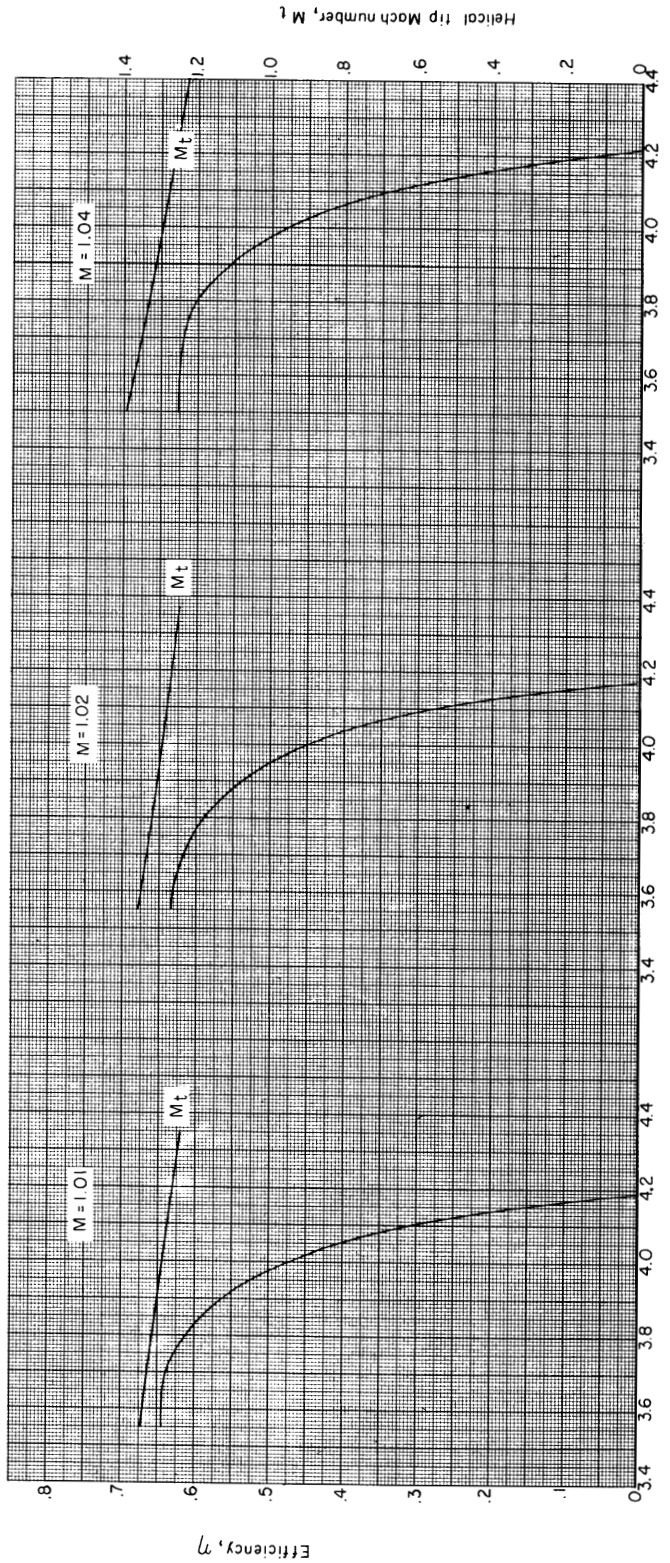

(c) Efficiency.

Figure 18.- Concluded.

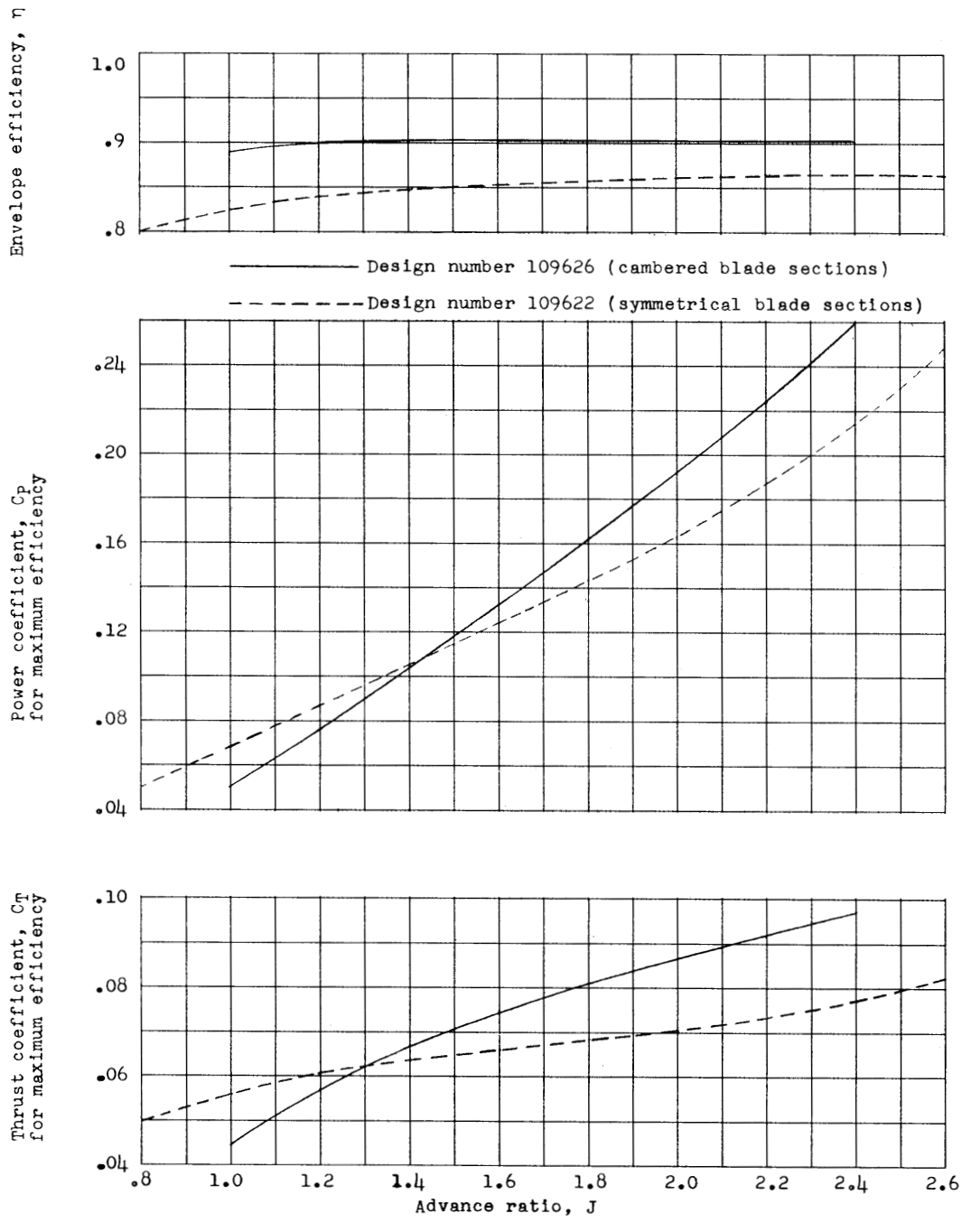

Figure 19.- Comparison of the envelope efficiency and the thrust and power coefficients for maximum efficiency of the Curtiss-Wright cambered propeller (design no. 109626) with the symmetrical propeller (design no. 109622) at a constant rotational speed of 1,600 rpm.

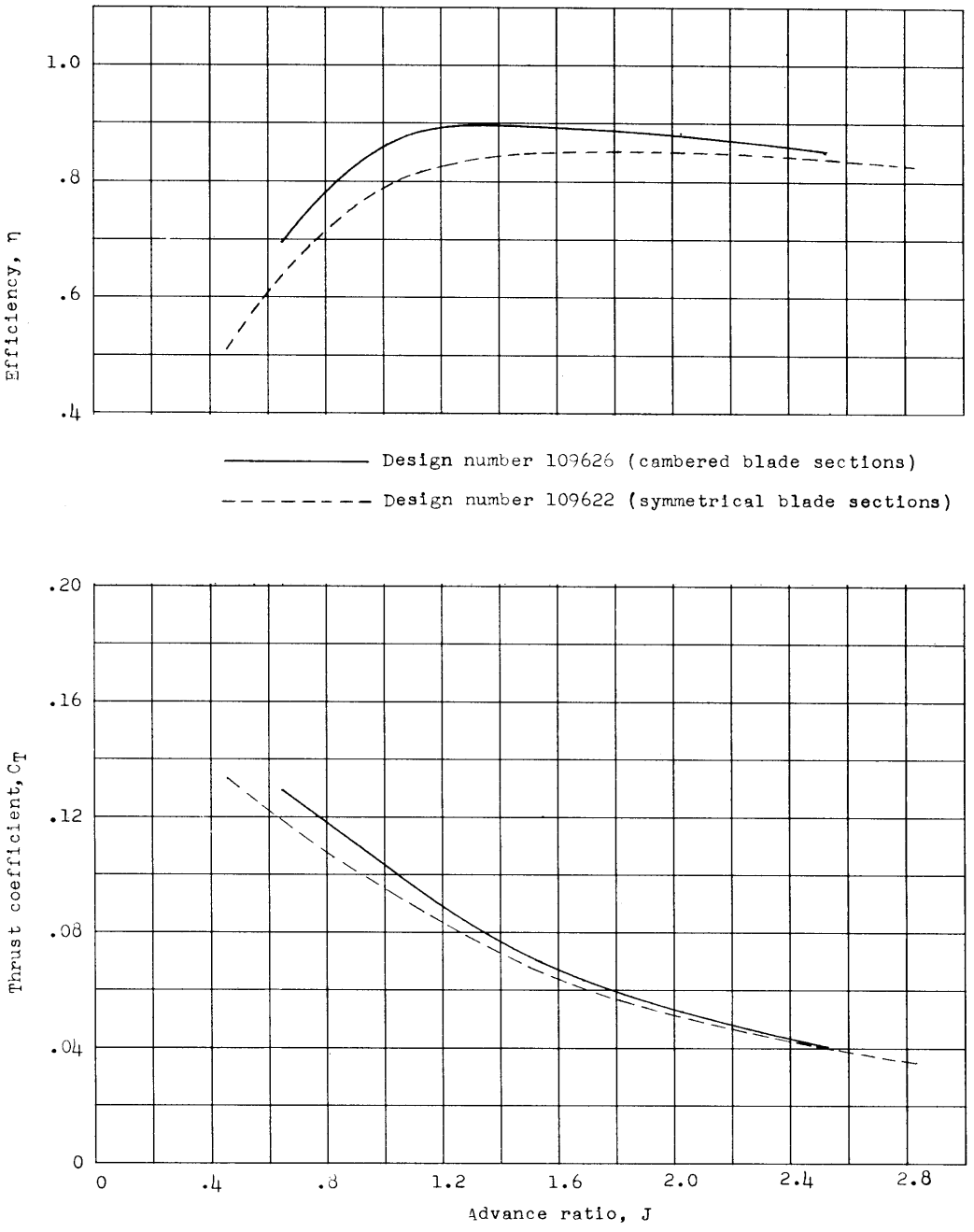

(a) $C_p = 0.12$.

Figure 20.- Characteristics of the Curtiss-Wright cambered propeller (design no. 109626) and the symmetrical propeller (design no. 109622) when operating at constant power and a constant rotational speed of 1,600 rpm.

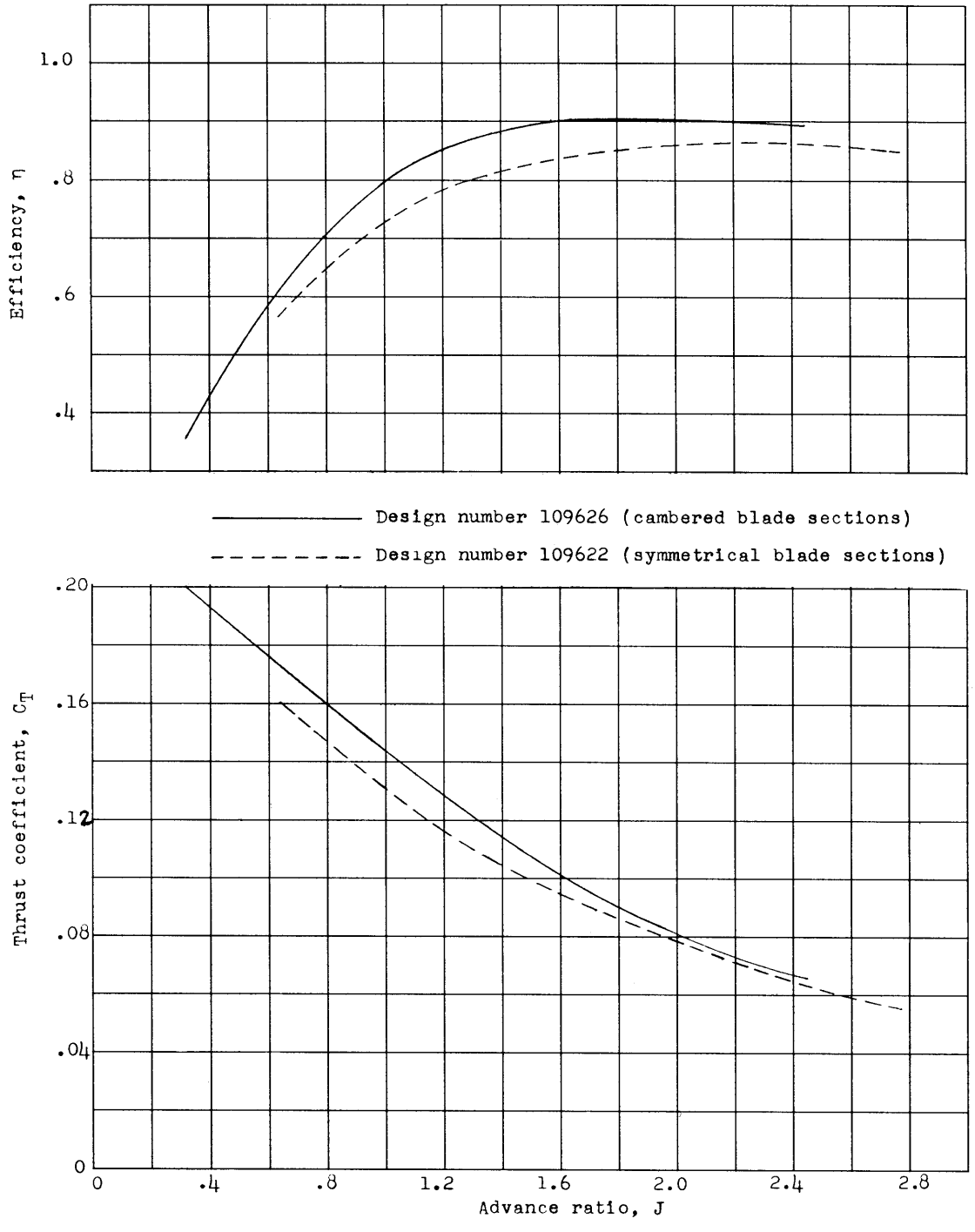

(b) $C_P = 0.18$.

Figure 20.- Concluded.

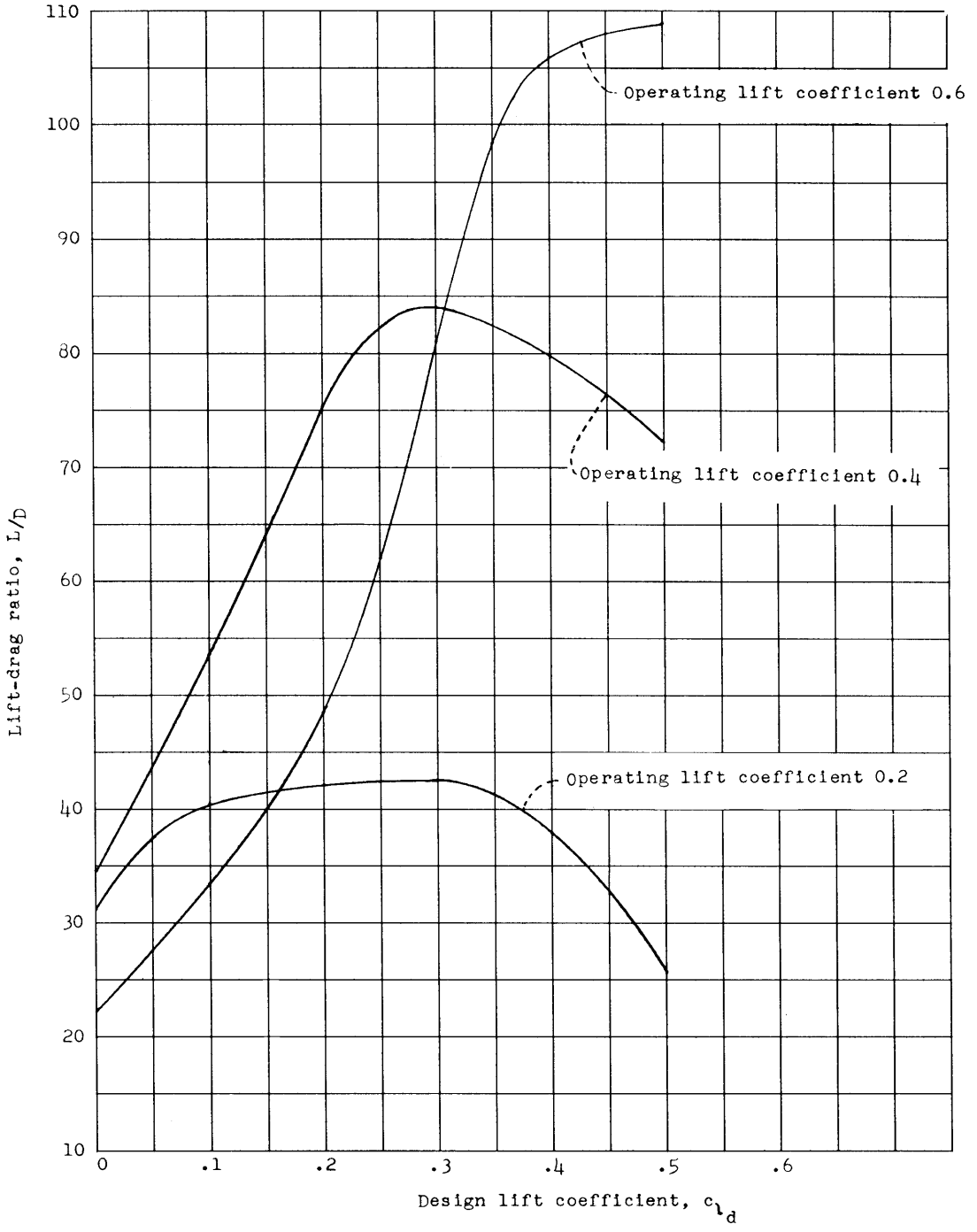

Figure 21.- The effect of design lift coefficient or camber on the lift-drag ratio of 4-percent thick 16-series airfoil sections at a Mach number of 0.7 (from ref. 8).

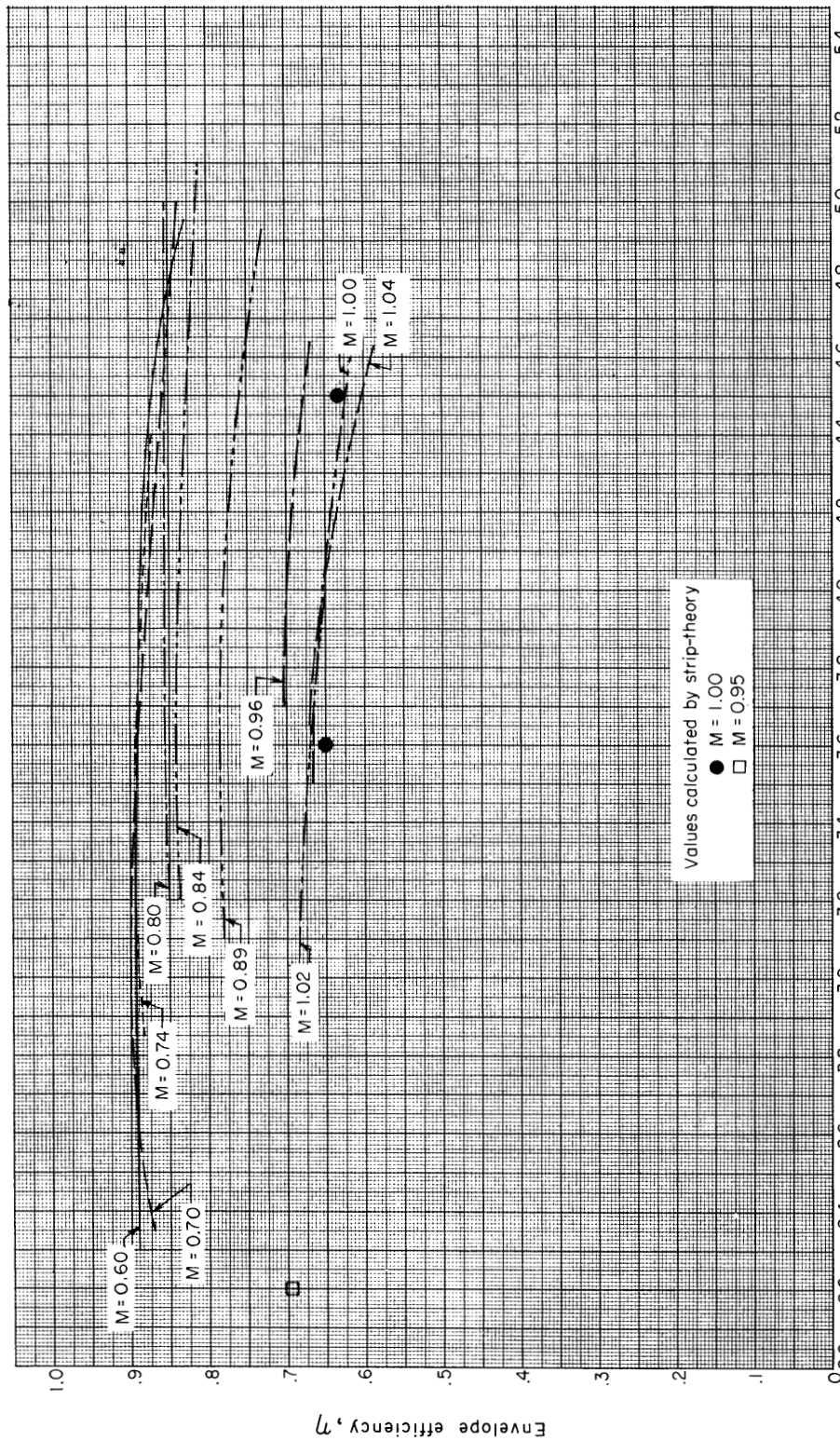

Figure 22.- Variation of envelope efficiency of the Curtiss-Wright cambered propeller (design no. 109626) with advance ratio for various Mach numbers.

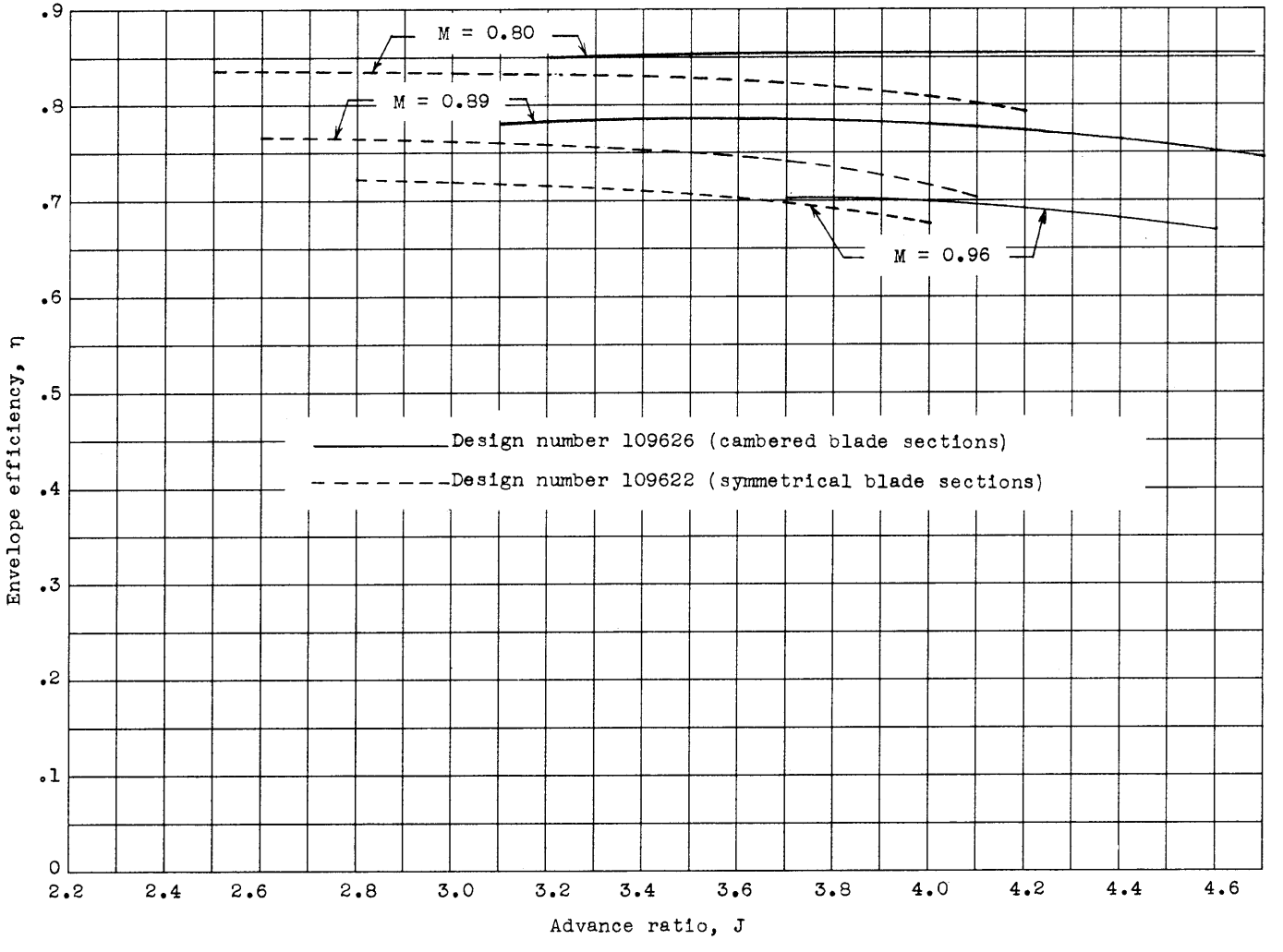

Figure 23.- Variation of envelope efficiency with advance ratio for the Curtiss-Wright cambered propeller (design no. 109626) and the symmetrical propeller (design no. 109622) at three Mach numbers.

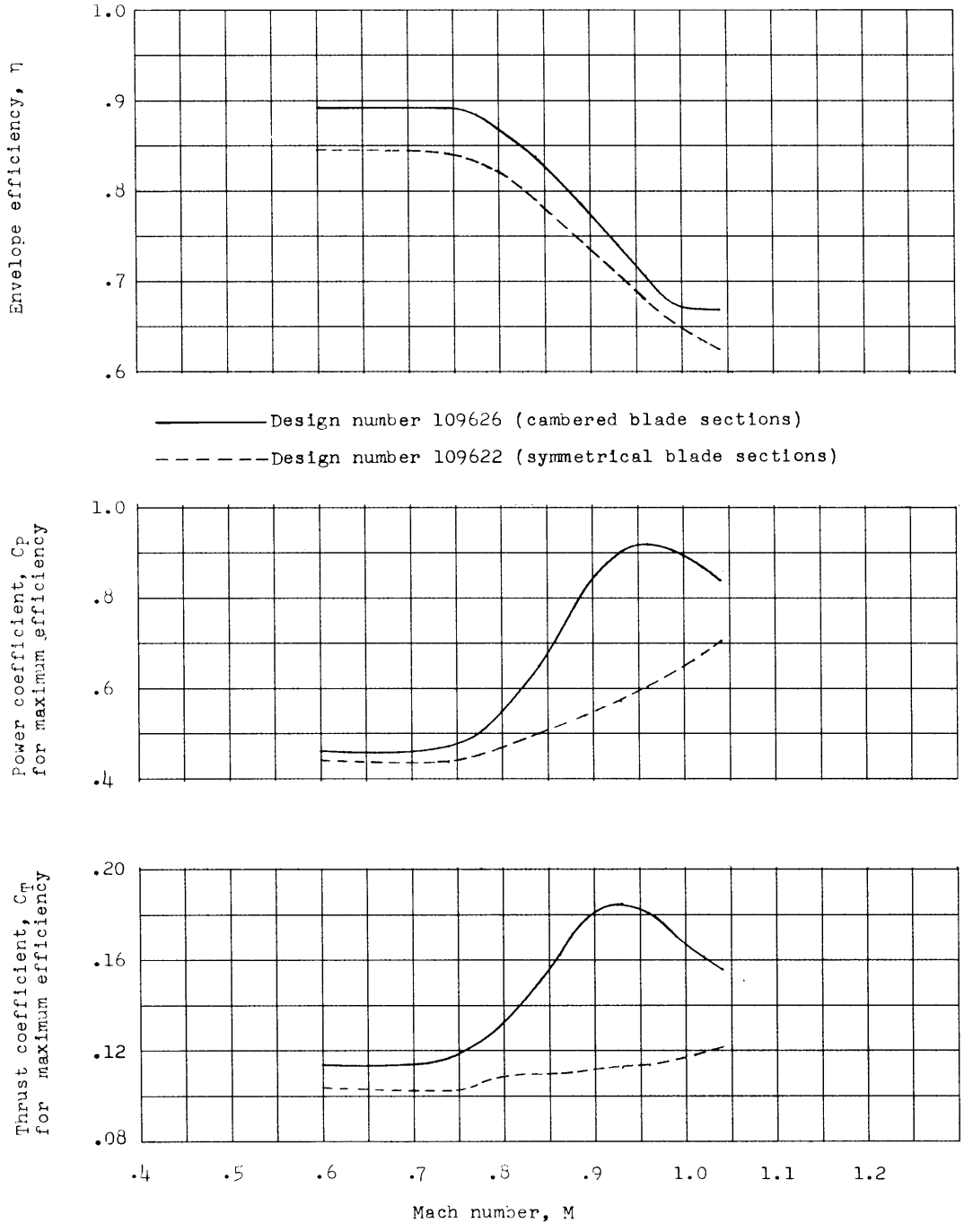

Figure 24.- Comparison of the envelope efficiency and the thrust and power coefficients for maximum efficiency of the Curtiss-Wright cambered propeller (design no. 109626) with the symmetrical propeller (design no. 109622) at an advance ratio of 3.6.

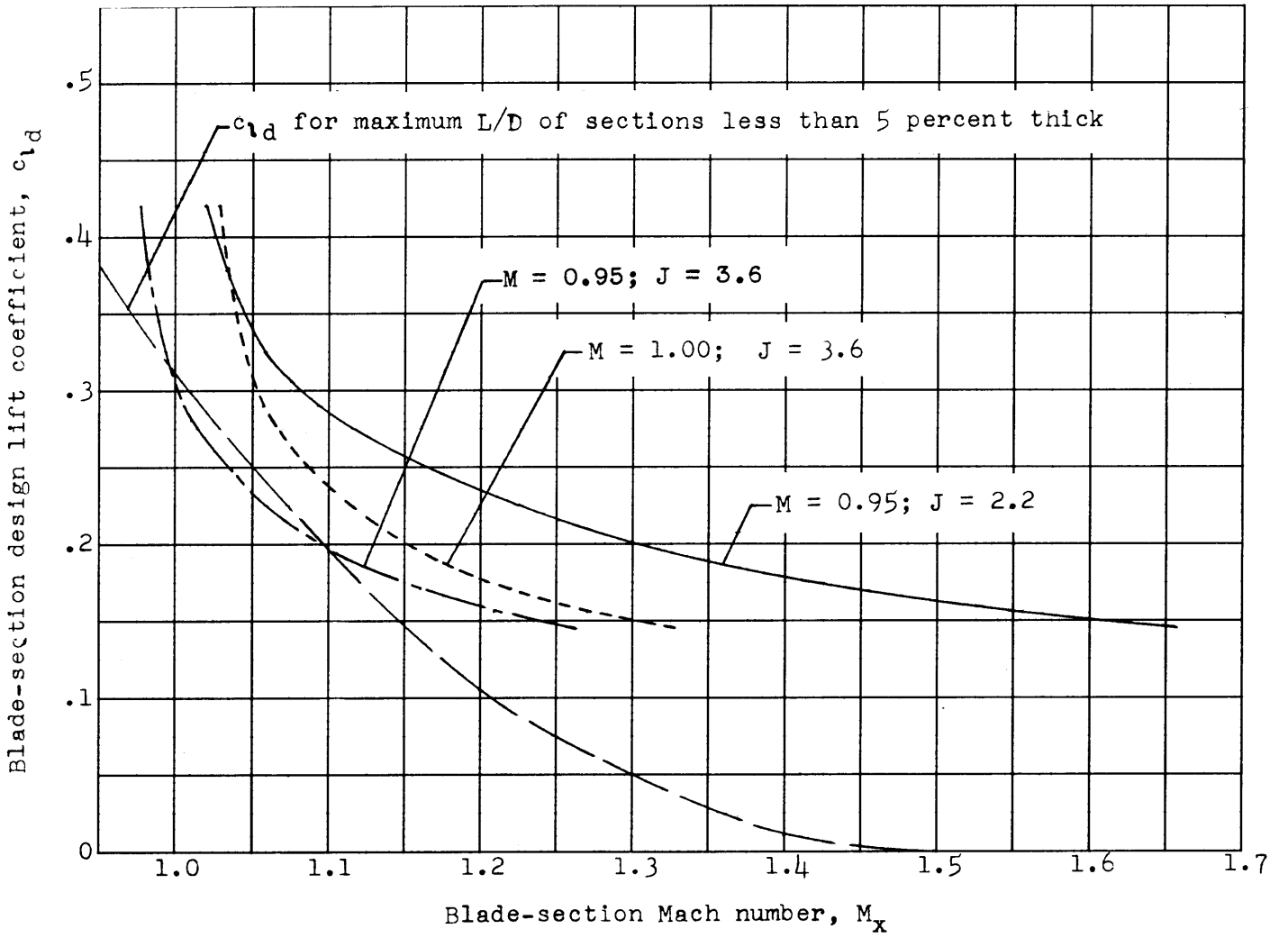

Figure 25.- Variation of blade-section design lift coefficient (camber) with section Mach number for the Curtiss-Wright cambered propeller (design no. 109626) at three operating conditions, and a comparison with the optimum distribution of camber for sections less than 5 percent thick.

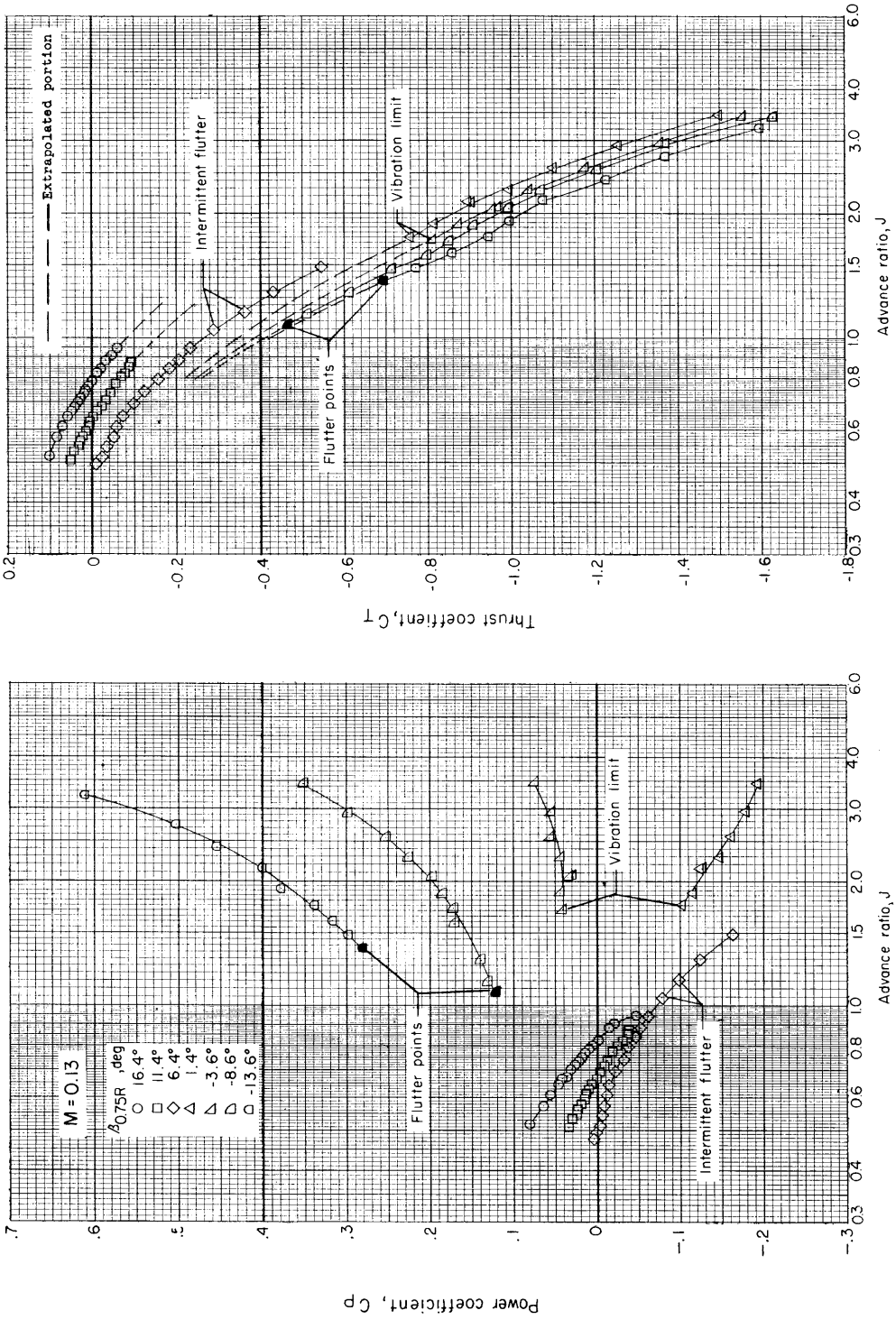

Figure 26.- Characteristics of the Curtiss-Wright cambered propeller (design no. 109626) at low and negative blade angles for a Mach number of 0.13.

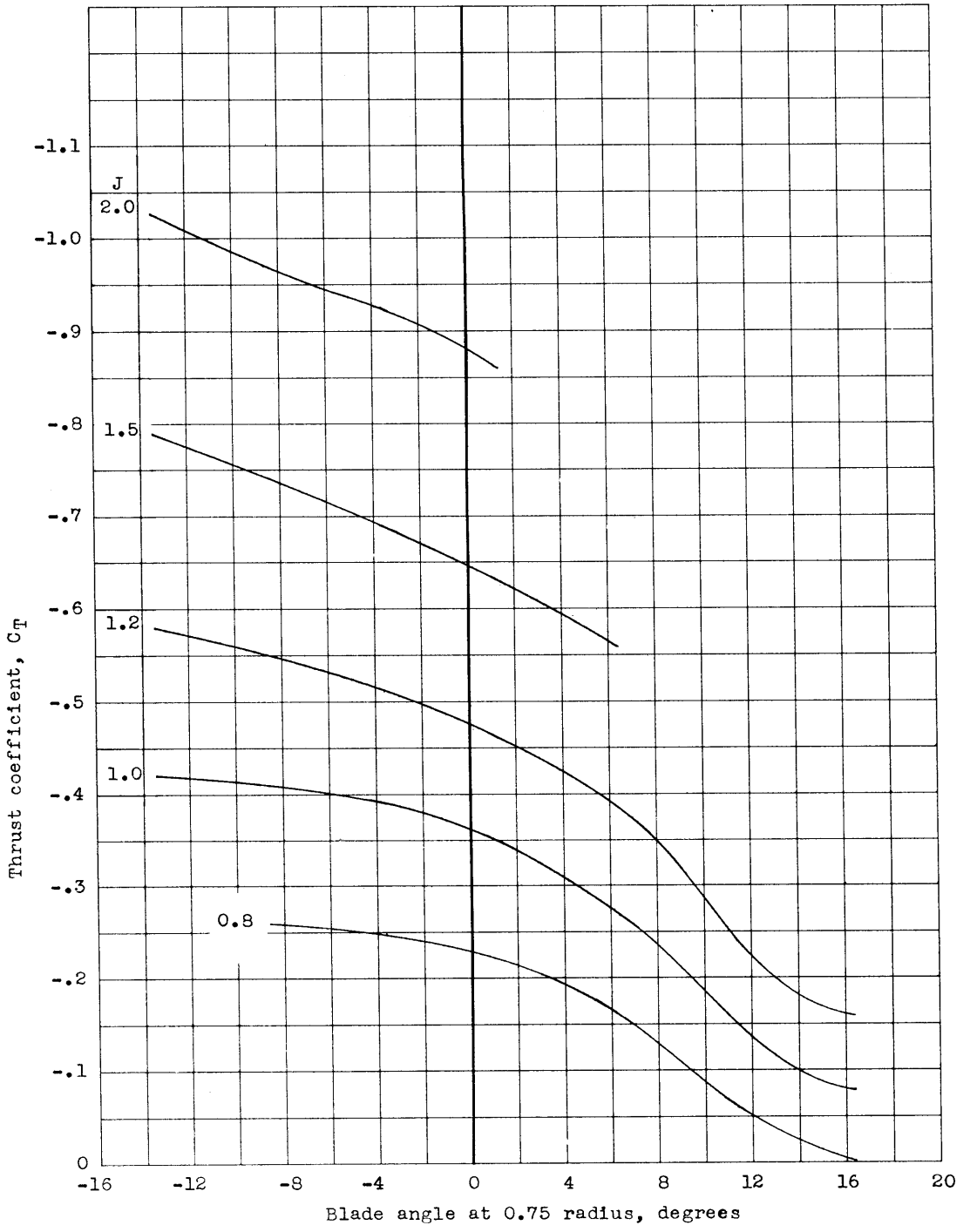

Figure 27.- Variation of negative thrust coefficient with blade angle at several values of advance ratio for the Curtiss-Wright cambered propeller (design no. 109626) at a Mach number of 0.13.

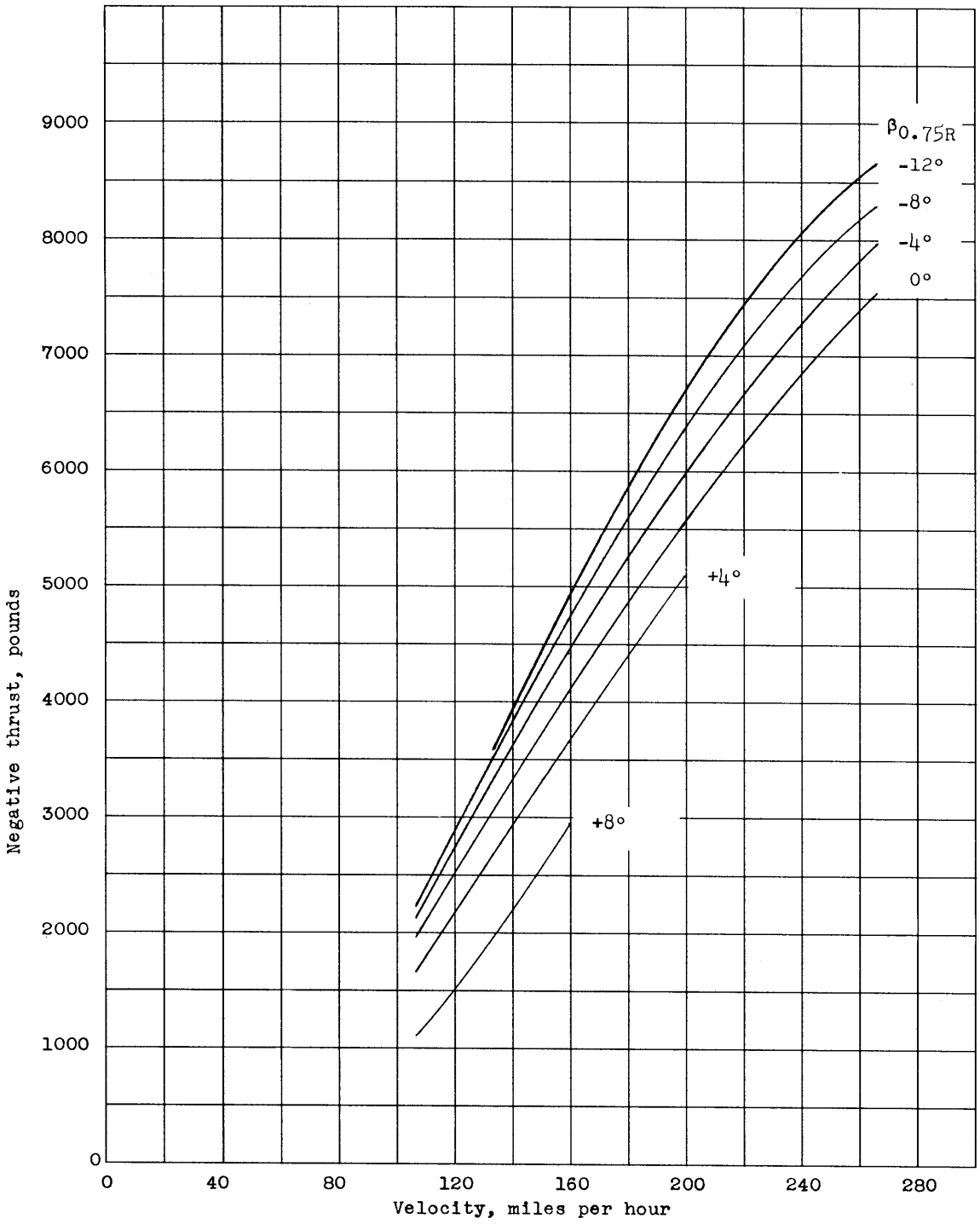

Figure 28.- Variation of negative thrust with velocity at several blade angles for the Curtiss-Wright cambered propeller (design no. 109626) at a constant rotational speed of 1,200 rpm. ρ = 0.002378.

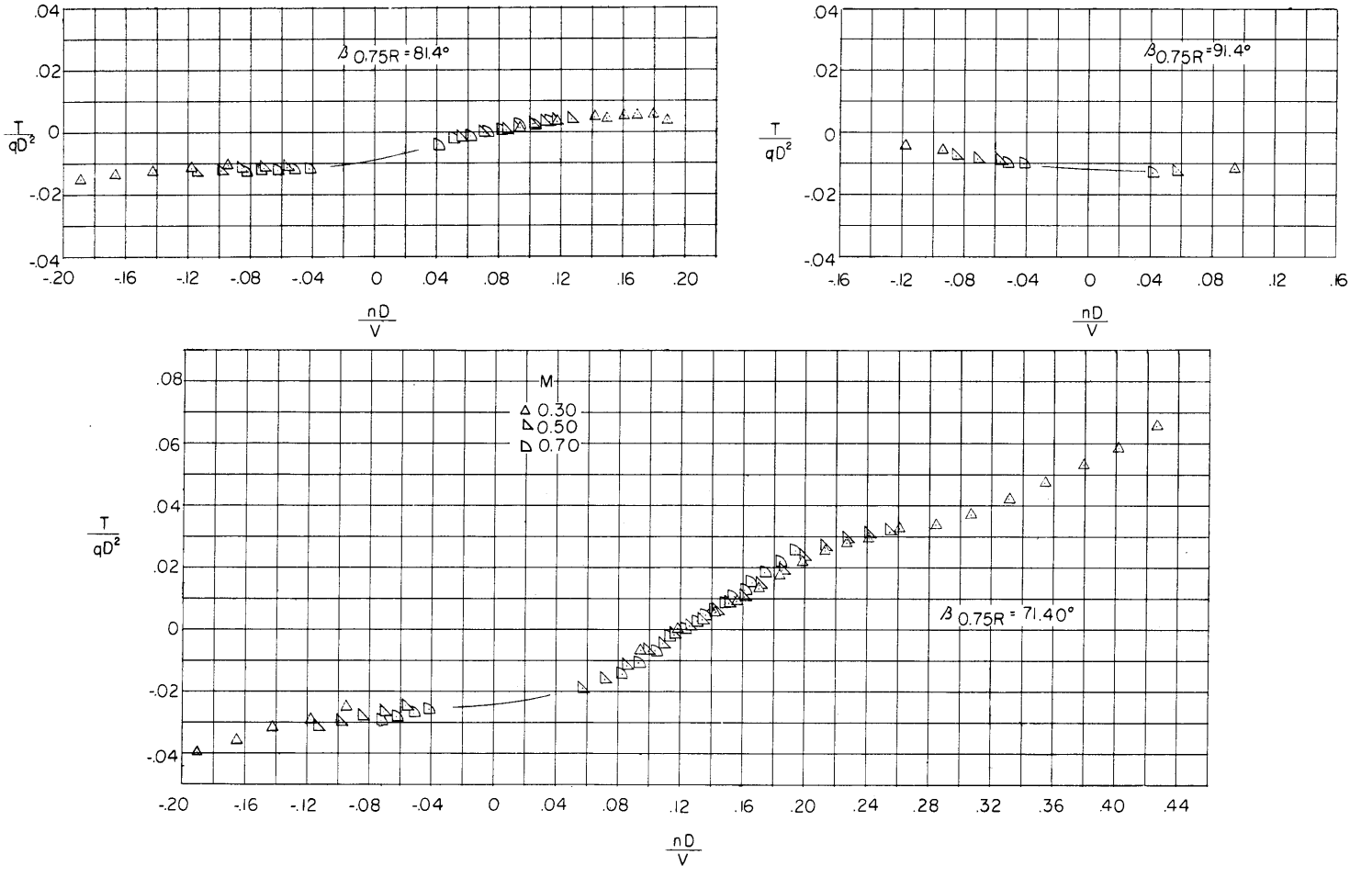

(a) Thrust.

Figure 29.- Characteristics of the Curtiss-Wright cambered propeller (design no. 109626) near the feathered condition for several Mach numbers.

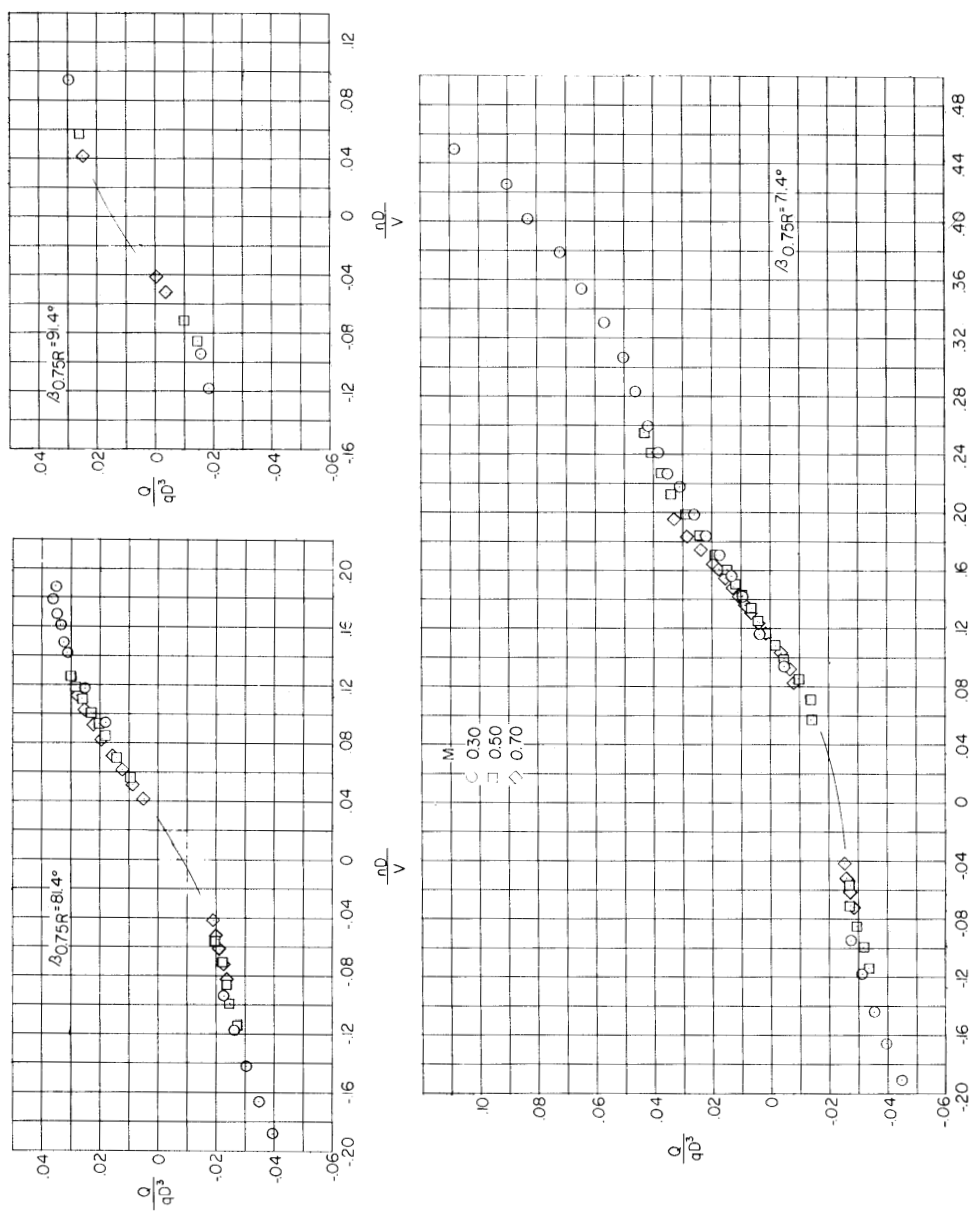

(b) Torque.

Figure 29.- Concluded.

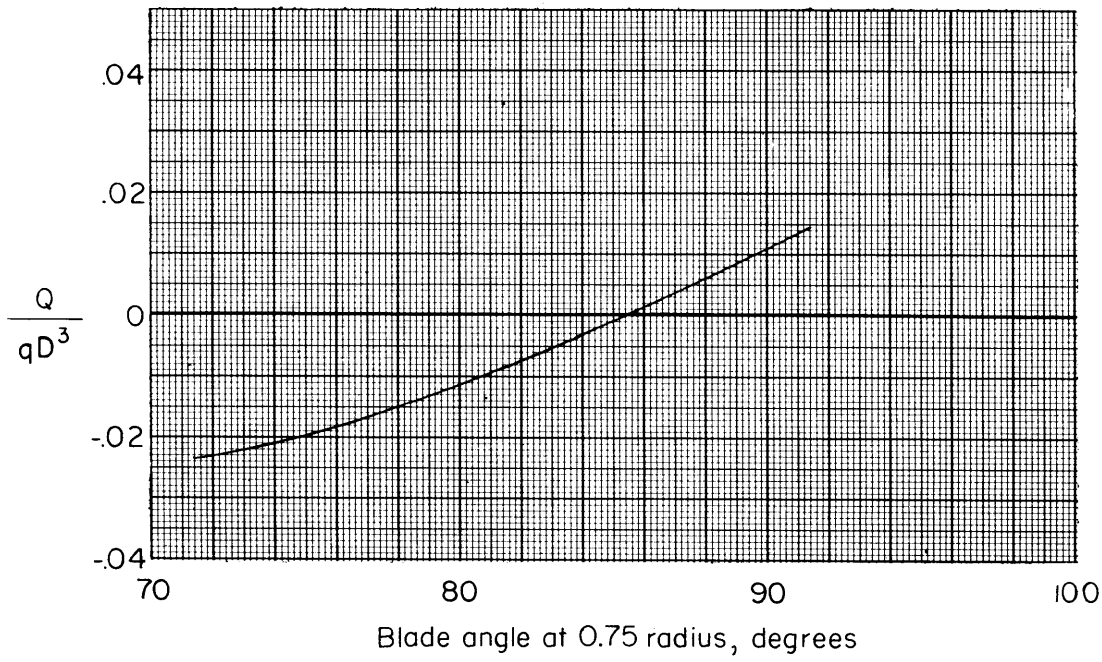

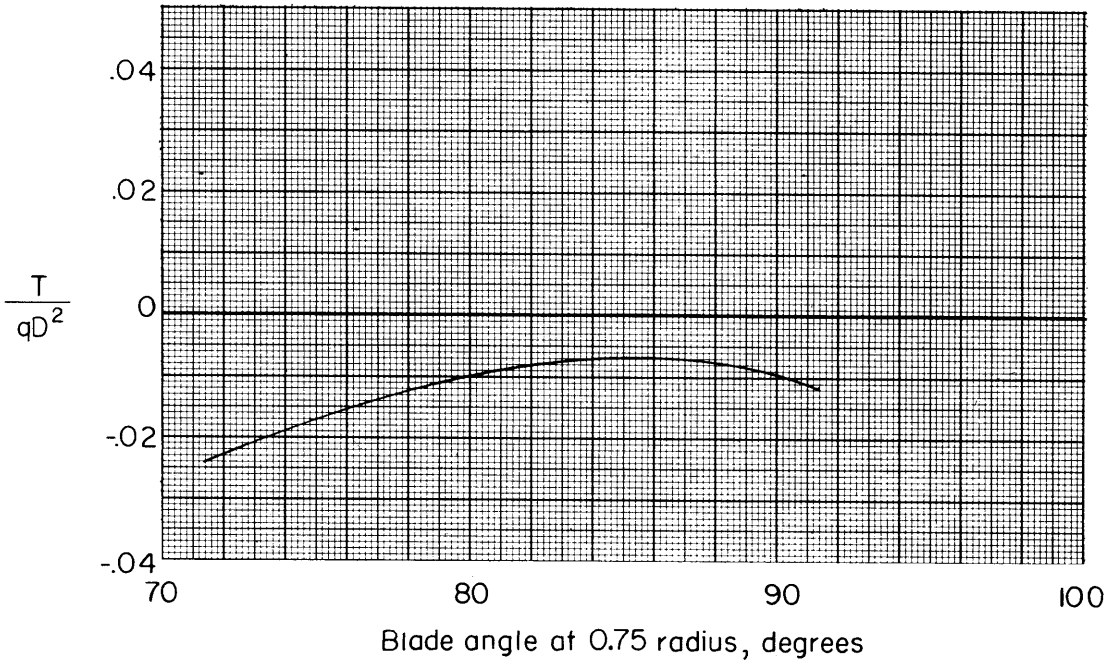

Figure 30.- Effect of blade angle on the thrust and torque characteristics of the Curtiss-Wright cambered propeller (design no. 109626) at zero rotational speed.

NACA - Langley Field, Va.